Table of Contents

Table of Figures

List of Tables

Table of Abbreviations

BSE	backscattered electrons
C_p	heat capacity at constant pressure
DSC	differential scanning calorimetry
EDX	energy-dispersive x-ray spectroscopy
EELS	electron energy loss spectroscopy
ESR	electron paramagnetic spin resonance spectroscopy
FIB	focused ion beam
ICDD	International Centre for Diffraction Data
ICTAC	International Confederation for Thermal Analysis and Calorimetry
PDF	powder diffraction file
SAED	selected area electron diffraction
SE	secondary electrons
SEM	scanning electron microscopy
STA	simultaneous thermal analyses
T_a	softening temperature
T_b	flow temperature
T_f	fictive temperature, freezing temperature
T_g	glass transition temperature, thawing temperature
T_m	melting temperature
T_s	sintering temperature
TEM	transmission electron microscopy
TG	thermogravimetry
XRD	x-ray diffraction

Abstracts

English

In this work the crystallization behaviour of stone wool is investigated. Systematic two-step heat treatments of stone wool fibres are conducted. The pre-heat treatment was performed at 0.8 • T_g, 0.9 • T_g, 1.0 • T_g, 1.1 • T_g and 1.2 • T_g where T_g = 957 K. The heat treatment was conducted both in air and in a reducing atmosphere (90 % N_2 + 10 % H_2) at 1.2 • T_g, 1.25 • T_g and 1.3 • T_g. Both treatments were executed for different durations (10, 30 and 60 min). Thermogravimetry (TG) of pre-heated and untreated fibres shows that between 500 and 700 °C a mass increase takes place which is associated with the oxidation of iron and the formation of surface crystals. It is observed by scanning electron microscopy (SEM) analyses of pre-heated fibres that the surface crystallization begins below T_g and that the size of the crystals accounts for between 20 and 50 nm. By differential scanning calorimetry (DSC) of untreated and pre-heated fibres it is found that between 850 and 1050 °C bulk crystallization occurs. In contrast to previous work (Kirkegaard & Korsgaard, 2004) by means of X-ray diffraction (XRD) albite ($Na[AlSi_3O_8]$) and gehlenite ($Ca_2Al[AlSiO_7]$) can be identified after the second heat treatment besides augite ($(Ca,Mg,Fe,Ti,Al)[(Si,Al)_2O_6]$). Quantification by the Rietveld program AutoQuan using ZnO as an external standard show that both the pre-heat and the heat treatment influence the mineralogical composition.

Deutsch

In dieser Arbeit wird das Kristallisationsverhalten von Steinwolle untersucht. Systematische zweistufige Wärmebehandlungen von Steinwollfasern werden durchgeführt. Die Vorbehandlung findet bei 0,8 • T_g, 0,9 • T_g, 1,0 • T_g, 1,1 • T_g and 1,2 • T_g statt, wobei T_g =957 K ist. Die Hauptbehandlung erfolgt sowohl in Luft als auch in einer reduzierenden Atmosphäre (90 % N_2 + 10 % H_2) bei 1,2 • T_g, 1,25 • T_g und 1,3 • T_g. Die Dauer beider Wärmebehandlungen wurde ebenfalls variiert (10, 30 und 60 min). Thermogravimetrische (TG) Untersuchungen von vorbehandelten und unbehandelten Fasern zeigen, dass zwischen 500 und 700 °C eine Massezunahme stattfindet, die mit der Oxidation des Eisens und der Bildung von Oberflächenkristallen verbunden ist. Rasterelektronenmikrospische Sekundärelektronenbilder (SEM-SE) vorbehandelter Fasern legen nahe, dass die Oberflächenkristallisation unterhalb von T_g beginnt und dass die Größe der Kristalle zwischen 20 und 50 nm beträgt. Untersuchungen mit der dynamischen Differenzkalorimetrie (DSC) von unbehandelten und vorbehandelten Fasern zeigen, dass es zwischen 850 und 1050 °C zu einer Volumenkristallisation kommt. Im Gegensatz zu früheren Arbeiten (Kirkegaard & Korsgaard, 2004) können mit der Röntgendiffraktometrie (XRD) nach der zweiten Wärmebehandlung Albit ($Na[AlSi_3O_8]$) und Gehlenit ($Ca_2Al[AlSiO_7]$) neben Augit ($(Ca,Mg,Fe,Ti,Al)[(Si,Al)_2O_6]$) nachgewiesen werden. Die Quantifizierung mit dem Rietveld-Programm AutoQuan unter Verwendung von ZnO als externem Standard zeigt, dass sowohl die Vor- als auch die Hauptbehandlung die mineralogische Zusammensetzung beeinflusst.

Dansk

I dette speciale bliver stenulds krystalliseringsopførslen undersøgt. En systematisk varmebehandling af stenuldsfibre ved forskellige temperaturer (forbehandling ved 0,8 • T_g, 0,9 • T_g, 1,0 • T_g, 1,1 • T_g og 1,2 • T_g, efterfølgende behandling ved 1,2 • T_g, 1,25 • T_g og 1,3 • T_g hvor T_g = 957 K) og varigheder (10, 30 og 60 min) bliver gennemført. Thermogravimetri (TG) undersøgelser af forbehandlet og ubehandlet stenuld viser, at en massestigning finder sted imellem 500 og 700 °C som kan relateres til jernens oxidation og overfladens krystallisering. Skanning elektron mikroskopi (SEM) analyser af forbehandlede fibre viser, at overfladens krystallisering begynder neden for T_g og at krystallernes størrelse er imellem 20 og 50 nm. Differentiel skanning kalorimetri (DSC) undersøgelser på ubehandlede og forbehandlede fibre viser, at bulk krystallisering finder sted imellem 850 og 1050 °C. Den mineralogiske sammensætning som opstår som følge af anden varmebehandling bliver identificeret med Røntgendiffraktometri (XRD) som augit ($(Ca,Mg,Fe,Ti,Al)[(Si,Al)_2O_6]$) ± albit ($Na[AlSi_3O_8]$) ± gehlenit ($Ca_2Al[AlSiO_7]$) og kvantificeret med Rietveld programmet AutoQuan, hvor ZnO bliver brugt som en ekstern standard.

1 Introduction

Climate change and the tightening of fossil fuels have brought energy efficiency into focus since the 1970s. Stone wool fibres which had been used for isolation of buildings for decades have been used more and more also in high-temperature applications, especially since the health hazards associated with asbestos products loomed. The high-temperature behaviour of stone wool has already been investigated by others (e.g. Kirkegaard et al., 2005; Moesgaard et al., 2007). The application possibilities of stone wool at high temperatures are limited by the shrinking of the fibres and can be improved by a pre-heat treatment.

In this work the effect of a pre-heat treatment on the formation temperature, the identity and the amount of crystalline phases is investigated. Pre-heat treatments are performed in air at different temperatures and for different durations. The pre-heated samples are investigated using SEM and TEM to measure the size and the composition of the surface crystals, TG is used to determine their formation temperature. DSC analyses are performed on pre-heated fibres to determine their crystallization temperature and enthalpy in dependence on the pre-heat treatment. The pre-heated samples are heated a second time to reach different degrees of crystallization and different mineralogical assemblages depending on the time, the duration and the atmosphere of this second heat treatment which simulates the heat exposure in high-temperature isolation applications. These samples are analyzed with XRD to determine this relationship. Until now only qualitative analyses have been performed and diopside ± anorthite could be determined (Kirkegaard & Korsgaard, 2004). This work shall close this knowledge gap and provide information about the connection between the identity and quantity of the crystalline phases and the shape stability of the fibres. Shape stability in this thesis means that the fibres do neither sinter nor shrink at high temperatures.

The findings of this work will give a deeper understanding of the relation between pre-heat treatment, bulk crystallization and shape stability. This might help the producers of stone wool fibres to optimize the duration and the temperature of the pre-heat treatment depending on the prospected application conditions (T, t, f_{O2}). The aim is to reach a maximal degree of crystallization without shrinkage of the fibres. The results will supply basic knowledge about the kinetics and thermodynamics of silicate glass systems which can be used both in geology and materials science. For example the tempering conditions for glass ceramics might be optimized and the formation of crystalline phases in obsidian and pitchstone might be understood better.

2 Theoretical Basis

For the understanding of this thesis some basic knowledge about glasses in general and stone wool in particular is needed because stone wool is a glassy material. Hence this chapter provides this knowledge for those who are not familiar with the topic.

2.1 Fundamentals of Glass Science

In this chapter the fundamentals of the glassy state shall be outlined. First a definition of glasses will be given before the structure and the properties of this non-crystalline solid state will be described in more detail.

2.1.1 Glass Definitions

In this chapter three different glass definitions are given. Heide (2002) defines them as non-crystalline solids which possess an equivalent, structurally and thermodynamically similar non-solid reference state, the metastable undercooled melt, into which it is converted above the glass transition temperature. In contrast to this the reference state of amorphous solids is the stable crystalline state which they tend to reach within long periods of time without a heat exposal. Alternatively they can melt or can be converted into another instable state. Although the atoms in glasses have no periodic long-range order (Shelby, 2005), different “structural areas” can be defined and the short-range order of the atoms can be observed (Heide, 2002). This obeys to a frequency distribution and is not characterized by discrete values like in crystals. Although glasses behave therefore structurally more like a liquid they are dynamically rather solids. This means that the relaxation time which a glass needs to convert a mechanical stress into a strain is larger than the observation time. Since the latter depends on the analytical method a clear transition from the glassy to the liquid state cannot be defined. The position of the glasses within the field of condensed matter is shown in Figure 1:

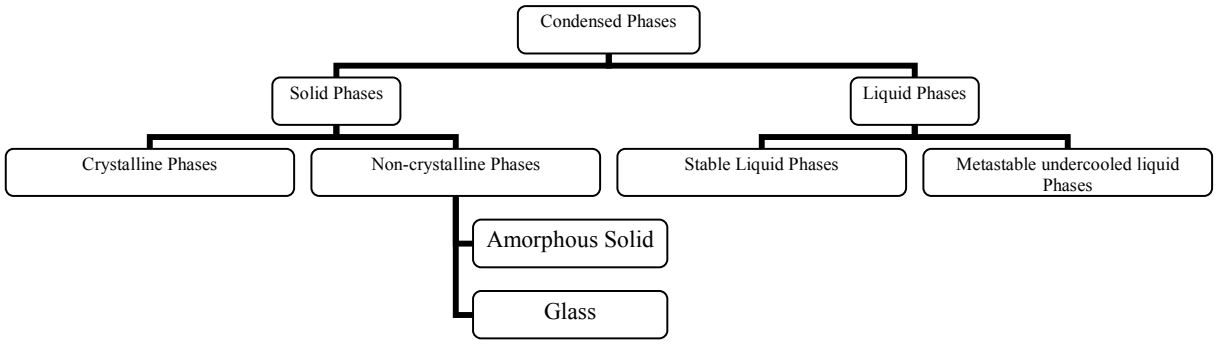

Figure 1: Classification of Condensed Matter (modified after Heide, 2002)

Apart from these characteristics no other criteria are needed for the definition of a glass: Although most glasses in geology and technology are silicates, both organic and inorganic substances can occur in the glassy state. Furthermore glasses can form not only by the cooling of a liquid but also by the heating of a gel (Heide, 2002). This definition contradicts the German Industry Norm DIN 1259 stating that glasses are always inorganic and melt-derived. Another definition made by Shelby (2005) states that glasses are defined by their glass transition behaviour (chapter 2.1.3). From the linguistic point of view this definition is not satisfying because it explains one word by using a composite word of itself. However this definition does not contradict to that of Heide (2002), but only focuses another aspect.

2.1.2 Glass Structure

The glass structure is described in this chapter for the special case of silicate glasses which are the most common type of glasses and include also stone wool fibres. The basic theory in this field was developed by Zachariasen (1932). They consist of network formers (e.g. Si, Ge) which build up a polyhedral structure and network modifiers (e.g. Ca, Na) which occupy the interstitial positions of this structure. The former are coordinated by three or four, the latter by at least six oxygen atoms respectively ions. Some elements (e.g. Al, Fe) can act both as network formers and network modifiers (Zachariasen, 1932). In silicate glasses like stone wool silicon acts as a network former and is coordinated by four oxygen atoms (Figure 2).

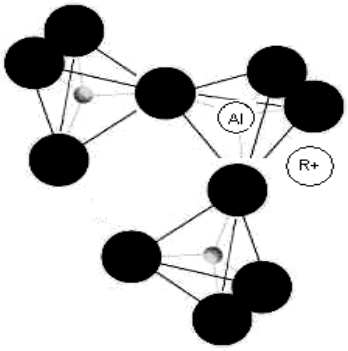

Figure 2: The structure of stone wool (small spheres in the center: Si, large black spheres: O) (Kirkegaard & Korsgaard, 2004)

In silicate glasses Al acts as long as a network former, e.g. it occupies a tetrahedral position, as its molar concentration is lower than that of the alkali / alkaline earth metals. This is the case in stone wool fibres (chapter 2.2.1). Otherwise it acts as a network modifier and occupies octahedral positions with three bridging and three non-bridging oxygen atoms. Alternatively the formation of clusters of three tetrahedral with a trigonal coordinated oxygen atom in the middle is discussed (Shelby, 2005). Apart from network formers and network modifiers glasses also contain fluxes, colorants and fining agents. A flux is a material, often an alkali oxide, which reduces the melting point of the raw materials for about 400 °C. Fining agents like arsenic and antimony acids, sodium and potassium nitrates, sodium chloride, sulphates or fluorides remove bubbles from the melt (Kirkegaard & Korsgaard, 2004). Although all these other chemical components might be present in alumosilicate glasses they contain structural elements which remind of cristobalite and quartz (Heide, 2002).

2.1.3 Glass Properties

For the understanding of this thesis a basic knowledge about the **thermal properties** of materials is required. Hence some important expressions have to be defined:

"The [molar] **heat capacity** is the energy required to raise the temperature of one mole of a material by one Kelvin (K) or one degree Celsius (°C)" (Askeland, 1996). This means that the heat capacity is measure for the resistance of a material against heating or cooling. In this work the heat capacity at constant pressure, C_p, is used. The hypothetical heat capacity at 0 K is zero. Then it increases material-dependent up to a maximum of 25 J/(mol*K). Phase transitions lead to jumps or peaks in the $C_p = f(T)$ curve (Askeland, 1996). C_p is a very important for the glass transition: When a liquid crystallizes at its freezing point T_m, the heat capacity C_p decreases suddenly (Vogel, 1992). This sudden decrease is associated with the

formation of a atomic long-range order (Shelby, 2005). If the crystallization is suppressed due to kinetic reasons, C_p decreases only slowly and continuously, the undercooled liquid does not crystallize. Instead of a sudden structural change only a slow temperature-dependent rearrangement of the atoms takes place (Shelby, 2005). The glass formation needs rapid cooling (around 10^{-6} K/s for alumosilicates and 10^2 K/s for metals). At the fictive temperature (freezing temperature) T_f the C_p deviates from that of the undercooled liquid which equals the formation of a glass. The term "fictive temperature" refers to the fact that during heating nothing happens at this temperature. Instead the enthalpy follows the enthalpy function of the glassy state which is referred to as the superheating effect (Höhne et al., 1996). In contrast to this Shelby (2005) defines the fictive temperature T_f as the interception of the lines which describe the enthalpy of the liquid and the glass. It is the temperature where the structure is frozen in. The viscosity increases and prevents a further rearrangement of the atoms. This phenomenon is referred to as the freezing of a liquid (Shelby, 2005). When the glass is heated again C_p reaches the curve of the undercooled melt at the glass transition temperature T_g which is also referred to as the dewing temperature. Above T_g the material is called an undercooled melt again. Exsolution and crystallization processes may occur because the kinetic barrier is overcome. Then energy is released, the enthalpy decreases and C_p reaches a minimum. Both the freezing of an undercooled melt and the thaw of a glass occur continuously and not abruptly and depend on the heating and cooling rate, respectively (Heide, 2002). In contrast to this clear distinction between freezing and dewing temperature, according to Shelby (2005) T_g is only vaguely defined by thermoanalytical methods. The dependence of the enthalpy which is linked with the heat capacity by the equation

$$C_P = (\partial H / \partial T)_P \qquad (1)$$

on the temperature and the cooling rate is visualized in Figure 3:

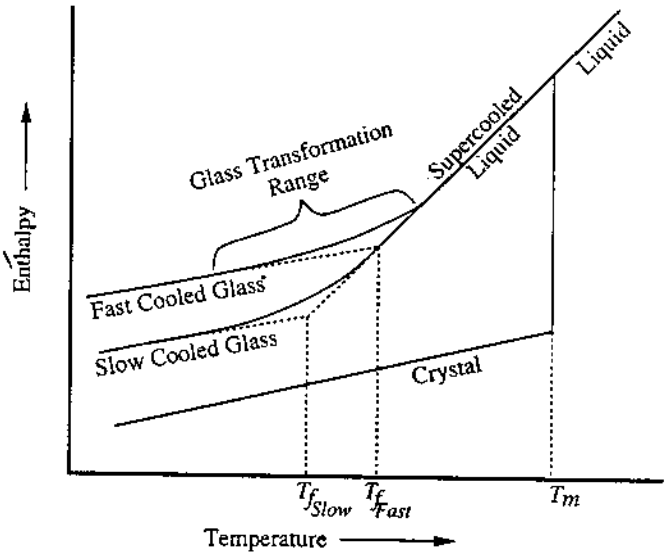

Figure 3: The glass transition. T_f = fictive temperature. T_m = melting temperature (Shelby, 2005)

Below the glass transition the enthalpy is determined by the heat capacity of the glass. High T_f values signify that the structure of the glass is more like that of a liquid, low T_f values mean that it is more ordered. The faster the cooling of a glass, the higher is T_f. Hence stone wool has a higher T_f than common glasses (Kirkegaard & Korsgaard, 2004). Furthermore in Figure 3 it can be seen that slower cooling rates shift the transformation range to lower temperatures because of a lower viscosity. These thermodynamic changes also effects the mechanic properties of the material: When the viscosity of an undercooled melt increases with decreasing temperature the mobility of the atoms is reduced and the enthalpy increases compared with that of a liquid. Finally the viscosity reaches a value of 10^{12} Pas, the atoms stop fluctuating and the structure of the melt is frozen in the solid state (Shelby, 2005).

This thesis deals with crystalline phases, hence the two basic processes for crystallization, **nucleation and crystal growth**, shall be discussed. The formation of a nucleus is associated with the creation of a surface for which the surface free energy is needed. On the other hand the so-called volume free energy is released when a certain volume is transferred from the energetically less favourable state of an undercooled melt to the more favourable crystalline state. The surface free energy increases by the power of two with increasing radius of the particle whereas the volume free energy decreases – because of its negative algebraic sign – by the power of three. Hence there is an energy maximum for a certain radius. This radius is referred to as the critical radius. There are two barriers which avoid the formation of sufficient large nuclei (Shelby, 2005). In the temperature range directly below T_m the thermodynamic barrier increases the critical radius (Askeland, 1996) and decreases therefore the probability of

crystallization; hence this region is called the metastable region of undercooling (Kirkegaard & Korsgaard, 2004). If the temperature is below T_g, the kinetic barrier increases the viscosity of the glass so much that to the atoms are not able any more to form nuclei. One distinguishes two kinds of nucleation: Homogeneous nucleation occurs if the nucleus has the same composition as the forming crystal. Heterogeneous nucleation is a process in which pre-existing solid particles, e.g. the rim of a furnace, act as nuclei. In the case of heterogeneous nucleation the critical radius can be reached with a smaller expense of material because the heterogeneous nuclei itself, the impurity, contributes to this critical radius (Askeland, 1996).

Crystal growth is the accretion of atoms, ions or molecules on the surface of a crystal. Since high viscosities disturb the transport of atoms to the crystal surface, crystal growth is slow for low temperatures. The higher the temperature is, the faster the crystals grow until the thermodynamic barrier increases in the vicinity of T_m and the crystal growth decreases again. However, the maximum of the crystal growth occurs at higher temperatures as that of the nucleation. As a conclusion it can be stated that growth occurs whenever nuclei are present and the temperature is below T_g (Moesgaard & Pedersen, 2005). Figure 4 shows the rates of nucleation (KB, german: “Keimbildung”) and crystal growth (KG, german “Kristallisationsgeschwindigkeit”) for a material that tends to crystallize (top) and those of a material that tends to vitrify (bottom). In the first case the two curves overlap each other, in the second they are separated from each other. η is the viscosity.

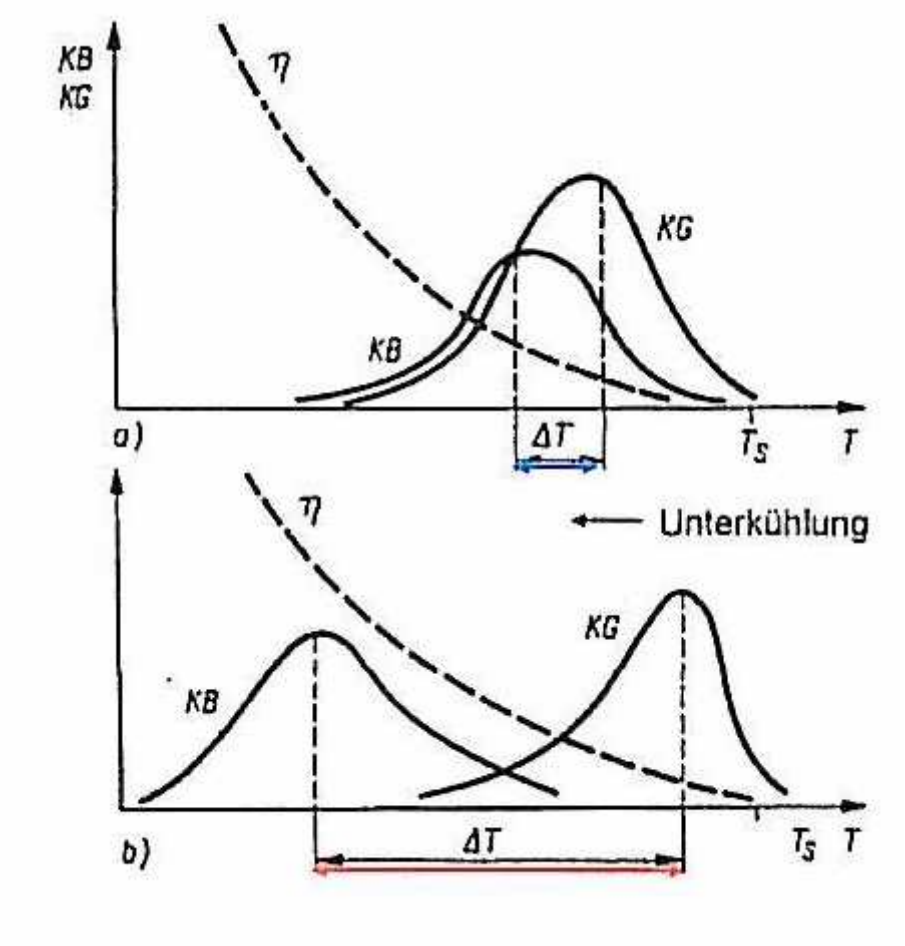

Figure 4: Phases of Crystal Growth, T_m is the melting temperature and T_g is the glass transition temperature (Götze, 2006)

2.2 Fundamentals of Stone Wool

In this chapter the present knowledge about stone wool which is needed for the understanding of the following parts of this thesis shall be summarized. The high-temperature behaviour of stone wool is described in detail to demonstrate the aim of this thesis and to justify the experimental design (chapter 3).

2.2.1 Production, Composition and Application of Stone Wool

Stone wool is a fibrous, glassy material which is used as a thermal and acoustical isolator. Untreated stone wool is completely amorphous. Since the main components of stone wool are SiO_2, Al_2O_3, CaO, MgO and FeO, it is an alkaline earth alumosilicate glass. The positive charge of the earth alkaline cations is neutralized by the substitution of Si^{4+} by Al^{3+} in the tetrahedral sites (Moesgaard & Pedersen, 2005). Since the concentration of Al is lower than that of Ca, Fe and Mg, Al occupies tetrahedral positions (Shelby, 2005). A mixture of basalt, limestone, recycling products and dolomite is used as a raw material. Together with additives like olivine, bauxite or slags they are melted in a cupola furnace (Moesgaard & Pedersen, 2005). In the Rockwool® production plant in Doense/DK the raw materials, among them a large amount of recycling materials, are pressed to briquettes before the melting process which I could see myself during a visit in the Doense production plant. During the process an exsolution of two melts occurs: One metallic iron melt which sinks down to the bottom of the furnace and which must be removed frequently and a silicate melt which is the basis for the fibre formation (Kirkegaard & Korsgaard, 2004). The silicate melt flows through an opening out of the tank onto a winder of spinning wheels whose centrifugal force converts the melt droplets into fibres while they freeze into glass (Figure 5) (Moesgaard & Pedersen, 2005):

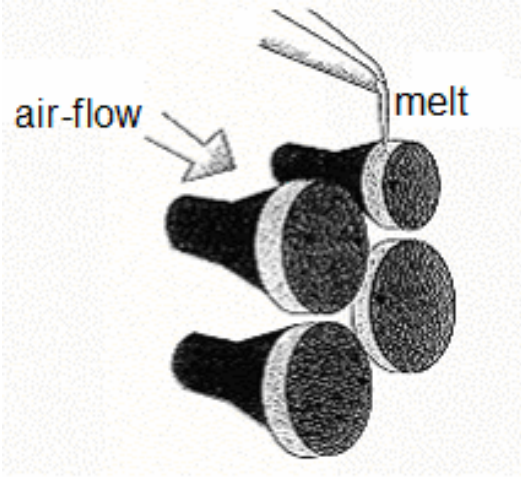

Figure 5: Fibre formation by rotating spinning wheels (Kirkegaard & Korsgaard, 2004)

The cooling rate accounts for 10^6 K/s (Pakosch, 2006). An air flow spins blows the fibres into a spin chamber where they are coated with a phenolic resin which acts as a binder. In the future also inorganic binders might be used (Kirk, in preparation). During the finishing process they are sprayed with silane (SiH_4) to improve the coherence between the fibres and their coating. After the coating has dried the stone wool can be cut, packed and sold (Moesgaard & Pedersen, 2005). The whole process is shown in Figure 6:

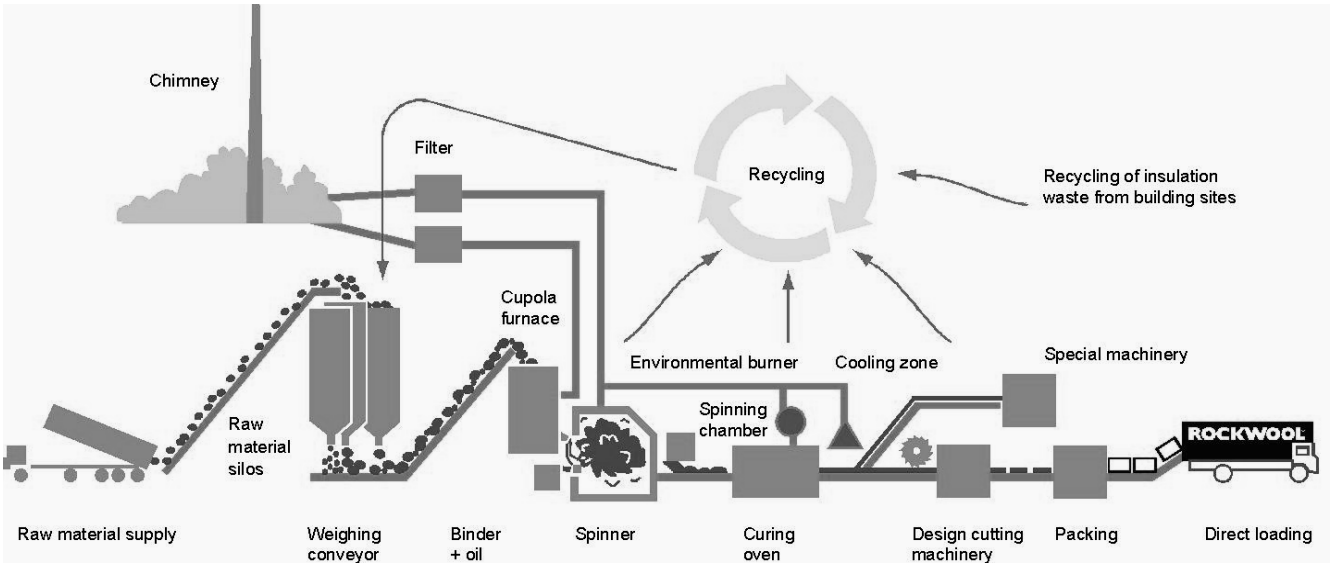

Figure 6: Production of stone wool fibres (Rockwool A.S.)

There are different kinds of stone wool fibres produced by Rockwool International A/S and its daughter companies. In this work predominantly HT (high temperature) fibres are examined,

but for the study of the influence of the iron content two more types were used who are called "white fibres" and "mixed fibres" in this work. These fibres have the following composition:

Table 1: XRF analyses of Rockwool HT fibres (Rockwool International A/S)

	Identification	SiO_2	Al_2O_3	TiO_2	FeO	CaO	MgO	K_2O	Na_2O	P_2O_5
HT		40.6	20.8	1.6	7.1	13.6	11.4	0.8	1.6	0.3
mixed	FI070182-00	39.5	19.4	0.5	4.4	26.5	5.1	0.6	1.5	0.5
white	FI070171-00	37.7	20.7	0.4	0.8	32.8	4.7	0.4	1.6	0.1

In the following part the behaviour of stone wool during a heating process is described. During the production of stone wool fibres energy is stored in the energetically unfavourable structure that results from rapid cooling (Figure 3). If the fibres are heated to a temperature between 475°C to 665°C the structure becomes energetically more favourable and the energy difference is released (Moesgaard & Pedersen, 2005). Like all really existing glasses (cooling rate < 0) stone wool fibres show below Tg the so-called thermometer effect. This is a volume relaxation (shrinking) caused by a decrease of the Gibbs free enthalpy down to the level of an ideal glass (cooling rate = 0) (Heide, 2002). The glass transition temperature in HT stone wool fibres is 684 °C according to own DSC measurements (Figure 22). In this temperature region Fe^{2+} is oxidized to Fe^{3+}:

$$4\ Fe^{2+} + O_2 \Leftrightarrow 4\ Fe^{3+} + 2\ O^{2-} \qquad (2)$$

Since the use of coal in the production process creates a reducing atmosphere, iron occurs in stone wool fibres in the ferrous state. When the fibres are cooled down rapidly there is not enough time for an efficient diffusion. Hence Fe^{2+} remains the dominant species. However, there is a gradient of the chemical potential of oxygen between the surface and the interior of the fibre which acts as a driving force for oxidation. As soon as efficient diffusion is possible the oxidation will take place in order to reduce this gradient (Kirkegaard & Korsgaard, 2004). This process is associated with a change in colour from grey to yellow, an embrittlement of the fibres and a change in the role of iron in the glass network: Since the ionic radius of iron decreases from 0.82 Å to 0.67 Å during oxidation a tetrahedral coordination becomes more favourable than an octahedral one when the Fe^{3+}/Fe^{2+}-ration exceeds 1:2 (Moesgaard & Pedersen, 2005). Besides this reaction also Ti^{3+} might be oxidized to Ti^{4+}. Furthermore also Fe^{2+} diffuses to the fibre surface at elevated temperatures. This diffusion is inhibited if the

bulk crystallization of the fibres has started, and it does not take place if the fibres were pre-heated in air (Kirkegaard & Korsgaard, 2004). The oxidation process covers a wide temperature range: The onset of the mass increase can be observed by TG already at 500 °C (Figure 7) and the formation of the surface layer can be seen clearly by secondary neutral mass spectrometry at 640 °C. DSC measurements show an oxidation peak at 705 °C (Moesgaard & Pedersen, 2005) and finally at 1000 °C all the iron ions are in the ferrous state according to Mössbauer spectroscopy measurements (Figure 7) (Kirkegaard & Korsgaard, 2004):

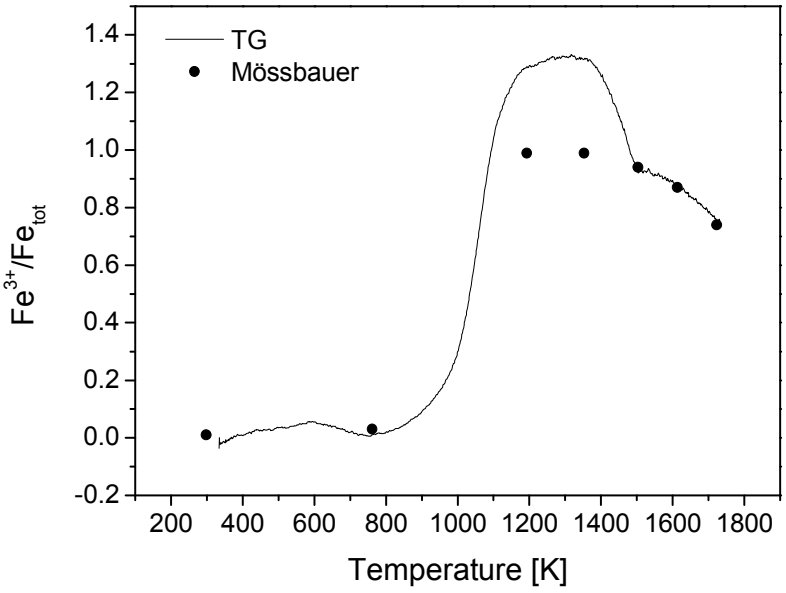

Figure 7: The degree of oxidation of HT stone wool fibres as a function of temperature (Kirkegaard & Korsgaard, 2004)

The oxidation process is not only a thermodynamic process it has also a kinetic dimension. Its dependence on temperature and time is shown in Figure 8:

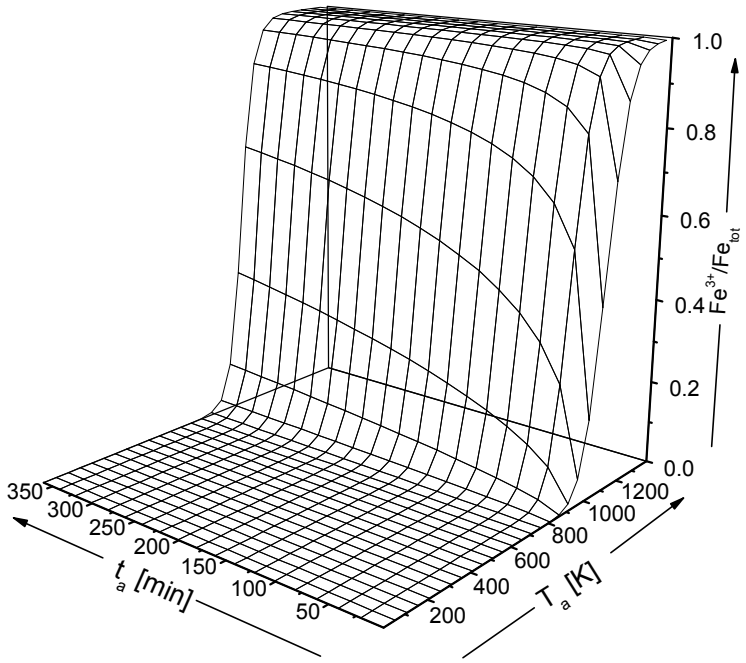

Figure 8: Degree of oxidation as a function of temperature (T_a) and duration (t_a) of the heat treatment (Kirkegaard & Korsgaard, 2004)

Apart from temperature and time of the heat also the heating rate has a certain influence on the oxidation. Although the increase in weight and therewith the oxidation rate does not increase with increasing heating rate, the oxidation temperature increases. Furthermore it is interesting to see that the maximum weight increase caused by oxidation of iron occurs at the same temperature as the onset of the crystallization (Kirkegaard & Korsgaard, 2004). This means that for rapid heating rates both processes occur simultaneous.

The oxidation of iron is associated with the formation of a nanocrystalline oxide layer: When the electrons are released from the iron ions, empty bonding points ("holes") remain in the fibre. New electrons fill these holes and leave other holes behind. A flux of positively charged holes from the surface to the oxidation front in the interior of the sample is the result. This flux is balanced by a flux of Ca^{2+} and Mg^{2+} ions onto the surface, where these ions form crystalline oxides (Moesgaard & Pedersen, 2005). Kirkegaard & Korsgaard (2004) identified the surface layer to be periclase (MgO) by XRD. They found by atomic force microscopy (AFM) that the width of the crystals varies between 200 and 300 nm and their height between 10 and 40 nm. However, Kirkegaard & Korsgaard (2004) discussed if also other crystal phases are constituents of the surface layer and interpreted differences in TG and Mössbauer measurements as a result of the oxidation of Ti^{3+} to Ti^{4+}. They also suggested the formation of

an iron rich surface layer might form. The divalent oxygen needed for the formation of the surface layer is produced by the incorporation of molecular oxygen from the atmosphere and the reduction hereof. Therefore it can be measured by thermogravimetry (TG). Parallel to the diffusion of divalent ions to the surface monovalent ions like Na^+ diffuse to the oxidation front. They charge balance the FeO_4^{5-} tetrahedra that form during the oxidation (Kirkegaard & Korsgaard, 2004).

One of the most important processes for the industrial use of stone wool is its contraction at elevated temperatures. In argon in the temperature range **between 775 °C and 850 °C** untreated stone wool starts fusing superficially (sintering) and shrinks therefore. The sintering temperature T_s increases with T_g: $T_s = 1.1\ T_g$. The sintering process begins in the interior of the sample and moves towards the surface. In the industrial application the sintering is not prevented by the formation of the surface layer, because during rapid heating both processes occur almost simultaneously (Kirkegaard & Korsgaard, 2004; Moesgaard & Pedersen, 2005). In air stone wool fibres show no sign of sintering until 1100 °C (Kirkegaard & Korsgaard, 2004). The authors think that they do not sinter up to the melting point at around 1200 °C. In contrast to this Rockwool International made the experience that it sinters at 1000 °C in air (personal information given by Dorthe Lybye, Rockwool International A/S).

Thermally treated stone wool behaves different. Here a nanocrystalline periclase layer has formed during the pre-heat treatment and protects the fibres form shrinking. The temperature up to which the contraction can be inhibited in argon depends on the pre-heat treatment. A pre-heat treatment for 30 minutes at 0.8 T_g increases the contraction temperature to between 800 and 900 °C, fibres pre-treated for 2 minutes at T_g do not show a significant contraction until 1050 °C and a pre-heat treatment at higher temperatures lifts the contraction temperature even to 1100 °C (Moesgaard & Pedersen, 2005). Since the iron ions play the main role in the formation of the surface layer, an iron content of 5 wt-% is necessary to maintain the shape and flexibility during pre-heat treatments under oxidizing conditions (Kirkegaard & Korsgaard, 2004).

2.2.2 Crystalline Phases in Thermally Treated Stone Wool

This chapter deals with the bulk crystallisation of stone wool fibres which takes place both in air and in argon at a temperature range **between 850 °C and 936 °C** (Moesgaard & Pedersen, 2005). The crystallization temperature increases with increasing heating rate because of the time needed for nucleation and crystal growth (Kirkegaard & Korsgaard, 2004). The identity of the minerals formed during the crystallization of stone wool is not completely clear. Typical crystalline phases which form above Tg in glasses are pseudowollastonite ($Ca[Si_2O_6]$), feldspars, mullit ($3\ Al_2O_3 \bullet 2\ SiO_2$), corundum ($Al_2O_3$), tridymite and crystobalite (both SiO_2) (Jørgensen et al., 1994).

The atmosphere of the heat treatment during which the crystallization occurs influences the mineralogical assemblage: If the crystallization takes place in **air** the mineralogical assemblage consists of plagioclase and a pyroxene like diopside ($CaMg[Si_2O_6]$). In this case the pyroxene crystallizes at 850 °C and the plagioclase at 920 °C (Burkhard, 2001). In contrast to this Pakosch (2006) and Kirkegaard & Korsgaard (2004) found pyroxene to be the only phase in air. Sørensen et al. (2005) found diopside as the major phase and traces of anorthite in some samples. Moesgaard & Pedersen (2005) observed two crystallization peaks in the DSC but only one crystalline phase, e.g. diopside, in the XRD. In an **argon** atmosphere only pyroxene crystallizes at a temperature of 936°C (Burkhard, 2001). In contrast to this Kirkegaard & Korsgaard (2004) found anorthite to be the dominant and diopside as a minor phase. Both authors used HT Rockwool® fibres. The atmosphere has also an influence on the crystallization speed. In argon the crystal growth is slower because the cation mobility is smaller due to the lower oxygen gradient (Kirkegaard & Korsgaard, 2004).

The mineralogical composition is also different, if the fibres have been subjected to a pre-heat treatment in air before: Kirkegaard & Korsgaard (2004) investigated the influence of the pre-heat treatment on the crystallization peaks for DSC measurements in **air**. They found that the peaks seem to unify for longer pre-heat treatments. The unification takes place the earlier the higher the temperature of the pre-heat treatment is and the peak shifts towards lower temperatures if the duration of the pre-heat treatment is increased. The last effect might be explained by the relaxation of the glass fibres which leads to a more crystal-like structure in which the energy needed to form crystals is lower. An interesting aspect is that they found three melting peaks in the DSC which are subscribed to three different crystal phases (Kirkegaard & Korsgaard, 2004). If the fibres pre-heated in air are heated again in **argon** the same mineralogical assemblage forms as for untreated fibres heated in air, e.g. only diopside

(Kirkegaard & Korsgaard, 2004). In contrast to this Sørensen et al. (2005) who analyzed oxidized glasses of the same composition as HT fibres found anorthite ($Ca[Al_2Si_2O_8]$) and akermanite ($Ca_2Mg[Si_2O_7]$) to form at the onset temperature of crystallization but only diopside at the crystallization peak temperature which suggest a phase transition. Akermanite is the end member of the melilite solid solution whose other end member is gehlenite ($Ca_2Al[AlSiO_7]$). All melilithes might contain some amount of iron and sodium (http://www.mineralienatlas.de/lexikon/index.php/Melilith). For the different results of the two authors there might be the explanation that Sørensen et al. (2005) examined bulk glass and Burkhard (2001) powdered glass, because diffusion processes are of greater importance in fibres than in bulk glass. After a pre-heat treatment for 44 hours and a continuous heat treatment in **air** up to 1100 °C at T_g Kirkegaard & Korsgaard (2004) found diopside as the only phase.

The pre-heat treatment influences not only the mineralogical composition of the crystalline phases but also their crystallization temperature and speed and their crystallinity. The longer the duration and the higher the temperature of the heat treatment are, the earlier (referring to the temperature) the crystallization starts, but the later it reaches its climax in the DSC measurement. This means that the crystallization interval in the DSC measurement increases with increasing duration of the heat treatment. The former effect could be due to the existence of more nuclei and therefore more crystallization sites after a longer heat treatment. The latter might be caused by the arising difficulties concerning the transport when the number of the components forming the crystals decreases (Moesgaard & Pedersen, 2005).

The chemical composition also influences the mineralogical composition: Higher amounts of Fe and Ti lead to the crystallization of Fe-Ti-oxides like ilmenite [$FeTiO_3$] simultaneously with the pyroxene (Burkhard, 2001). But the iron content does not only influence the mineralogical composition, but also the crystallization kinetics: Firstly the crystallization occurs the faster the higher the iron content of the fibres is. Secondly it depends on the redox state of the iron and therefore on the pre-heat treatment. Reduced glasses crystallize faster and at lower temperatures than oxidized glasses. For this behaviour several explanations are discussed. One approach is to consider the structure of the crystalline phases. Pyroxene minerals are the main host mineral for iron in crystallized stone wool fibres (Kirkegaard & Korsgaard, 2004) and Fe^{2+} fits better in the crystal structure of pyroxenes than Fe^{3+}. Another approach is to consider the glass structure. Here Fe^{2+} acts as a network modifier and is hence more mobile than Fe^{3+} as a network former. Furthermore the mobility of Mg^{2+} and Ca^{2+} is

reduced, if the network is strengthened by Fe^{3+} (Sørensen et al., 2005). The heating rate has no influence on the mineral assemblage formed: Slow heating up to 860°C or 910 °C leads to the formation of the same crystal phases as the fast heating up to the same temperatures. However, the crystallization increases, if the heating rate in the DSC analyses is decreased. This can be explained by an inhibition of the crystallization during rapid heating (Moesgaard & Pedersen, 2005). This effect might be caused by a lack of time for the formation of nuclei (Kirkegaard & Korsgaard, 2004).

The crystallization starts at the surface and spreads into the interior of the fibre, because the MgO layer forms a heterogeneous nucleus for the crystallization. The nucleation process is limited to a small temperature range so that a longer heat treatment above this range leads to bigger crystals, since no nuclei are formed after some time whereas crystal growth continues. Shortly after the beginning of the crystallization process the crystallization becomes faster, because apart from the formation of new nuclei the growth of already existing nuclei contributes to the process. After 2000 s the crystallization becomes slower again, because the diffusion of the atoms taking part in the crystallization decreases, since fewer and fewer atoms are available for the diffusion. Additionally the ratio between those atoms taking part in the crystallization and those which remain in the glass network becomes less advantageous. The crystallization of stone wool is therefore a diffusion-controlled process (Moesgaard & Pedersen, 2005).

3 Procedures and Design

Starting from the facts given in chapter 2 an experimental design was developed to answer the questions given in the abstract. Before this thesis no quantitative analyses of systematically heat-treated stone wool were performed. Hence the idea of this work is to investigate the dependencies of the mineralogical composition on a two-step heat treatment. The first heat treatment (pre-heat treatment) in the glass transition range is used to increase the shape stability of stone wool fibres (Kirkegaard & Korsgaard, 2004), the second heat treatment serves as a simulation of the application of stone wool under high temperatures. The changes induced in the material during both heat treatments are observed by microscopic, thermoanalytic and diffraction methods. Figure 9 summarizes the experimental design which is explained in this chapter:

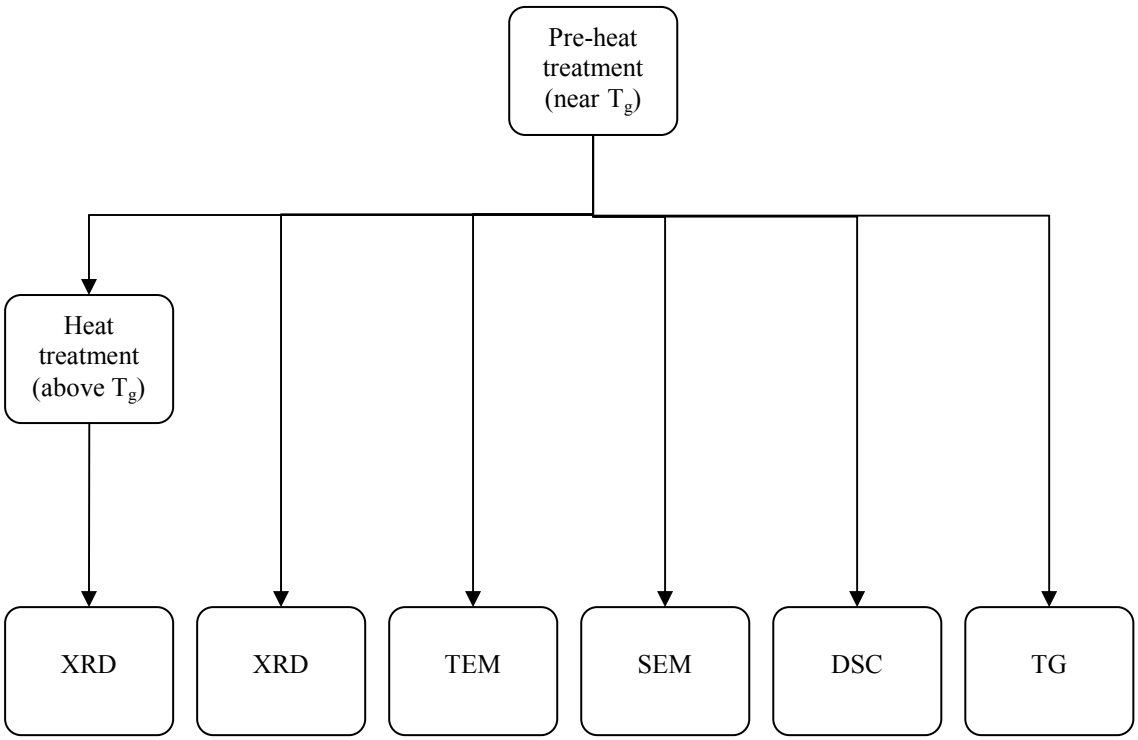

Figure 9: Experimental Design

Before the experiments shown in Figure 9 were performed the HT Rockwool© fibres were sieved to a particle size < 63 µm to remove the droplets that change the size distribution of the fibres. Later the droplets, a black residual, were analyzed with XRD and found to be completely amorphous like the rest of the fibres. However, since no chemical analyses of both fractions were performed, it remains unclear, which differences exist between both fractions. This approach is according to the previous work performed at the section of chemistry at Aalborg University; hence the results are comparable. On the other hand they might differ

from the results that would be produced using all the fractions and that would be closer to the behaviour of "complete" stone wool in reality.

3.1 Thermal Treatments

3.1.1 Pre-heat Treatment

For the heat treatment a Scandia Ovnen K10 with a current of 10 Ampere, a power of 2.1 kW and a heating rate of 10 °C per minute was used. For the temperature measurement a Bentrup Thermocomputer TC 507 was applied. For each heat treatment 4 g stone wool fibres were heated in platinum crucibles. The pre-heat treatment was performed according to the following scheme where all temperatures are multiples of T_g which was determined to be 684 °C (chapter 4.2). The multiples refer to values in K and were converted afterwards into °C:

Table 2: Variations of the pre-heat treatment conditions

	0.8 • T_g = 493 °C	0.9 • T_g = 588 °C	1.0 • T_g = 684 °C	1.1 • T_g = 780 °C	1.2 • T_g = 875 °C
10 min			x		
30 min			x		
60 min	x	x (only 0.5 g for DSC)	x	x (only 0.5 g for DSC)	x

3.1.2 Heat Treatment

The heat treatment in the furnace was performed both in air and in a reducing atmosphere (90 % N_2 + 10 % H_2). The treatment in air was conducted in the same furnace which had been used for the pre-heat treatment according to Table 3.

Table 3: Variations of the heat treatment in air

	1.2 • T_g = 875 °C	1.25 • T_g = 923 °C	1.3 • T_g = 971 °C
10 min			x
30 min			x
60 min	x	x	x

The heat treatment for 60 min at 971 °C was conducted for all the samples, the other variations were only chosen for the sample pre-heated for 60 min at 684 °C. The heat treatment in a reducing atmosphere was performed in a self-made furnace by Ass.-Prof. Ralf Keding. The sample was put into the cold furnace; afterwards the furnace was evacuated and heated. The time given in Table 4 is the standing time at the elevated temperature. Afterwards the furnace was cooled down and the sample was removed. The real temperature was about 20 °C lower than the thermo couple showed according to experiences in the Section of Chemistry of Aalborg University. Therefore the temperature was chosen always 20 °C higher than it should be according to the experimental design. In the reducing atmosphere an alumina shuttle was used as a crucible. The heat treatment in a reducing atmosphere was only conducted for the samples pre-heated for 60 min at 684 °C and according to the Figure 5:

Table 4: Variations of the heat treatment in a reducing atmosphere

	1.2 T_g = 875 °C	1.25 T_g = 923 °C	1.3 T_g = 971 °C
6 min			x
30 min			x
60 min	x	x	x

The names given to the samples result from the two heat treatments: A sample with the code 684-60-971-60 has been heated in the pre-heat treatment for 60 min at 684 °C and in the main heat treatment for 60 min at 971 °C. Samples marked with “H” at the end were heated in a reducing atmosphere. Two samples with different amounts of FeO (white and mixed fibre, Table 1) were heated only in one-stage treatment for 60 minutes at 884°C.

3.2 Microscopy

Microscopic methods were used ton investigate the surface crystallization that occurs during the pre-heat treatment according to Kirkegaard & Korsgaard (2004). Since the size of these particles is too small (< 300 nm, Kirkegaard & Korsgaard, 2004) for light microscopy (resolution 1 µm, Wenk, 1976; 200 nm, Becker et al., 2003) electron microscopy was applied. The theoretical basis is given in the Appendix.

3.2.1 Scanning Electron Microscopy (SEM)

In this work five samples (untreated, 493-60, 684-10, 684-30, 684-60, 875-60) were selected for these measurements. It was expected that the sample pre-heated at 493 °C would show the beginning of the formation of the surface layer, that the samples pre-heated at 684 °C would illustrate its development and the sample pre-heated at 875 °C would visualize its final stadium. This development was expected to be expressed in an increase in thickness and an enrichment in Mg and maybe also in Ca and Fe at the surface. The former should be analyzed by SEM-SE and the latter by SEM-EDX. The sample was prepared for SEM analyses in two different ways. For a first series a small amount of fibres was stuck on a carbon tape without any further preparation. For a second series the fibres were embedded into epoxy resin at the Department of Mechanical Engeneering at Aalborg University and polished afterwards using a Struers LaboPol-5. The polishing was started with coarse grained sand paper (type 220), afterwards the grain size was decreased step by step until type 4000. Each sample was polished for five minutes with each type of sand paper (220, 500, 1000 and 2400). The measurements were performed in the Department of Nanotechnology of Aalborg University with a Zeiss 1540 XB microscope using the field emission canon Gemini. A low acceleration voltage of 2 kV was chosen to avoid charging of the samples which had not been coated before because the coating covered all useful features of the surface (Figure 12). The working distance was set initially at 3 mm, afterwards it was reduced until the resolution was optimal. A focused ion beam (FIB) with gallium ions and an ion current of 1 nA was tried to use to create a cross section through a fibre.

3.2.2 Transmission Electron Microscopy (TEM)

The fibres which had been investigated by SEM should also be analyzed by TEM in Risø National Laboratory. Therefore the samples embedded in eposy resin were used for further sample preparation. The preparation caused some problems because the epoxy was to rubbery. Therefore no TEM results could be won.

3.3 Thermonalysis

In this work a Netzsch STA 449C was used. STA stands for simultaneous thermal analyses and refers to a combination of DSC and TG. The measurements were performed in the following way: First the measuring parameters were set: For the DSC program a starting temperature of 60 °C was chosen. Then the temperature was increased with a rate of 20 °C /

min up to 1050 °C. For the cooling process the same rate was used. The purge gas flow accounted for 40 mL/min, the protection gas flow for 18 mL/min. Then two empty platinum crucibles were measured to determine the zeroline. After the crucibles were placed in the DSC and the apparatus was closed, it was waited for several minutes until the mass signal remained constant. Then the measurement was started and the zeroline was determined. In a second step a sapphire standard was placed into the sample crucible, the file of the zeroline was opened and the standard was measured. Finally the samples were measured. Also in this case the file of the zeroline was opened before. Each sample was weighed out before it was put into the DSC. The measurements were carried out twice for each sample to check the repeatability. After the measurement the files of the sapphire standard and the measured sample were opened. The TG signal was smoothed by the factor 8 and the DSC signal was converted into the specific heat capacity. After each measurement the sample was removed from the crucible with a pincer than the crucible was used again.

3.4 X-ray Diffraction (XRD)

To identify and quantify the minerals that formed during a heat treatment according to the DSC results (chapter 4.2.3) X-ray diffraction (XRD) was used at Freiberg University of Mining and Technology. XRD analyses need very fine grained material; hence a McCrone mill was used to crush the fibres. Since this kind of mill has not been used before for stone wool, it was tested if the necessary median of the grain size of 8 µm could be reached also for fibres. Therefore the grain size distribution of the grinded fibres was determined with a SympaTec Helos KF laser granulometer. Since the grindability depends on the brittleness of a material and since this brittleness is different for crystalline and non-crystalline solids two samples were chosen for this measurement. The crystallinity should increase with the temperature of the heat treatment: Therefore one sample with the lowest temperature in the second heat treatment (875 °C) and one with the highest temperature (continuous heating up to 1100 °C) were chosen. Furthermore also samples which have been subjected only to a pre-heat treatment were analyzed by XRD to check if the surface crystals account for a measurable volume percentage. The fundamentals of this standard method for phase analysis are given in the appendix. In this work the XRD analyses were performed at the Institute of Mineralogy at Freiberg University of Mining and Technology. The fibres used for the XRD measurements were weight out exactly and 10 % (referred to the overall weight) of an external standard, ZnO, were added to every sample. The X-ray diffraction analyses were conducted with a URD-6 produced by the company Seifert and the Freiberger

Präzisionsmechanik GmbH. A Co tube was used to create the X-rays. The parameters of the measurement are listed in Table 5:

Table 5: Parameters for XRD measurements

Parameter	Setting
wavelength	CoKα = 1.78901 Å
scan axis	2:1, symmetrical constant area
mode	stepscan
range	5 – 80 °
step	0.03 °
constant area	15 x 15 mm
counting time per step	5 s
sample holder	steel, diameter 26 mm, depth 0.6-2.5 mm
total measuring time	3:28:25

The angle range was chosen smaller (< 80° instead < 145°) and the step size are larger (0.03° instead of 0.02° than the suggested by Allmann (2003), the measuring time per step (=time between the signals) lies in the range given there. Therefore the measuring time is only a third of that resulting from Allmann (2003). This decision was made to be able to analyze more samples in the same time and because the weak peaks at large angles are not used for phase quantification whereas Allmann (2003) suggests his parameters for a structure refinement. The first step of data evaluation was the determination of the background by hand with an extrapolated line using between five and ten staging points. A $K\alpha_2$ correction was not conducted. The identification of the crystalline phases was done with the program ANALYZE. It was begun with an automatic peaksearch where each phase with at least three peaks in the diffraction pattern was shown. The sensitivity index was set on “2”. In a second step additional peaks were added manually. The program compares the peak positions of the measurement with those of the powder diffraction file (PDF) from the International Centre for Diffraction Data (ICDD) and suggests dozens of suitable phases. The decision for a certain phase was made according to the fit of the peak position and the chemical composition of the phases. These structural models for these phases were used as a starting model for the Rietveld refinement. Among the parameters which were refined in this thesis are the

occupation factors for the variable lattice positions of the phases which were solid solutions and the microstrain which results from a change of the lattice parameters within one crystal due to a chemical zonation. During the refinement process the differential plots and the development of the residuals were observed on the monitor. When there were no significant deviations in the differential plot any more the refinement was stopped. The final differential plots which are shown in the appendix of this thesis for each diffraction pattern.

4 Results

This chapter deals with the findings of this work. They are presented in three parts. In the first part the results from SEM-SE and TEM measurements are presented. The second part summarizes the TG, SEM-EDX, TEM-EDX and DSC results giving information about oxidation and crystallization. In the third part the findings from the XRD measurements are given.

4.1 Morphological Changes

The shape of stone wool fibres changes during a thermal treatment. In this section the processes of shrinking (4.1.1) and surface crystallization (chapter 4.1.2) are described.

4.1.1 Macroscopic Observations

Photos were taken from the fibres removed from heat treatments and DSC measurement to show the effects of a thermal treatment on the shape stability of stone wool. Figure 10 shows that even pre-heated fibres shrink and become black after a heat treatment in a reducing atmosphere.

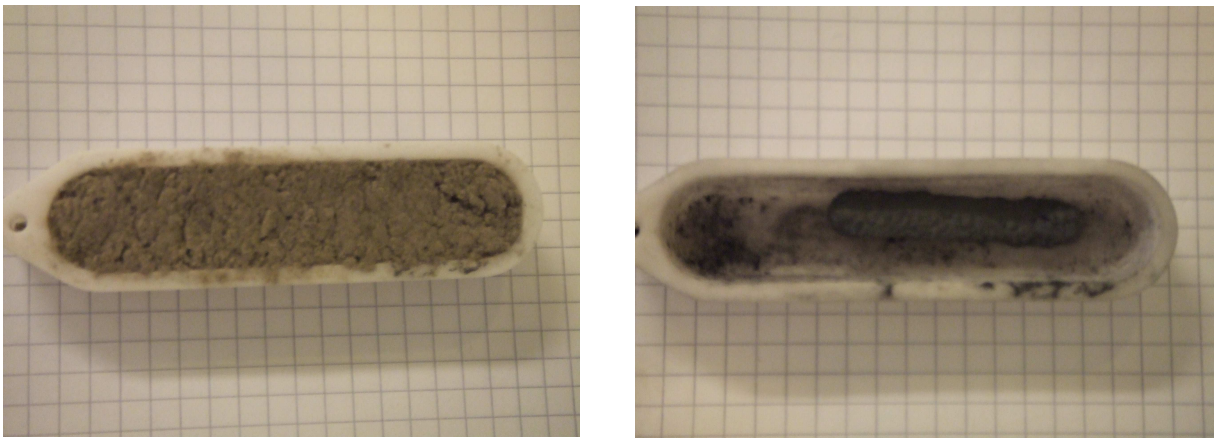

Figure 10: Stone wool after a 60 minutes heat treatment at 971 °C in air (left) and in 90 % N_2 + 10 % H_2 (right) and a 60 minutes pre-heat treatment at 684 °C

Figure 11 shows samples which have been subjected to a DSC measurement up to 1050 °C. It can be seen that the untreated fibres shrink and become black in argon (centre), but not in air (right). The shrinkage is a bit less drastic than in a reducing atmosphere (Figure 10). Fibres which have been pre-heated in air (60 minutes, 684 °C) shrink less and become less black (left) than untreated fibres (centre). It might be concluded that the surface crystals prevent the sintering of the glass, but that this effect is limited to a certain range of oxygen fugacity.

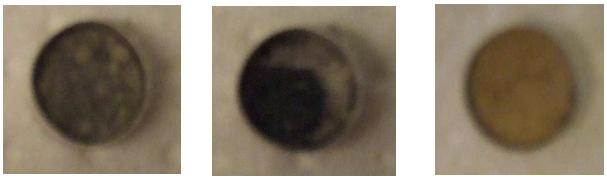

Figure 11: Pre-heated (left) and untreated fibres (centre and right) after DSC measurements in argon (left and centre) and air (right)

4.1.2 Microscopic Observations

Two electron microscopic methods, scanning and transmission electron microscopy (SEM and TEM, respectively) were used to investigate the character of the surface crystallization which takes place during the pre-heat treatment. In **SEM** analyses the secondary electron (SE) picture was used because of his better spatial resolution compared with the backscattered electron (BSE) image.

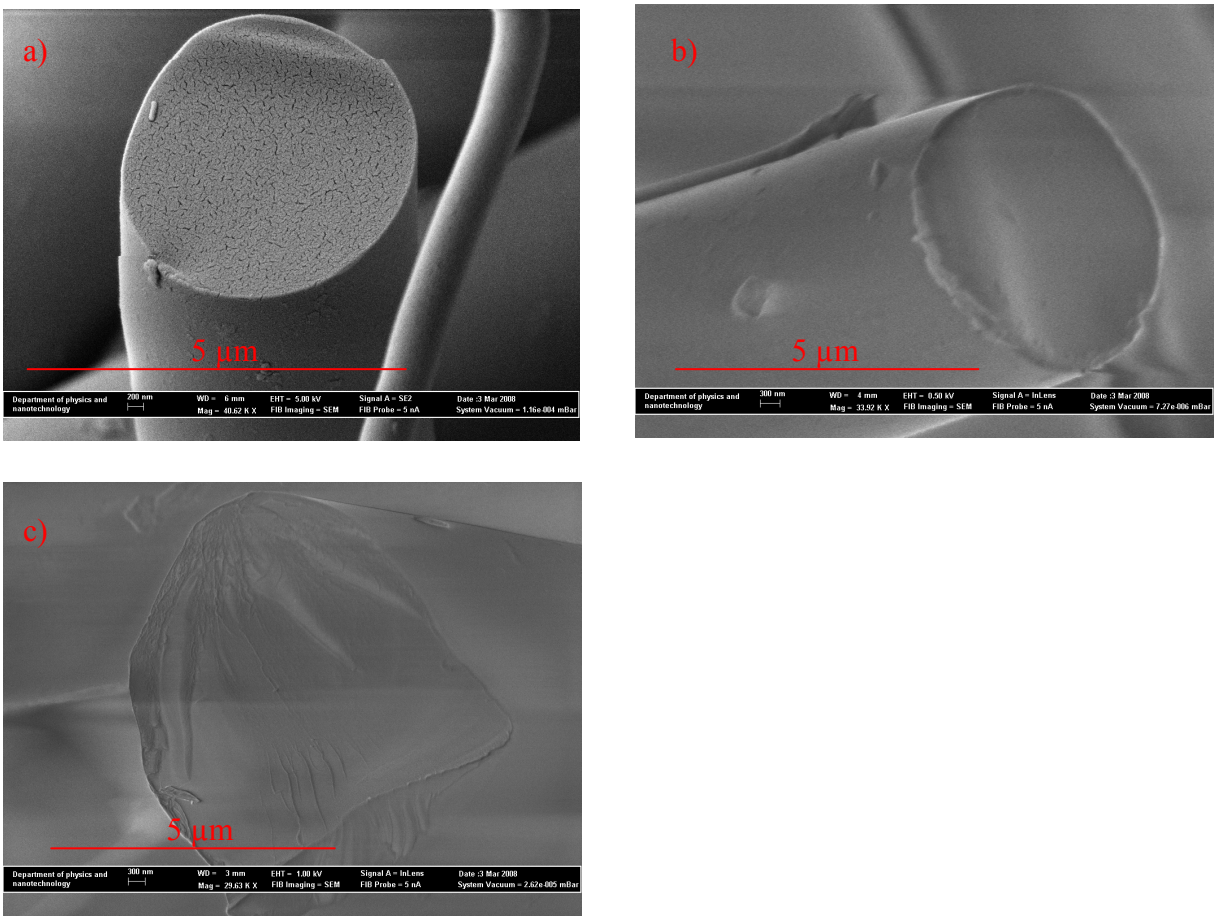

Figure 12: SEM-SE pictures of untreated stone wool fibres

Fig. 14a shows a fibre coated with gold. The surface structure of the gold makes it impossible to obtain any information about surface crystallization. Therefore the further measurements were performed without coating. The disadvantage of this procedure was that the fibres

became electrically charged and moved therefore while the pictures were taken. Hence all the following pictures lack sharpness. Fig. 14b shows an end of a fibre. On the edge there are excrescences which should result from the production process or from the sieving process because nothing else was done with the fibres. A fracture during sieving might look like this picture when the surface of the fibre has a different strength than the interior. Such a difference in strength might result from the different cooling rates between the interior and the surface during the production process. It has been observed by Rueda et al (2002) that the hardness of a glassy polymer decreases with increasing cooling rate. Glass fibres are cooled during the production by the air around them. Hence they cool faster there. If the results from Rueda et al. (2002) are transferable from the hardness of a polymer to the strength of stone wool the hardness should be lower at the surface than in the interior. Fig. 14c shows another end surface of the fibre which shows no excrescences. Instead of this the fracture plain is very irregular which is typical for amorphous materials. Considering the excrescences in the second picture as amorphous there are no surface crystals in untreated stone wool fibres.

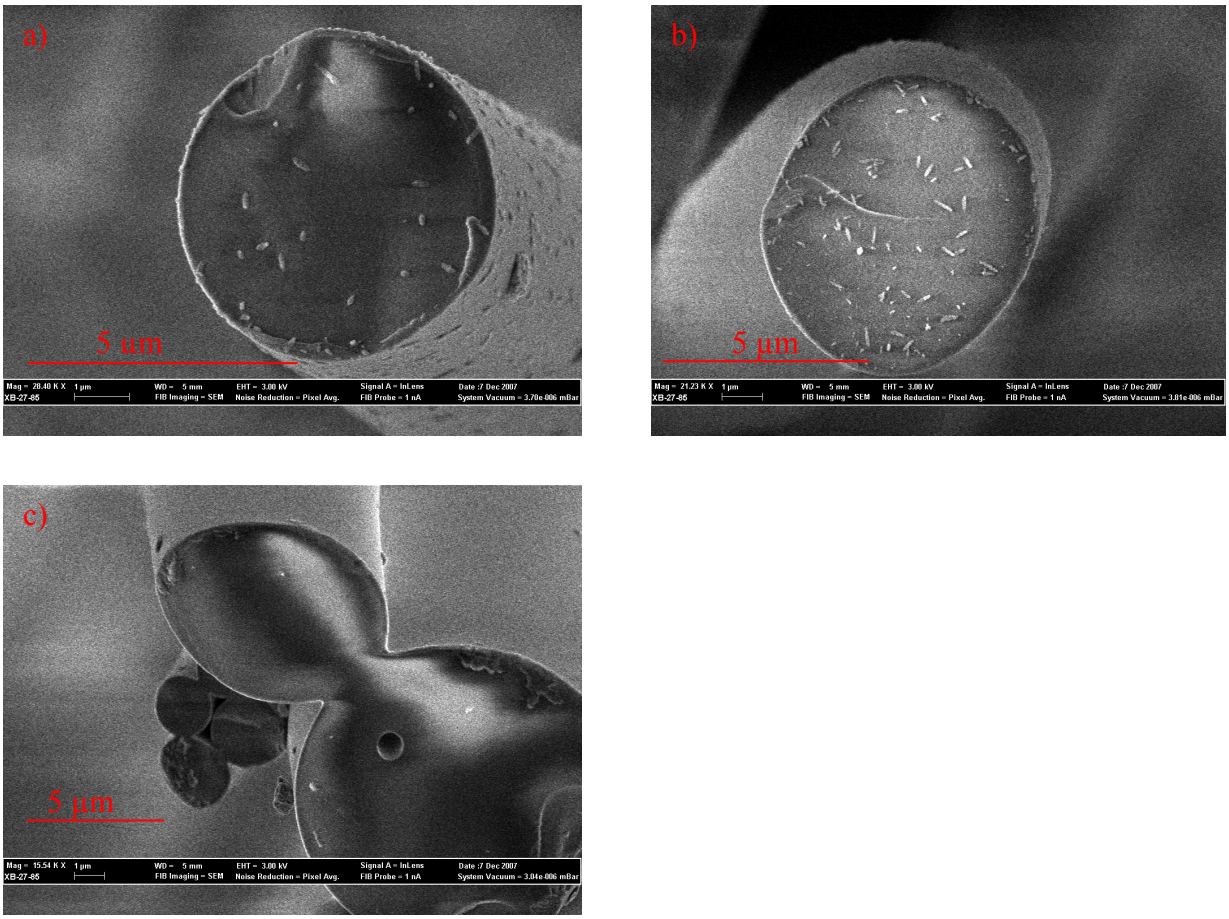

Figure 13: SEM-SE pictures of stone wool fibres pre-heated for 60 min at 493 °C

After a pre-heat treatment at 0.8 T_g (Figure 13) both the end and the mantel surfaces of the fibres are covered by white particles with a length between 100 and 500 nm and a width of few nm. It remains unclear what these particles are. Their large size, their formation at only 0.8 Tg and their non-isometric shape make it seem doubtful that these particles are crystals. Furthermore it cannot be seen in the pictures that any of these white particles penetrates the fibre, although this should be the case when a crystal grows on the surface. The white particles look more as if they were only loosely bonded to the surface or just lie on it. Furthermore the rod-shaped appearance is typical for bacteria. XRD analyses (chapter 4.3) showed that the fibres remain completely amorphous after a pre-heat treatment at 493 °C. Hence it seems not probable that the white particles are crystals. It remains unclear if there is already surface crystallization on the nanoscale because the spatial resolution of SEM-SE pictures is too low. It is interesting to see that the number of white particles varies a lot between the pictures, that there are more particles on the cylindrical surface than on the end surface in the picture top left and that the colour difference between the mantel and the end surface is the largest for the lowest particle density. The white edge can be interpreted as the so-called edge effect in secondary electron (SE) pictures. This is a topographical effect and is not connected to the surface crystallization or a change in the chemical composition. In the lower picture excrescences can be seen at the rim of the fibres which have been interpreted before as a result from different cooling rates during production.

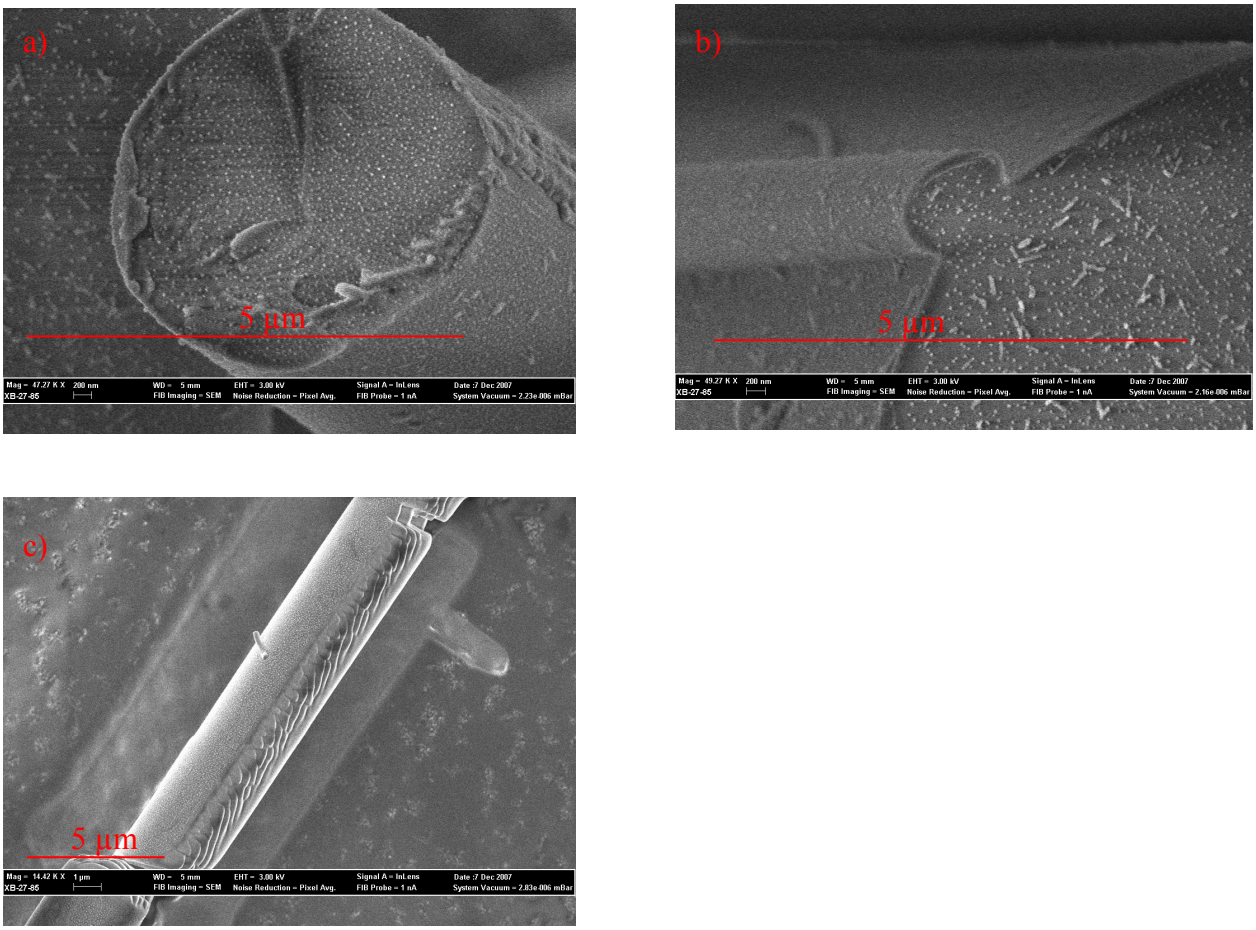

Figure 14: SE picture of stone wool pre-heated for 10 min at 684 °C

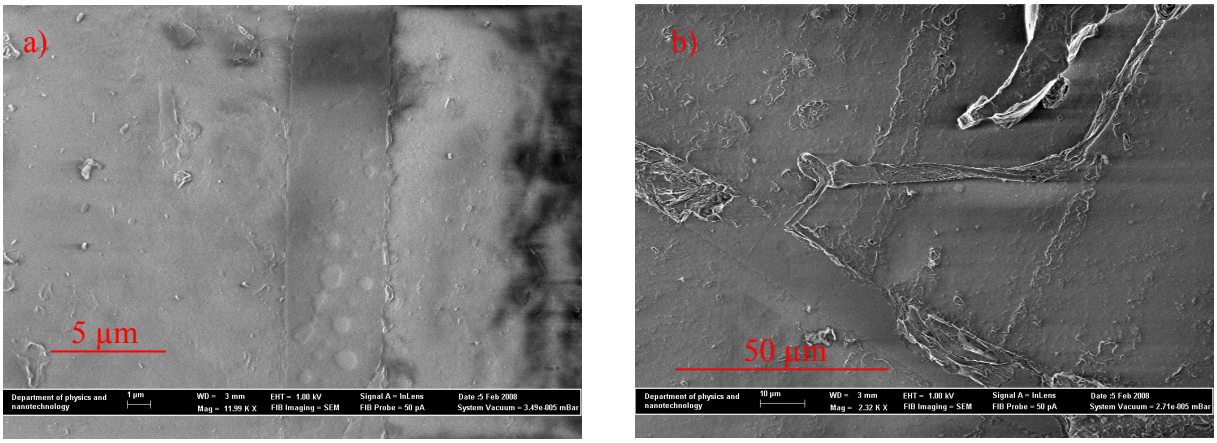

Figure 15: SE pictures of stone wool pre-heated for 10 min at 684 °C and embedded into epoxy resin

In the first two pictures (Fig. 16a+b) it can be seen clearly that after a pre-heat treatment at 684 °C besides the long particles known from the "colder" pre-heat treatments also isometric particles form. They have a size of approximately only 20 to 50 nm. Their shape might be a hint that they belong to the cubic crystal system. These white particles might indeed be crystals, because they are small and isometric which is typical for initial stages of crystal growth and because they are distributed regularly above the surface. Furthermore this sample

was subjected to a pre-heat treatment at T_g, this means that the crystals formed from an undercooled melt and not from a glass in the closer sense. Hence here crystallization is in agreement with the thermodynamic rule that glasses do not crystallize whereas undercooled melts do (chapter 2.1.3). Fig. 16c shows a fibre whose left side consists of rolls that are orientated parallel to each other and separated sharply from the rest of the fibres which are covered by small white particles. The rolls might be a part of the surface layer that grew faster than its other parts. Since faster growth needs higher temperatures, it might be possible that this part of the fibre had direct contact with the platinum crucible during heating and was heated therefore stronger than the rest of the sample. In the upper part of the fibre there is a notch with a width of about 750 nm. The notch is caused by a focused ion beam (FIB) used for producing a cross section along which the chemical composition could be measured. The pictures of the embedded fibres allow a look into the interior of the fibres. Fig. 17a shows circular shapes within a length section through a fibre. These shapes might be hollows which could have developed when the freezing melt was sprayed in the air flow (chapter 2.2.1). Fig. 17b shows a part of the fibre that has broken away from it, probably during the polishing process.

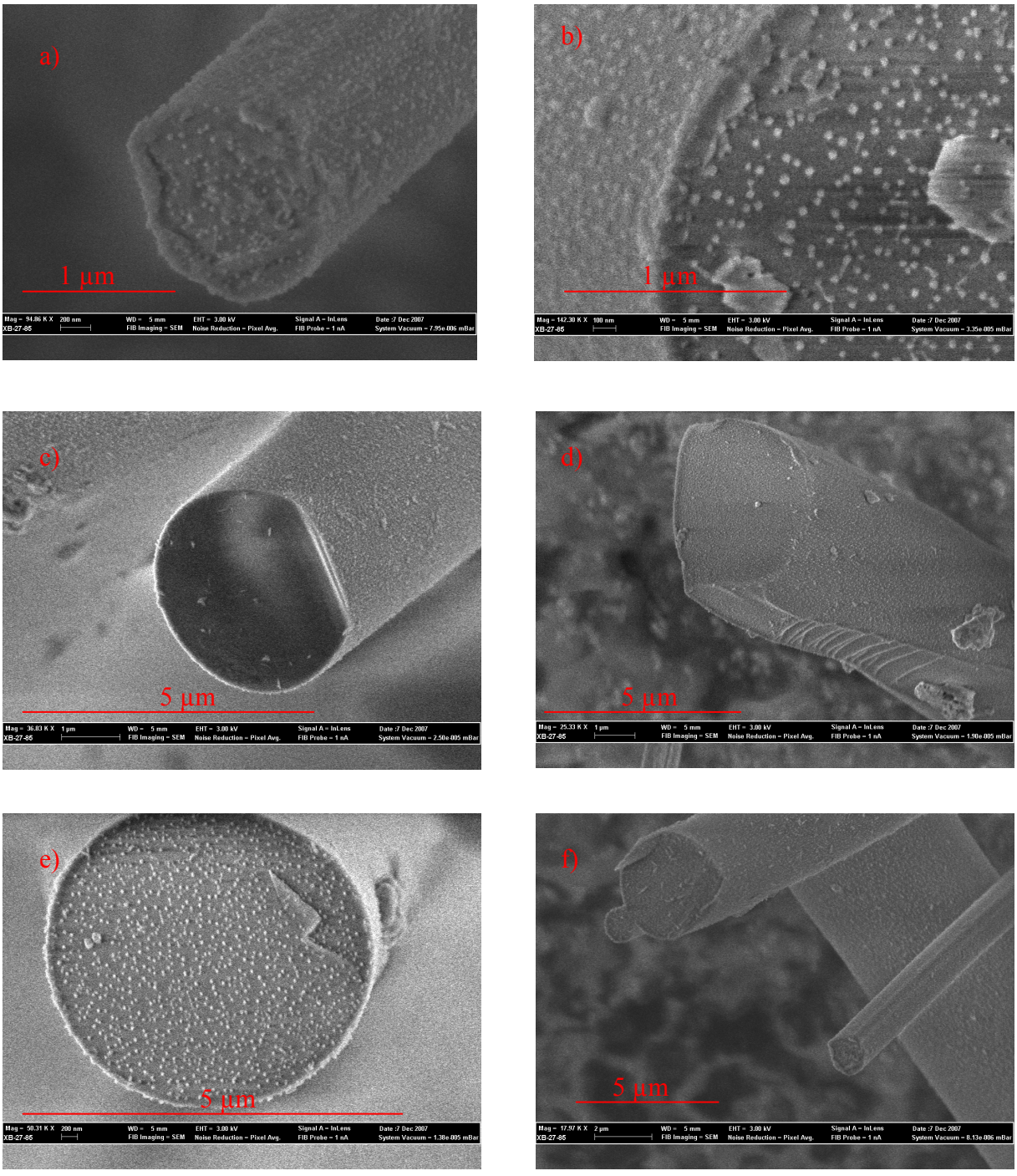

Figure 16: SE pictures of stone wool pre-heated for 30 min at 684 °C

Figure 16 shows that there are large similarities between the results of pre-heat treatments of 10 and 30 minutes. In both cases there are small isometric crystals, their number is in the same range, only the size might be a bit larger. This might mean that crystal growth continues, but nucleation does not. The excrescences in Fig. 18a are more pronounced than for shorter and colder pre-heat treatments. Hence they probably cannot be interpreted any more as effects

of the production. It seems possible that the relaxation of the fibres in connection with the shape stability of the surface layer might lead to the formation of the excrescences (Figure 17):

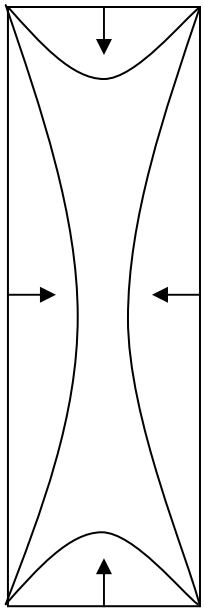

Figure 17: Explanation model for the growth of excrescences during the pre-heat treatment

The idea is that the edges of the fibres are mechanically more stable than the surfaces. This could be true if the crystal density there is higher, but this cannot be seen in the pictures because such a feature would be outshined by the edge effect. There are larger particles in the Fig. 18b on the fracture might be surface flatness imperfections. They do not seem to be dirt because there are surface crystals on them. The end surface in the Fig. 18c might be a fracture that occurred after the pre-heat treatment because the difference in colour is much more intense than in the other pictures and because the density of the white particles is so different. The light effect on this end surface is caused by charging whereas the effect on the edges is topographical. The stair-like structure which can be seen in Fig. 18d at the lower side of the fibre might be interpreted as a result of an abrasion process caused by another fibre. The concave shape might result from the convex formed other fibre which was harder than this fibre. A different hardness of two fibres could result from different strong surface layers which might be caused by the inhomogeneous heat distribution within the sample during the pre-heat treatment. The large particles (1 µm) sticking on the surface seem to be dirt. Fig. 18f contains a lightning-like shape which might result from a fracture which occurred along weakness zones within the fibre, perhaps zones with a different glass structure. The difference in the colour of the fracture and the other surfaces results from topographical effects. The

assemblage of fibres in Fig. 18f is characterized by long white particles of several hundreds µm length which cover both the ends and the other surfaces of the fibres. They are similar as the particles in the sample 493-60, but in this picture they are not so bright. However, shape and size are in the same range. Hence they might also be bacteria.

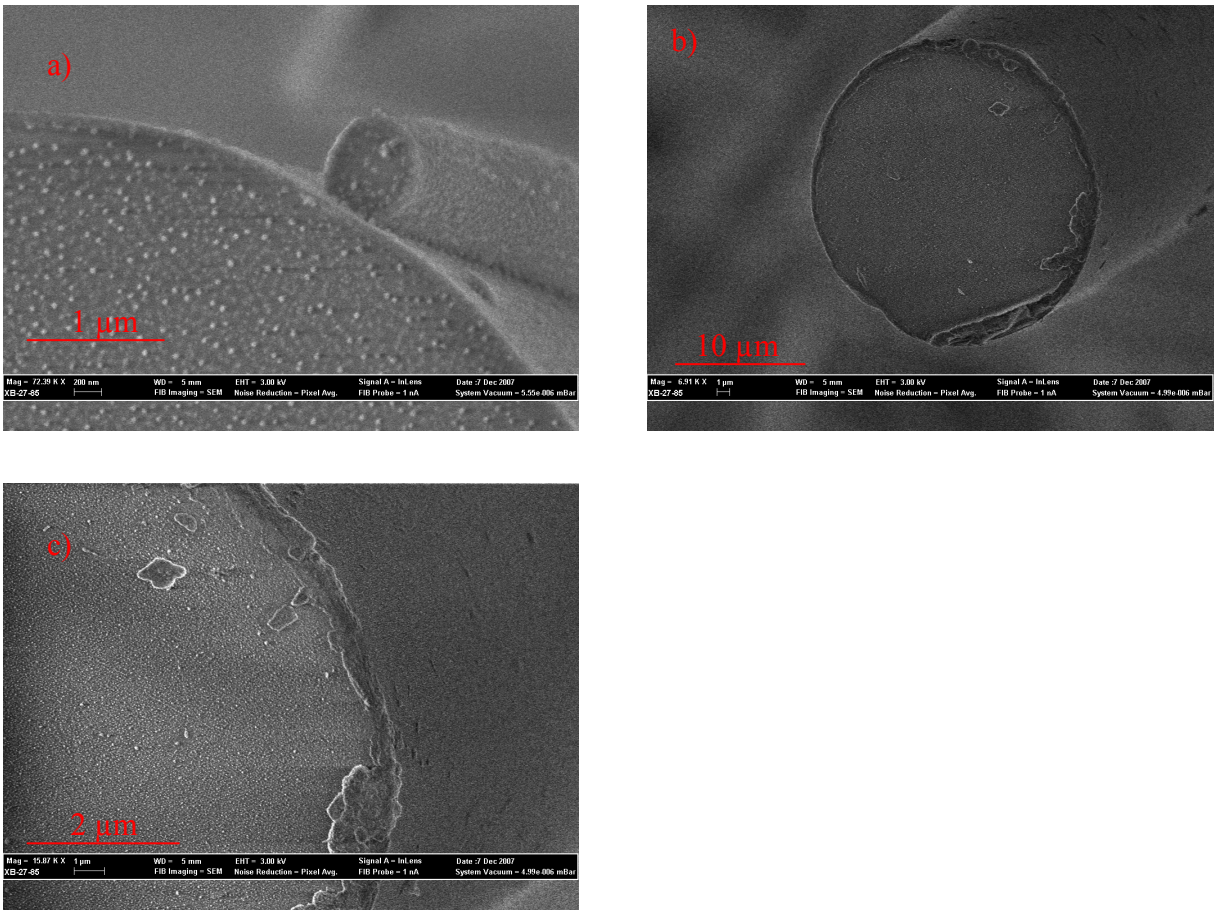

Figure 18: SE pictures of stone wool pre-heated for 60 min at 684 °C

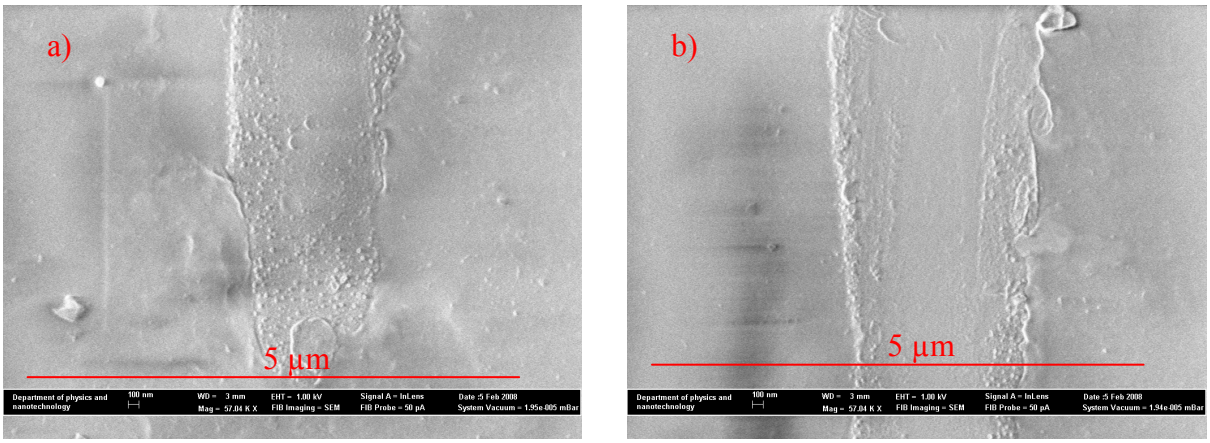

Figure 19: Inclined sections of a stone wool fibre pre-heated for 60 min at 684 °C and embedded into epoxy resin

Figure 18 shows that a prolongation of the pre-heat treatment has no further effects. Number and size of the crystals are in the same range as for shorter pre-heat treatments at the same temperature. The excrescences on the edge of the fibre in the Fig. 20 b and c are more than 1 µm large and distributed randomly at the edge. The former fact results from the longer pre-heat treatment which might have led to stronger relaxation (Figure 18) whereas the latter might be explained by inhomogeneous shrinking. This might result from a inhomogeneous heat distribution in the samples and / or from an inhomogeneous chemical composition since the production. The pictures of the samples embedded in epoxy resin (Figure 19) show a length section and an inclined length section of a fibre, respectively. Fig. 21a shows clearly that the crystals cover only the surface, because only the area where the fibre “dives” into the epoxy in the lower part of the picture, is covered by crystals: Here the surface can be seen. More upwards in the picture the length section penetrates the fibre deeper and it seems as if the crystals were ousted to the rim of the fibres. In Fig. 21b such a situation can be observed: Only at the rims of the length section the surface is cut and the crystals can be seen. These pictures prove that there is in fact only a surface and no bulk crystallization. This is in agreement with XRD results showing no crystalline phases after pre-heat treatment of 60 minutes at T_g which results from the small volume percentage of the surface crystals (chapter 4.3.2).

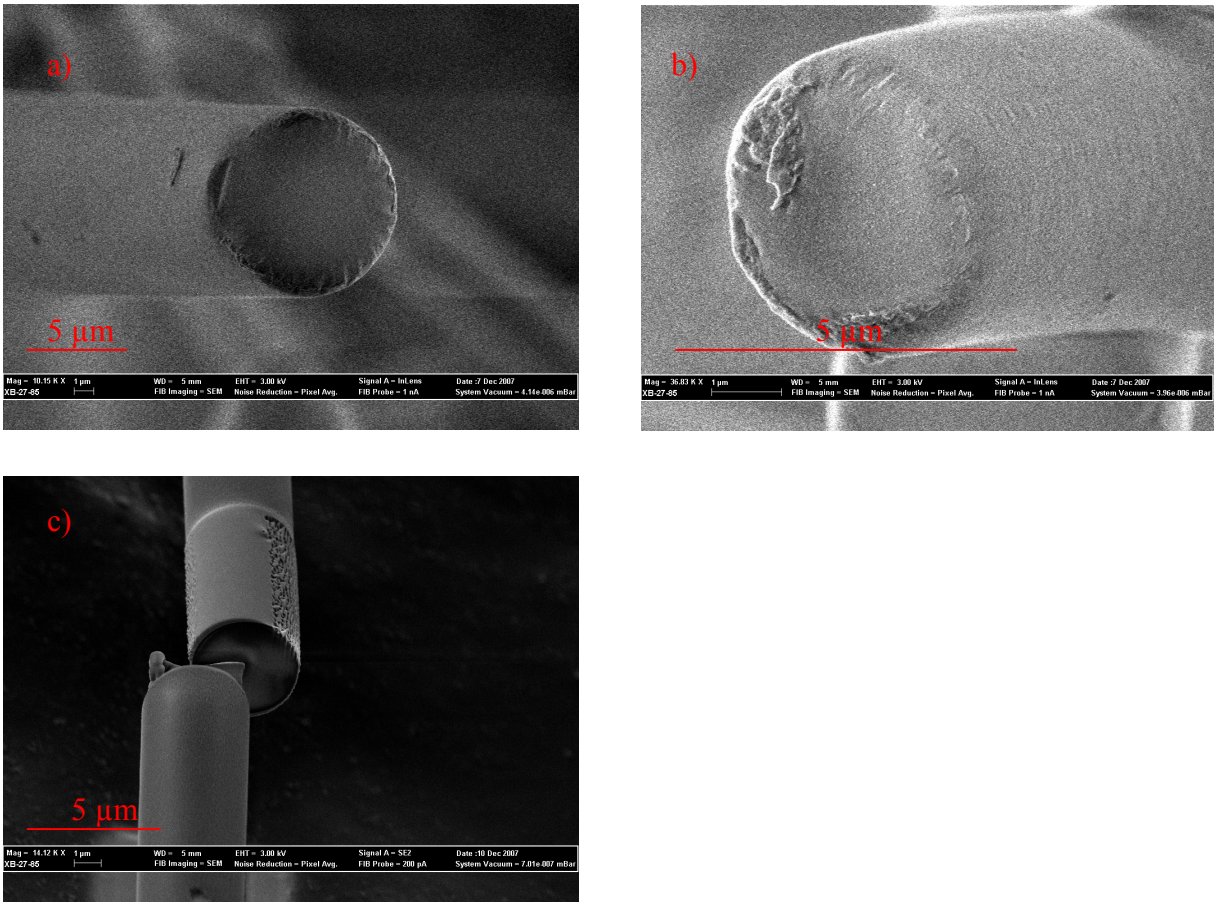

Figure 20: SE pictures of stone wool fibres pre-heated for 60 min at 875 °C

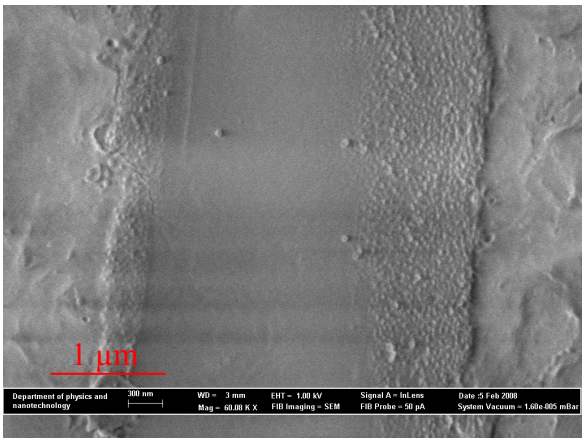

Figure 21: Inclined section of a stone wool fibre pre-heated for 60 min at 875 °C and embedded in epoxy resin

After a pre-heat treatment at 875 °C the fibres are characterized by rounded shapes. The sharp edges visible at the fibres pre-treated at lower temperatures disappeared. This can be seen as a result from sintering of the fibres. The fibres melted superficially and the melt solidified again thereby minimizing the surface energy by forming a smoother surface. The excrescences which can be seen in the second picture (top right) formed before the sintering process. This can be concluded from the fact that the fibres pre-heated at lower temperatures also show this feature. The growth of the excrescences continued during the sintering because they show a

fine-structured surface. If the growth had stopped, the partly melting would have rounded them, too. In the third picture (bottom left) there is a cut through a fibre which probably results from the focused ion bean (FIB) which was used to receive a cross section of the fibre for chemical analyses with SEM-EDX (chapter 4.2.1). The cutting plane is darker than the other surfaces which might result from the fact that it was produced after the pre-heat treatment. Hence this might be a real cross section which proves that in the interior there are no crystals. This hypothesis is confirmed by the picture of the embedded fibre (Figure 21) which shows a length section in whose interior there are no crystals visible. The surfaces in the third picture in Figure 20 are partly even and partly full of pores whose origin remains unclear. Both regions are separated sharply and occur only in a part of the fibre which is thinner than the rest of the fibre.

TEM measurements shall still be performed at the Risø National Laboratory. The only results obtained until know just confirm that the crystals only grow on the surface.

4.2 Chemical Changes

In order to develop an experimental design (chapter 3.1) for the heat treatments the glass transition temperature, T_g, was determined. Afterwards multiples of T_g were used as temperatures for the heat treatments.

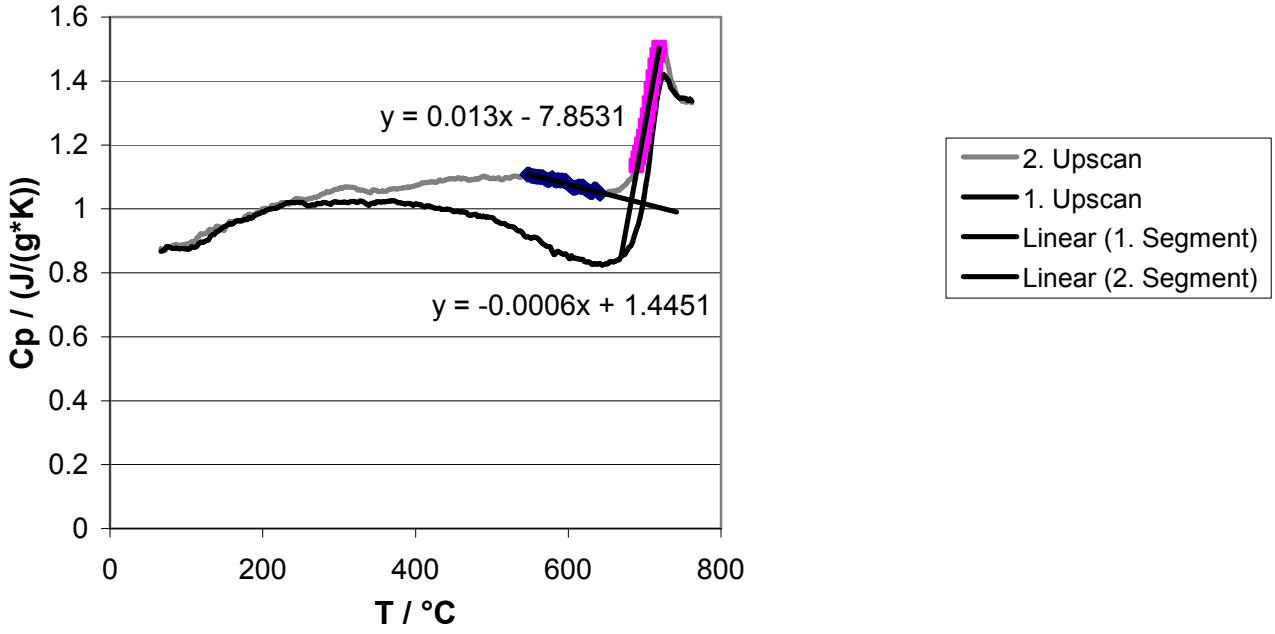

Figure 22: Determination of T_g, heating rate 20 °C/min

During the first upscan the heat capacity rises slowly until it reaches a maximum at 372 °C. Then it decreases as a result of the release of energy stored in the fibres during their production until a minimum at 649 °C which is followed by a steep increase in the glass transition range to a maximum at 729 °C. Shortly after this maximum the measurement was concluded and the sample was cooled down to room temperature. In the second upscan the first maximum is shifted to 552 °C, but both the following minimum (647 °C) and the maximum (724 °C) remain almost at the same temperature. The heat capacity in the second upscan is almost always higher as in the first upscan because less energy is released any more. Two linear approximations were performed for the segments between 546 °C and 642 °C and between 689 °C and 720 °C in the second upscan. The intersection between both lines is the glass transition temperature T_g: 684 °C.

4.2.1 SEM-EDX results

In this chapter the SEM-EDX data are presented. The idea of these measurements was to find an enrichment of certain elements like Mg at the surface in pre-treated fibres compared to untreated fibres and to reason from this that there was diffusion from the interior to the surface. This diffusion is said to be associated with the oxidation of iron (Kirkegaard & Korsgaard, 2004). The measurements were begun with the analyses of untreated fibres. The idea was to investigate one area on the mantel surface and one area on a fresh fracture which can be seen in Figure 23:

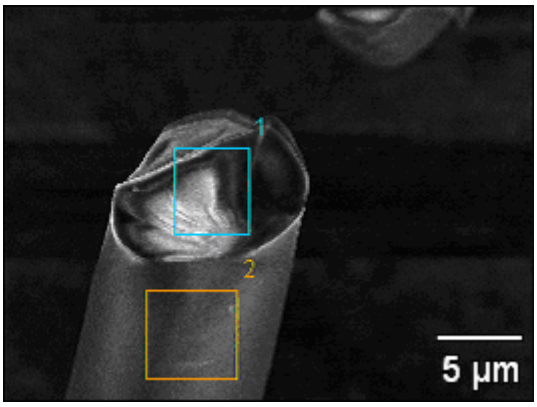

Figure 23: SE picture of untreated fibres

An acceleration voltage of 8 kV and a magnification of 9239 were used. The following composition (in weight-%) was determined:

Table 6: SEM-EDX analyses of untreated stone wool (weight-%)

Area	F	Na	Mg	Al	Si	S	Ca	Ti	Fe
1	1	1	2	6	12	0	8	0	6
2	1	0	1	3	7	0	17	1	4

There are differences between the chemical compositions of the different areas. This means either that the fibres are not homogeneous after the production or that the analytical precision of the method is so low that the differences are only random. In both cases there is the consequence that SEM-EDX does not allow to determine a slight difference in the chemical composition of a surface which is expected after the heat treatment, especially because the spatial resolution of the characteristic X-ray is lower than the estimated thickness of a possible surface. This means that the signal can be used maximally to say something about enrichment or depletion trends between different parts of the fibres, but not to obtain absolute

values for chemical concentrations of certain elements. In order to confirm the chemical differences within the fibre a chemical profile from the end via the edge to the mantel surface was measured (Figure 24). The same magnification (9239) and the same acceleration voltage (8 kV) as before were used.

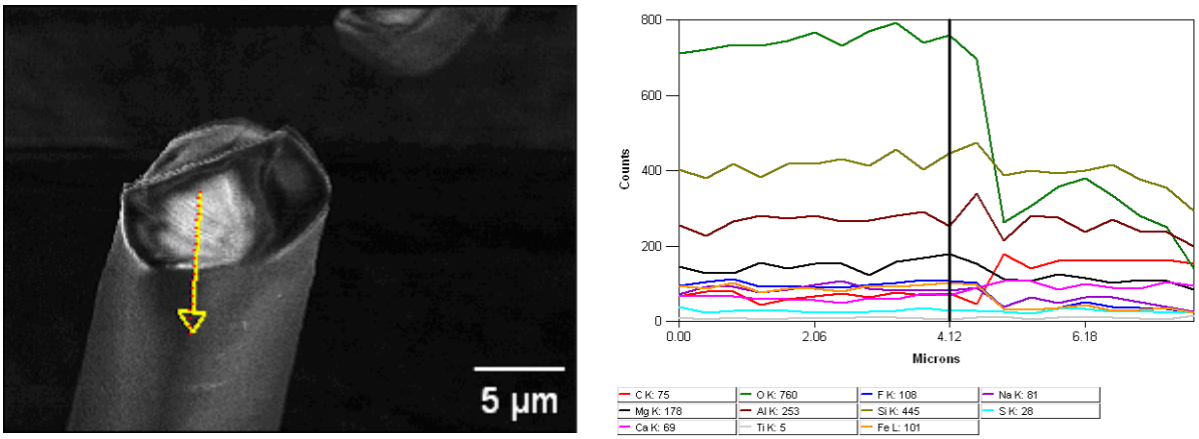

Figure 24: Line scan of untreated fibres (left), chemical profile (right)

Although the chemical analyses of the two different sites show clear differences between them, the chemical profile has no significant change in the intensities of the relevant elements. The fluctuations of the intensities within one area are larger than the fluctuations between the areas. This means that the inhomogeneous distribution of the elements in the untreated samples is random. However, further analyses were performed because larger differences between the surface and a fresh fracture- which was difficult to find – might have been possible.

The sample 493-60 was also analyzed according to the same scheme. The acceleration voltage was the same as before (8 kV), but the magnification in the picture was with a factor of 3474 smaller.

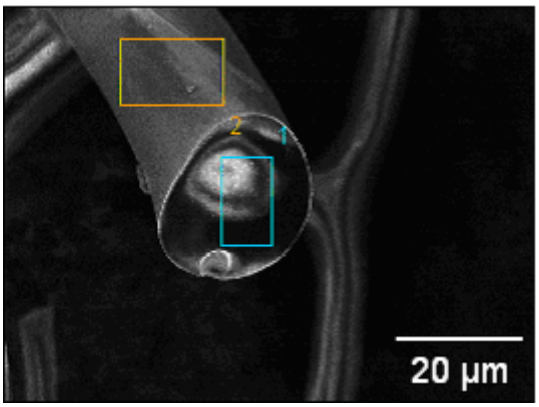

Figure 26: Analyzed sites in stone wool pre-heated for 60 min at 493 °C

Table 7: SEM-EDX analyses of stone wool pre-heated for 60 min at 493 °C (weight-%)

Area	Na	Mg	Al	Si	S	Ca	Ti	Fe	Ga
1	2	4	9	22	0	16	2	4	0
2	1	3	7	13	0	10	1	14	0

Since also the untreated fibres are not homogeneous, chemical differences up to 100 % referred to the lower value should not be interpreted as characteristic for a certain part of the fibre. In this case only Fe is strongly enriched on the fracture at the end of the fibre. It remains unclear why iron should diffuse into the interior of the fibre if a Ti-rich surface layer forms. Perhaps it replaces the Ti in the glass network. However it has to be doubted that the fracture occurred really after the pre-heat treatment. If this is not the case, both analyzed sites represent the surface and their differences result from the natural inhomogenity of the fibres which could be seen in the untreated fibres.

Whereas no analyses were performed on the sample 684-10, the sample 684-30 was analyzed again with the same method (Figure 24) where the magnification was 19330 and the accelerating voltage 8 kV.

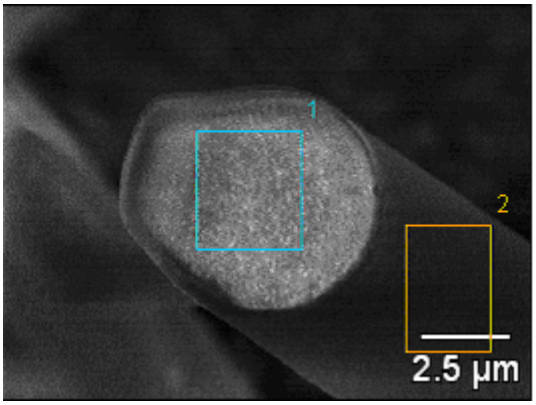

Figure 25: Sites of EDX analyses in stone wool pre-heated for 30 min at 684 °C

Table 8: EDX analyses of stone wool pre-heated for 30 min at 684 °C (weight-%)

Area	Na	Mg	Al	Si	S	Ca	Ti	Fe	Ga
1	2	3	7	16	0	18	0	8	1
2	0	2	4	8	0	33	3	8	0

To check the reproducibility of the results the measurement of this sample was repeated at another site (Figure 26):

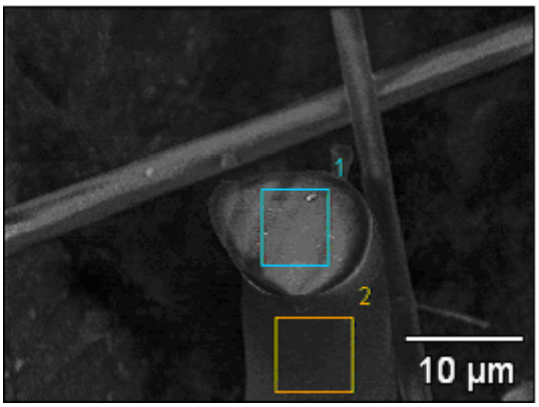

Figure 26: Sites of EDX analyses of stone wool pre-heated for 30 min at 684 °C (II) (magnification: 6416, acceleration voltage: 8 kV)

Table 9: EDX analysis of stone wool pre-heated for 30 min at 684 °C (II) in weight-%

Area	Na	Mg	Al	Si	S	Ca	Ti	Fe	Ga
1	2	3	8	14	0	12	1	11	0
2	1	1	3	7	0	27	1	7	0

Although this measurement was performed on the same sample as the measurement before, the results are different. Mg and Al are depleted on the mantel surface whereas Ca is enriched.

It can be concluded that all the changes in the chemical composition observed by this method are only random. The results for the sample 684-60 show also large fluctuations, the sample 875-60 was not analyzed. Summarizing this chapter it can be stated that SEM-EDX is not an appropriate method to investigate the surface chemistry of thermally treated stone wool because the spatial resolution is too bad. Furthermore it seems probable that all the "fractures" analyzed in this chapter developed before the pre-heat treatment and are therefore "surfaces" which should have the same chemical composition as other surfaces.

4.2.2 TG results

In a next step **thermogravimetry (TG)** was used to measure the incorporation of atmospheric oxygen with is associated with the oxidation of iron (chapter 2.2.1) and the formation of the MgO surface layer. In a first step measurements in air were conduted. TG analyses of untreated and pre-heated fibres were performed to investigate how the pre-heat treatment influences the oxygen incorporation afterwards. Figure 27 shows the dependence of the mass increase during the TG measurement on the temperature of the pre-heat treatment:

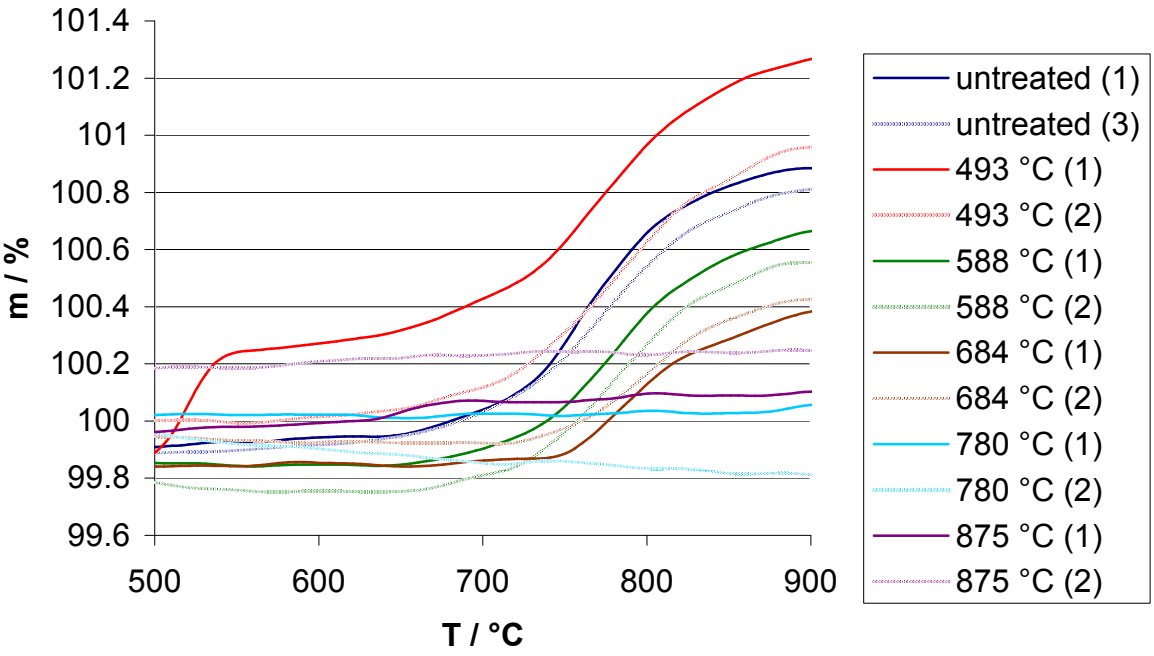

Figure 27 : TG in air after pre-heat treatments of 60 minutes at various temperatures

In this series a general trend can be seen: The higher the temperature of the pre-heat treatment the smaller is the mass increase during the TG measurement. This can be explained by a partial oxidation during the pre-heat treatment. The higher the temperature of the pre-heat

treatment the faster is the diffusion during it. Hence for a constant duration the rate of oxidation increases with increasing temperature. All deviations from the main trend seem to be within the uncertainty range (Kirkegaard & Korsgaard, 2004). At 780 °C the formation of the surface crystals is completed and in the TG measurement no further mass increase can be detected. The first scan of the sample pre-heated at 493 °C is a exception from the trend mentioned above and is characterized by a two-step mass increase. The additional mass increase between 500 and 600 °C might be caused by the oxidation of another element, for example from Ti^{3+} to Ti^{4+}. But this interpretation is very doubtful because the results are not repeatable and the untreated fibres show no second mass increase in this temperature region. The role of Ti might be proved by the use of electron paramagnetic spin resonance spectroscopy (ESR) in further work.

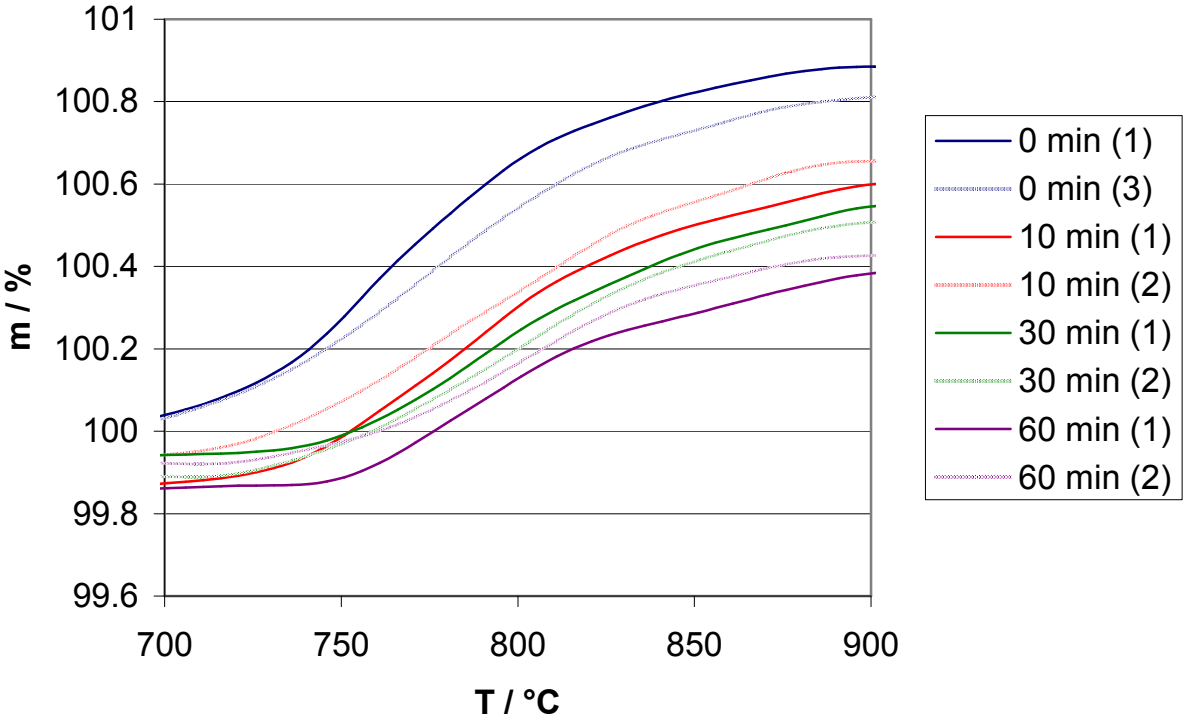

Figure 28 : TG in air after pre-heat treatment for different durations at 684 °C

An increase in the duration of the pre-heat treatment has the same effect as an increase in its temperature: The longer the pre-heat treatment the smaller is the mass increase in the TG measurement. This means that the formation of the surface layer during the pre-heat treatment proceeds with time if the temperature is constant. In comparison to the former series where this proceeding was reached by an acceleration of the crystallization speed via a raising

temperature it is reached here by an increase in time at constant speed. The effects are the same.

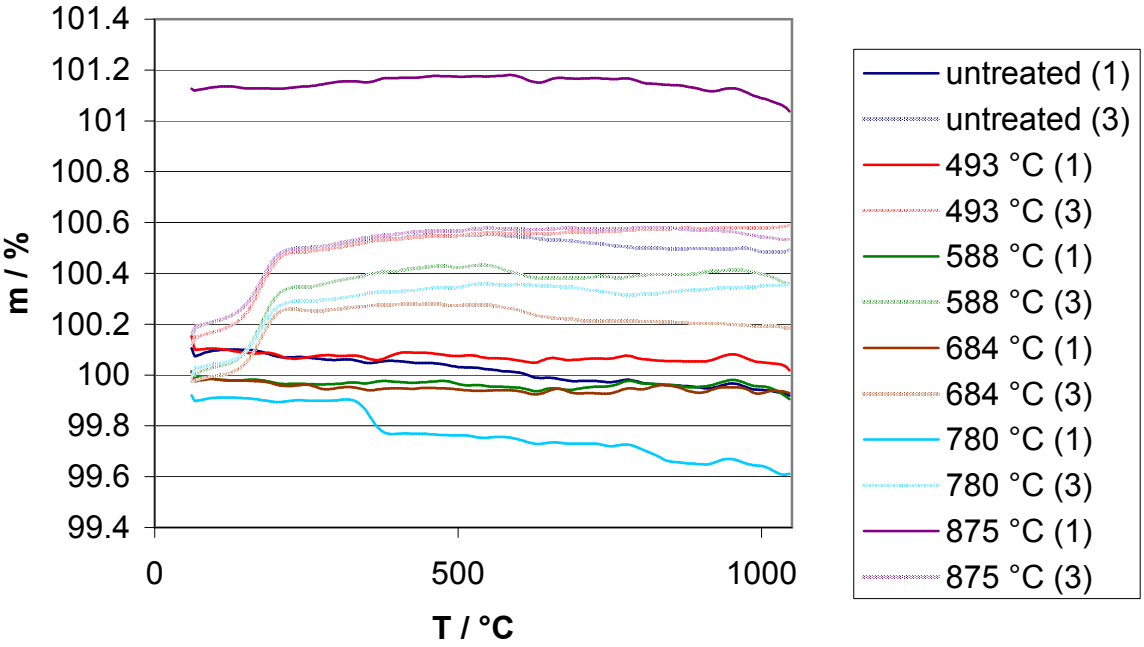

Figure 29: TG in argon after a pre-heat treatment for 60 min at different temperatures

The measurements in argon (Figure 29: TG in argon after a pre-heat treatment for 60 min at different temperatures) show no mass increase between 700 and 900 °C because no oxygen can be incorporated into the fibres in an argon atmosphere. But there is a mass increase at about 200 °C which can be seen in Figure 30 in more detail:

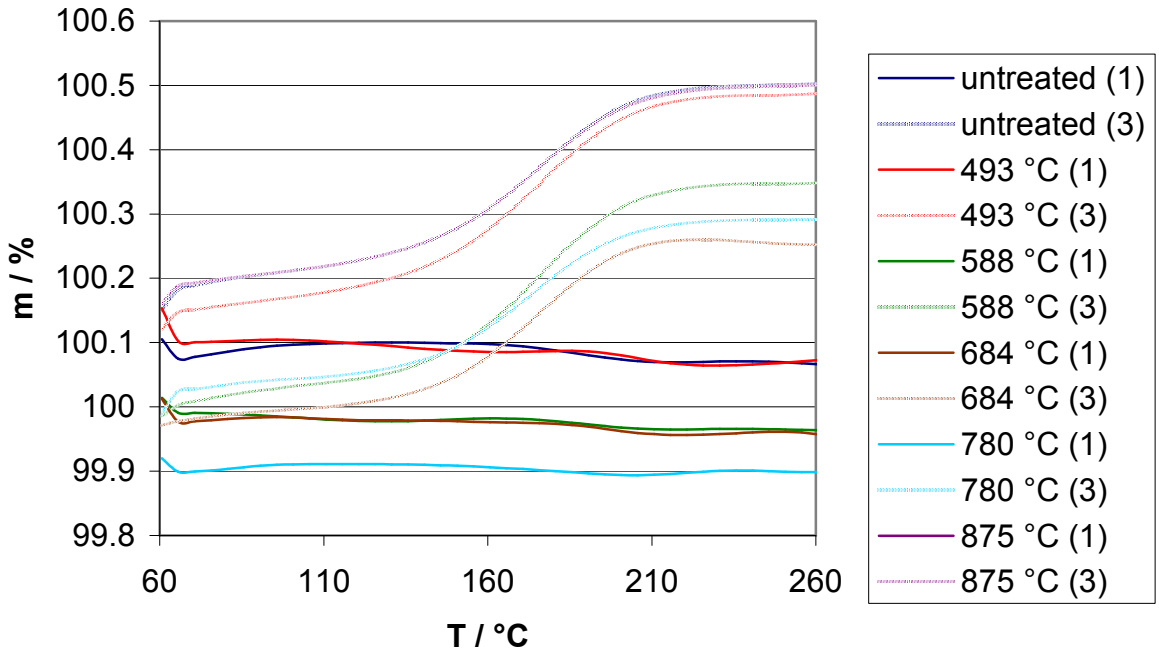

Figure 30: TG in argon after a pre-heat treatment for 60 min at different temperatures, mass increase at low temperatures

This mass increase only occurs with samples from the third series which was performed three months after the first, after the second gave wrong results due to handling errors. This means that the samples of the third series had been stored for three months in glasses or plastic containers. A mass increase at low temperatures could be explained by the adsorption of argon atoms. Adsorption is a surface process; hence the results might be explained by a change in the surface properties during the storing period. It might be that a kind of weathering took place during these three months where chemical bonds were broken that could be "used" for the adsorption of atoms. But it has to be seen that this mass increase does not occur in the second series of the measurements in air although the fibres used there had been stored also for two months. As a conclusion it can be said that the reasons for this mass increase which can also be seen in Figure 31 remains unclear.

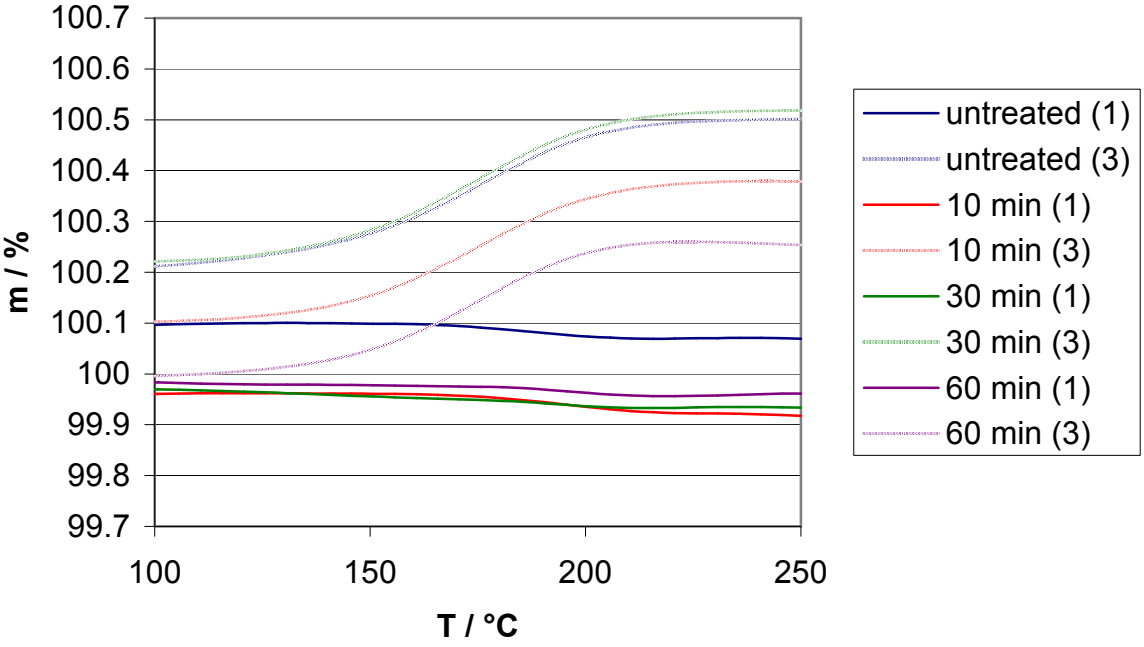

Figure 31: TG in argon after a pre-heat treatment at 684 °C for different durations, mass increase at low temperatures

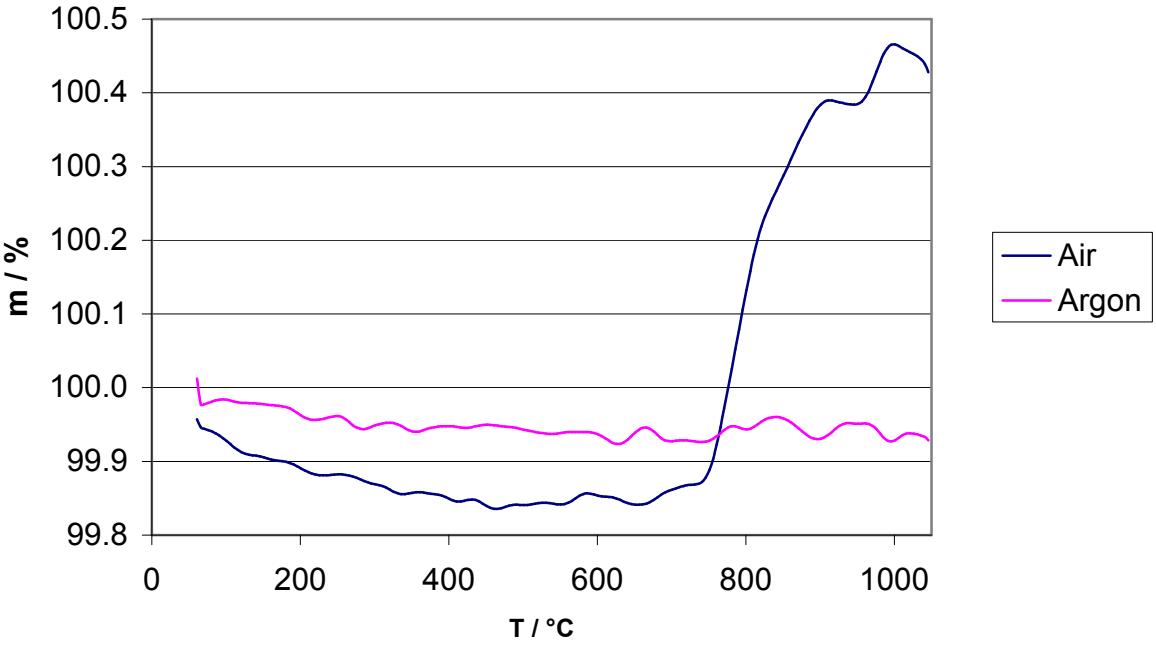

Figure 32: TG in argon and in air after a pre-heat treatment for 60 min at 684 °C

Figure 32 shows clearly that the mass increase between 750 and 1000 °C only occurs in air. That is why it is interpreted as the incorporation of atmospheric oxygen.

4.2.3 DSC results

To investigate the crystallization temperature and enthalpy differential scanning calorimetry (DSC) was used whose results are presented in this chapter.

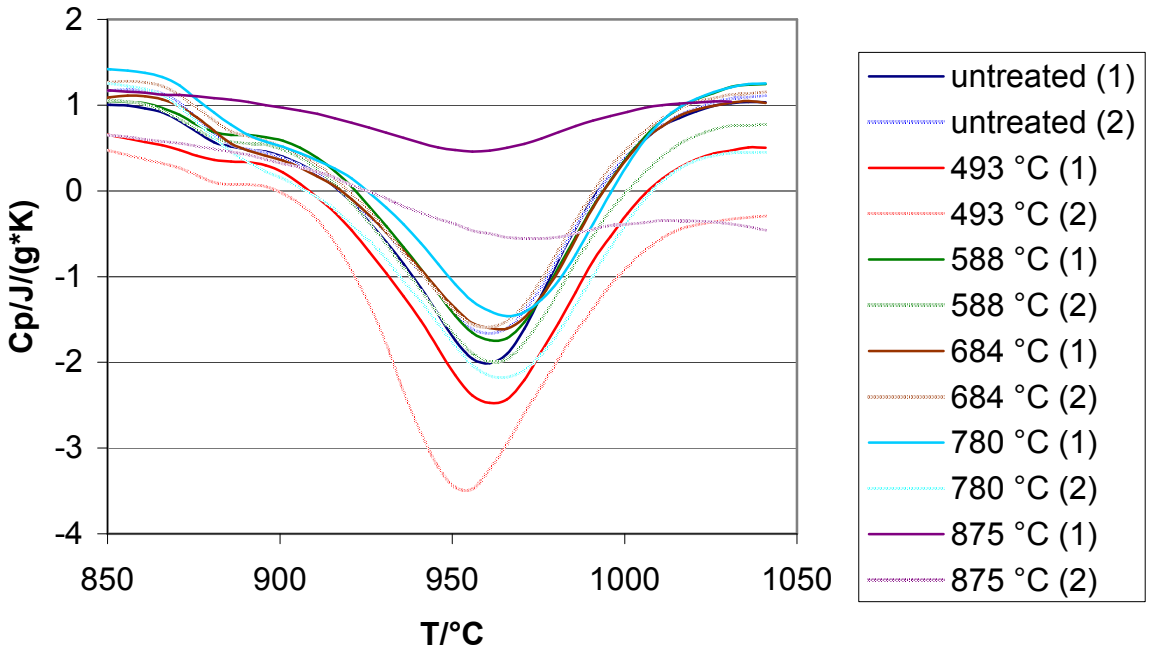

Figure 33: DSC in air after a pre-heat treatment for 60 min at different temperatures

Figure 33 shows the crystallization peaks of fibres which had been pre-heated at different temperatures. The position of the peak varies between 955 and 970 °C, but there is no trend depending on the temperature of the pre-heat treatment. All the fibres apart from the sample 875-60 show a very small peak at 880 °C. The position and the size of this side peak are independent from the temperature of the pre-heat treatment. It might be interpreted that the side peak corresponds to the formation of a minor phase and the main peak to the crystallization of the major phase. This interpretation should be doubted because there is no phase present in the fibres pre-heated at lower temperatures which is not present in the fibres pre-heated at 875 °C (chapter 4.3.2). Although the temperature of the main peak is higher than 875 °C, the onset temperature is not. This explains why during the pre-heat treatment at 875 °C crystals can already form (chapter 4.3.2). In a second step the crystallization enthalpies during the DSC measurements were calculated. Therefore the areas of the peaks were calculated by a numerical approach. The peaks were limited by an auxiliary line between the two adjacent maxima (with the exception of the second measurement for 875 °C) and divided into columns of 5 °C width. The area of each column was calculated by the formula:

$$A = 5\ °C \bullet mx + a - b \qquad (3)$$

In this formula 5 °C is the width of the column, "mx + a" is the equation of the auxiliary line (where x is the average temperature of the interval) and b is the C_p value at the middle of the interval. The areas of the different columns were summed up, negative values were neglected.

Table 10: Crystallization enthalpies calculated from DSC in air depending on the temperature of the pre-heat treatment

Sample	Crystallization enthalpy in J/g	Average crystallization enthalpy in J/g
untreated (1)	208	204
untreated (2)	199	
493 °C (1)	121	171
493 °C (2)	220	
588 °C (1)	195	179
588 °C (2)	162	
684 °C (1)	190	193
684 °C (2)	196	
780 °C (1)	217	218
780 °C (2)	219	
875 °C (1)	47	44
875 °C (2)	40	

Some measurements have good reproducibility, others do not. However, it becomes clear that fibres pre-heated at 875 °C have a significantly smaller crystallization enthalpy than the others. This means that the crystallization has already taken place during the pre-heat treatment. This hypothesis was proved by XRD data (chapter 4.3.2).

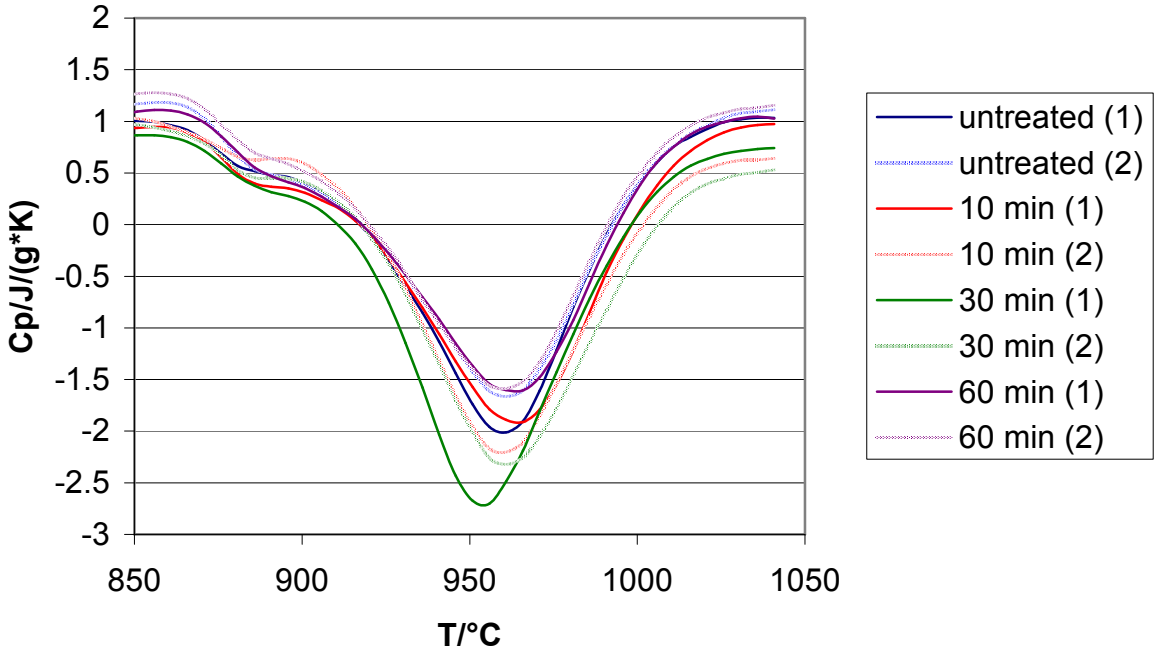

Figure 34: DSC in air after a pre-heat treatment for 60 min at 684 °C

Figure 34 shows that also for a variation in the duration of the pre-heat treatment the crystallization peak remains constant. However, the crystallization enthalpies were calculated (Table 11):

Table 11: Crystallization enthalpies calculated from DSC in air depending on the duration of the pre-heat treatment (T = 684 °C)

Sample	Crystallization enthalpy in J/g	Average crystallization enthalpy in J/g
untreated (1)	208	204
untreated (2)	199	
10 min (1)	197	193
10 min (2)	189	
30 min (1)	213	206
30 min (2)	199	
60 min (1)	190	193
60 min (2)	196	

There are no significant differences between the crystallization enthalpies. It might be concluded that the degree of crystallization is therefore identical but the XRD measurements (chapter 4.3.2) show that it increases with increasing duration of the pre-heat treatment. The reason for this effect might be the different crystallization enthalpy of albite and gehlenite compared to augite. It seems also possible that the enthalpy calculation is not precise enough to say something about crystallization.

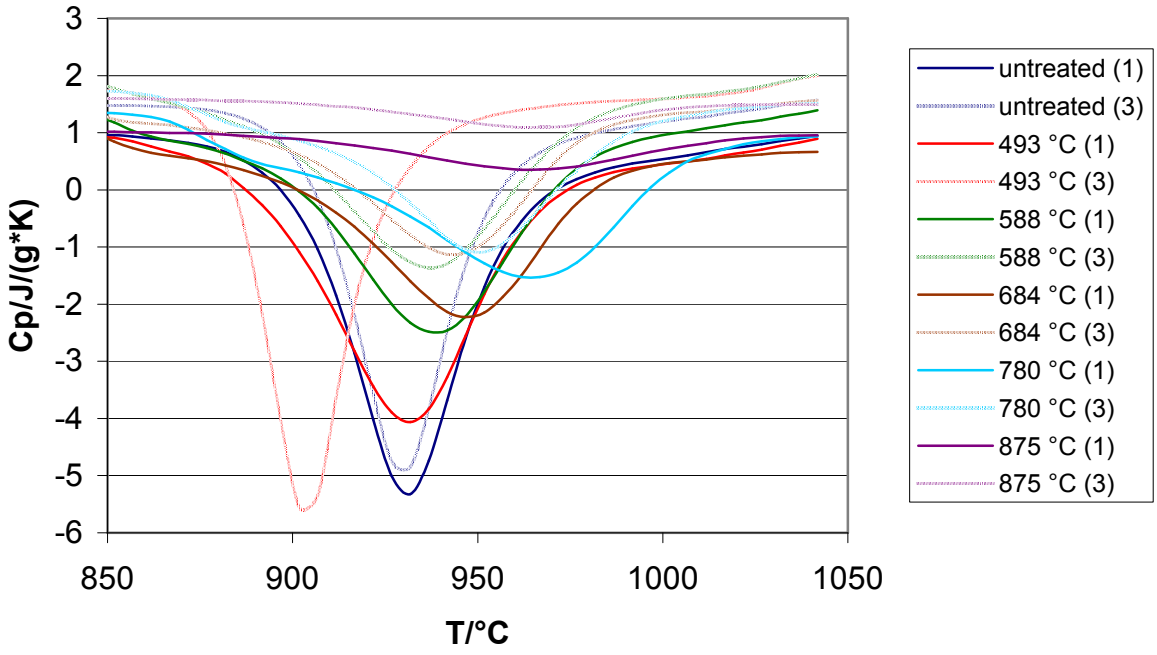

Figure 35: DSC in argon after a pre-heat treatment for 60 min at different temperatures

Three series of measurements were performed in argon to test the repeatability of a rightwards shift observed during the first series. There the untreated fibres and the sample pre-heated at 493 °C have the crystallization peak at 930 °C, increasing the temperature to 588 °C shifts the peak up to 940 °C, an increase to 684 °C shifts it to 945 °C, an increase to 780 °C to 965 °C and for the highest temperature of 875 °C the crystallization peak occurs even at 970 °C. The second series could not be used because it showed mass increases in the TG curves which hint to a handling error having caused the presence of oxygen in the apparatus. But also in the third series the results from the first could not repeated. It has to be stated that all peak temperatures in the third series are lower than in the first and the temperature difference is not constant. However, also the third series shows a slight shift to higher temperatures. This means that the right shift is reproducible although the precision of the temperature measurements is low. The shift of the crystallization peak might result from the sintering and

blackening of the fibres (chapter 4.1.1). Also for the measurements in argon the crystallization enthalpies were determined:

Table 12: Crystallization enthalpies calculated from DSC in argon depending on the temperature of the pre-heat treatment.

Sample	Crystallization enthalpy in J/g	Average crystallization enthalpy in J/g
untreated (1)	291	269
untreated (3)	247	
493 °C (1)	282	282
493 °C (3)	281	
588 °C (1)	252	246
588 °C (3)	240	
684 °C (1)	208	198
684 °C (3)	187	
780 °C (1)	209	196
780 °C (3)	183	
875 °C (1)	45	36
875 °C (3)	27	

The crystallization enthalpies show decreasing trend with two steps: one between 588 °C and 684 °C and one between 780 °C and 875 °C. The first step which is smaller than the second corresponds to the surface crystallization. Surface crystallization which has already taken place in the pre-heat treatment does not contribute to the crystallization enthalpy in the DSC. That is the explanation for the first decrease in the enthalpy because above T_g the surface crystallization becomes significant. The larger second step corresponds to the bulk crystallization whose onset temperature is below 875 °C. Here an analogous interpretation can be used. The repeated measurements have always smaller enthalpies than the first measurements. Such a systematic error might result from the baseline or from a change of the material used for the repeatability measurements during the three months between the sieving and the measurement.

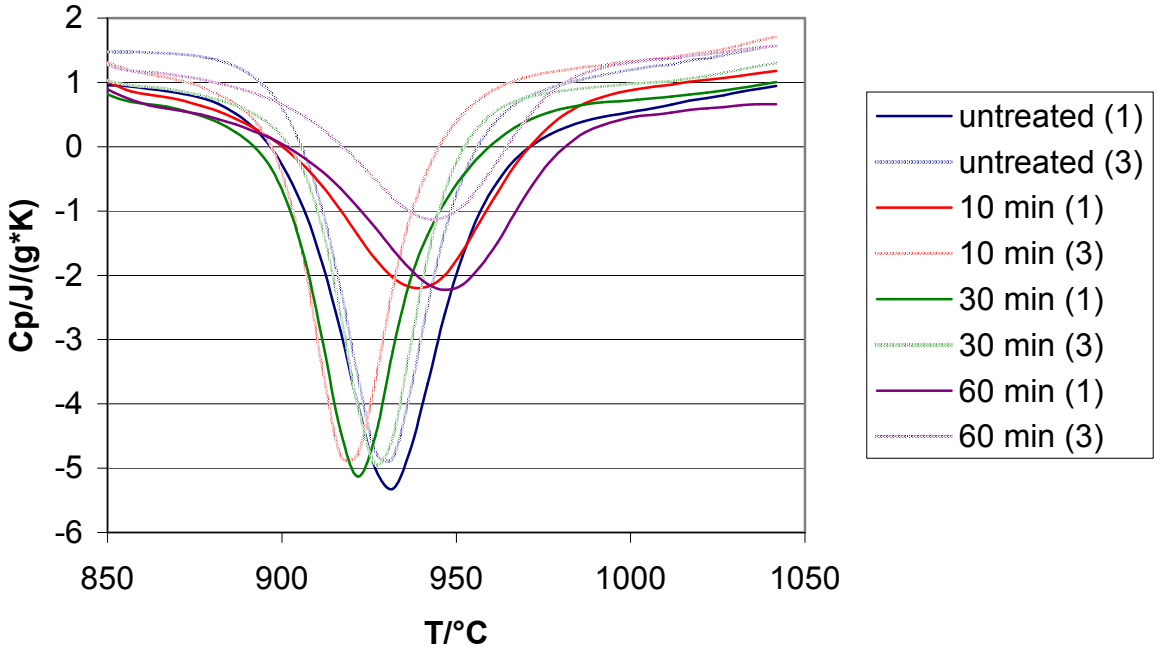

Figure 36: DSC in argon after a pre-heat treatment at 684 °C for different durations

The maxima of the crystallization peaks lie between 920 and 970 °C. It can be seen that the differences between the first and second measurements of the same sample are in the same range as the differences between the different samples. This means that there is no clear trend and no dependence of the crystallization temperature on the duration of the pre-heat treatment. The peak of the first measurement of the sample 684-10 does not fit into the series because it is to flat and occurs at a too high temperature. Also for the dependence on the duration of the pre-heat treatment the crystallization enthalpies were calculated:

Table 13: Crystallization enthalpies calculated from DSC in argon depending on the duration of the pre-heat treatment

Sample	Crystallization enthalpy in J/g	Average crystallization enthalpy in J/g
untreated (1)	291	269
untreated (3)	247	
10 min (1)	232	251
10 min (3)	269	
30 min (1)	275	263
30 min (3)	251	
60 min (1)	208	198
60 min (3)	187	

Only after a pre-heat treatment of 60 minutes the crystallization enthalpy decreases significantly. But also for the sample 684-60 no crystalline phases could be found with XRD (chapter 4.3.2). This means that the slight decrease of the crystallization enthalpy for long durations results only from the surface crystallization.

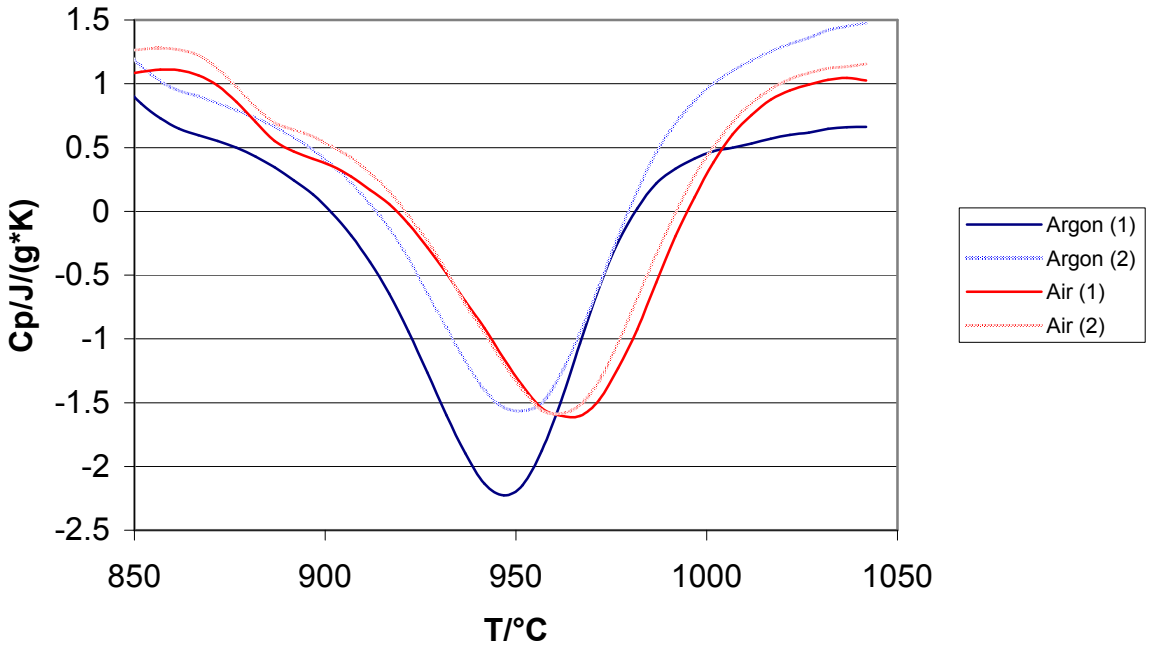

Figure 37: DSC in argon and in air after a pre-heat treatment at 684 °C for 60 min

According to Figure 37 there is a slight difference in the crystallization peak temperatures in air (960 °C) and in argon (950 °C). If this difference should be significant which should be tested with at least ten measurements there might be the explanation that the surface crystals inhibit the bulk crystallization for some minutes or degrees Celsius which is equivalent in a DSC measurement because the samples are heated. Alternatively it might be possible that the different crystalline phases which form under different redox conditions might have different crystallization temperatures.

4.3 Mineralogical Changes

Figure 38 shows the resulting grain size distributions from the grinding test (chapter 3.4) with and without a dispersing agent. 684-60-875-60 means that the pre-heat treatment was performed for 60 min at 684 °C and the heat treatment for 60 min at 875 °C. 684-60-1100 means that the sample was heated after a pre-heat treatment of 60 min at 684 °C continuously up to 1100 °C to pretend a DSC measurement:

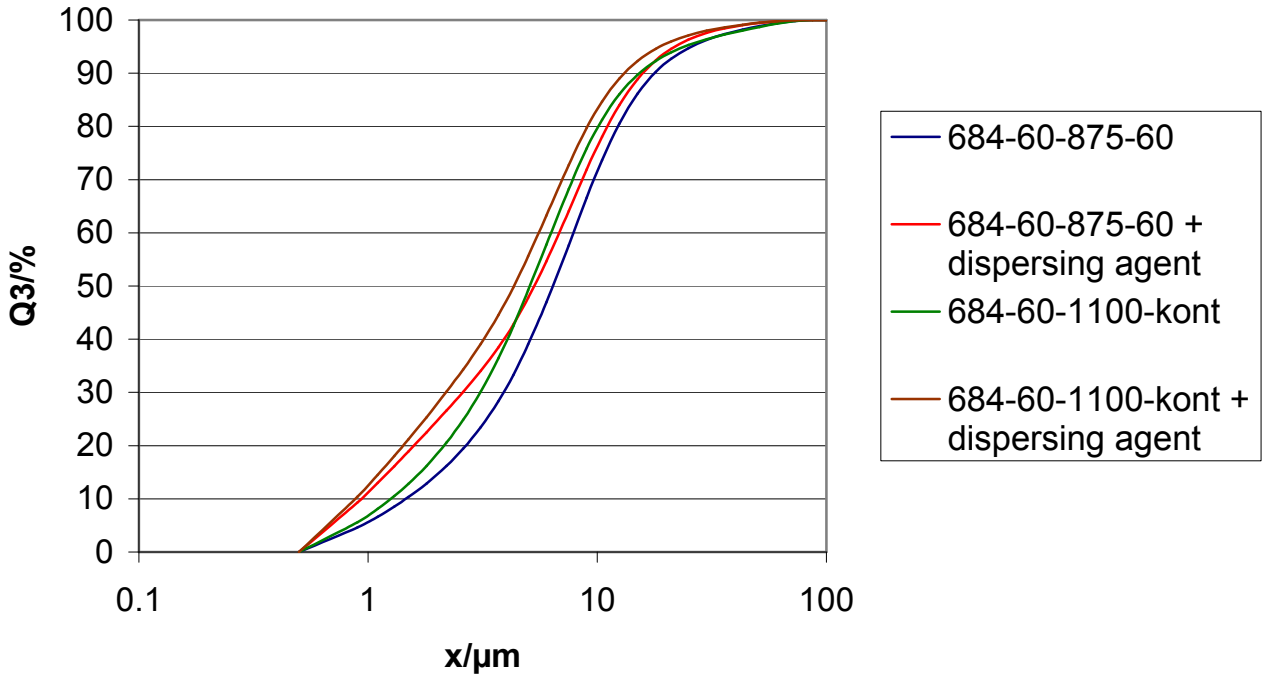

Figure 38: Cumulative frequence Q3 of the grain sizes x of stone wool fibres grinded with a McCrone mill

The median values are summarized in Table 14:

Table 14: Median values of the grain size distributions of grinded and pre-heated stone wool

Sample	684-60-875-60	684-60-875-60	684-60-1100	684-60-1100
Median in µm	6.4	5.3	5.1	4.3

In all cases the efficiency of McCrone milling was sufficient. Hence a cooling with liquid nitrogen during the grinding process like suggested by Allmann (2003) was not necessary. The fibres which were subjected to the "coldest" heat treatment have larger grain sizes than the fibres subjected to higher temperatures. This results from the embrittlement during the crystallization. The use of a dispersing agent decreases the grain size because agglomerates are destroyed.

4.3.1 Identification of Crystalline Phases

The general phase composition was found to be amorphous phase + augite ± albite ± gehlenite (Figure 39):

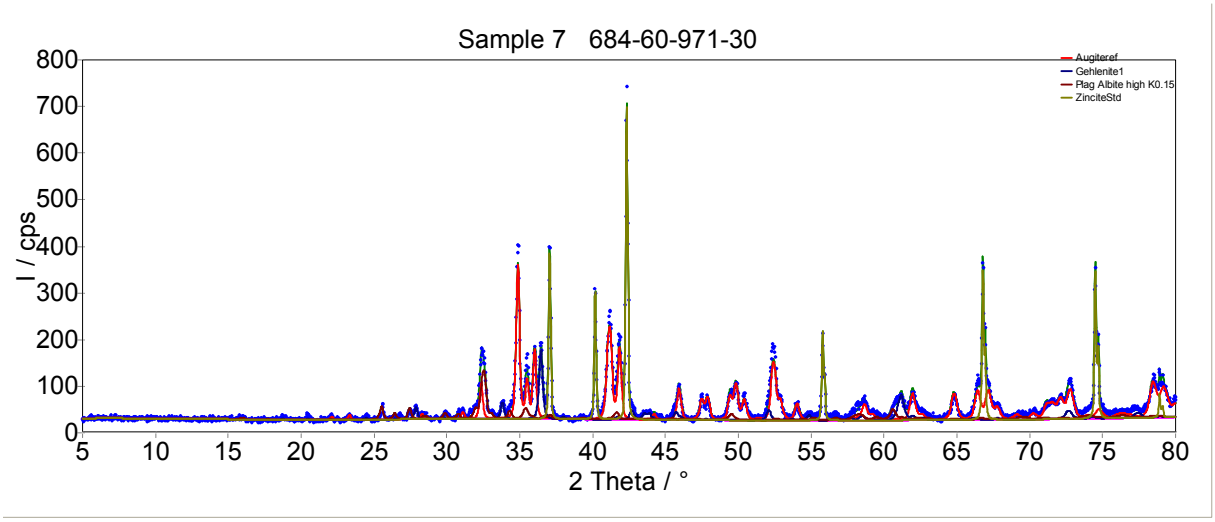

Figure 39: X-ray diffraction pattern of the sample 684-60-971-30

It can be seen how the different phases, augite (red), gehlenite (dark blue), albite (brown) and the external standard zincite (olive) contribute to the overall diffraction pattern. These phase assemblage was used as a starting model for the Rietveld refinement. All of these phases are members of solid solutions. The gehlenite peaks which could be found in the X-ray diffraction patterns at 61 ° are quite broad. This effect might result from lattice strain which leads to a variation in the lattice parameters within one crystal. This lattice strain might result from a chemical zonation within the crystal and was set at 0.3 % in the Rietveld refinement. It might be possible that the Mg-Al distribution which defines the melilithe solid solution akermanite

(Mg) – gehlenite (Al) is inhomogeneous. However, from the position of the peaks and from the chemical composition of the fibres (chapter 2.2.3) it could be concluded that the composition of this melilithe is close to the gehlenite end member. It could be seen that the gehlenite peaks were wider for larger angles. This is typical for small crystallites; hence the crystallite size was set at 100 nm for the Rietveld analysis. The albite structure which fitted best and was therefore used as a starting model for the Rietveld refinement was a high albite with a substitution of 15 % potassium on the sodium position ("Plag High Albite K0.15" in the program AutoQuan). If it is really true that high albite is present it is a metastable phase, this might happen because of the rapid cooling after the heat treatment. From the assumption that gehlenite can be neglected (which is more or less the case for the sample 684-60-971-60) the exact formula of augite was calculated from the bulk and the albite composition: $Ca_{0.69}Fe_{0.32}Mg_{0.91}Al_{0.08}[Al_{0.19}Si_{1.81}O_6]$. The charge of the anion complex is -4.19. From this it can be calculated that the 0.32 mol Fe must provide 0.75 charges. This means that the exact formula should be $Ca_{0.69}Fe^{2+}_{0.21}Fe^{3+}_{0.11}Mg_{0.91}Al_{0.08}[Al_{0.19}Si_{1.81}O_6]$. This formula was used to change the structural file "Augiteref" from the program AutoQuan which was used as a starting model for the augite structure. The assumption of a rest of divalent iron after a pre-heat treatment at 684 °C is according to Mößbauer analyses by Kirkegaard & Korsgaard (2004) who found complete oxidations not before 800 °C. The fast heating process in the second heat treatment might prevent further oxidation. After the Rietveld refinement the program stated that there is no iron in the augite which is chemically seen very unlikely because some samples are almost completely crystalline and albite can only incorporate traces of iron. Gehlenite might incorporate a certain amount of iron but accounts only for a small mass percentage.

4.3.2 Quantification of Crystalline Phases

Table 15 shows the results of the identification and quantification of the crystalline phases in thermally treated stone wool. Their dependence on different parameters will be explained and interpreted in the following chapters:

Table 15: Quantification of crystalline phases in thermally treated stone wool (n.d. = not detected)

	Amorphous	Augite	Albite	Gehlenite
untreated	100	n.d.	n.d.	n.d.
untreated-971-60	30 ± 2	70 ± 2	n.d.	n.d.
493-60	100	n.d.	n.d.	n.d.
493-60-971-60	26 ± 2	67 ± 2	7 ± 1	n.d.
684-10	100	n.d.	n.d.	n.d.
684-10-971-60	31 ± 2	69 ± 2	n.d.	n.d.
684-30	100	n.d.	n.d.	n.d.
684-30-971-60	20 ± 2	67 ± 2	11 ± 1	2 ± 1
684-60	100	n.d.	n.d.	n.d.
684-60-971-60	3 ± 3	65 ± 2	26 ± 2	6 ± 1
875-60	47 ± 2	50 ± 2	3 ± 1 (?)	n.d.
875-60-971-60	27 ± 2	71 ± 2	2 ± 1	n.d.
971-10	22 ± 3	70 ± 2	8 ± 2	n.d.
971-30	25 ± 2	65 ± 2	10 ± 1	n.d.
971-60	4 ± 3	82 ± 3	14 ± 2	n.d.
684-60-875-60	49 ± 2	46 ± 2	n.d.	6 ± 1
684-60-923-60	32 ± 2	65 ± 2	n.d.	3 ± 1
684-60-971-10	24 ± 2	74 ± 2	n.d.	2 ± 1
684-60-971-30	11 ± 3	60 ± 2	17 ± 2	12 ± 1
684-60-875-60-H	10 ± 3	68 ± 2	12 ± 1	10 ± 1
684-60-923-60-H	10 ± 4	54 ± 2	21 ± 3	16 ± 1
684-60-971-6-H	11 ± 4	49 ± 2	23 ± 3	17 ± 2
684-60-971-30-H	8 ± 3	66 ± 2	22 ± 2	4 ± 1
684-60-971-60-H	11 ± 3	59 ± 2	17 ± 2	12 ± 1
684-60-971-60 (with air in the H furnace)	13 ± 3	80 ± 2	7 ± 2	n.d.
684-60-1100 (continuos heating)	18 ± 2	73 ± 2	9 ± 2	n.d.
untreated-884-60-white fibre	10 ± 3	4 ± 1	12 ± 1	73 ± 2
untreated-884-60-mixed fibre	39 ± 2	32 ± 1	11 ± 2	18 ± 1
sieve remainder	100	n.d.	n.d.	n.d.

First the dependence of the phase assemblage on the pre-heat treatment shall be discussed (Figure 40):

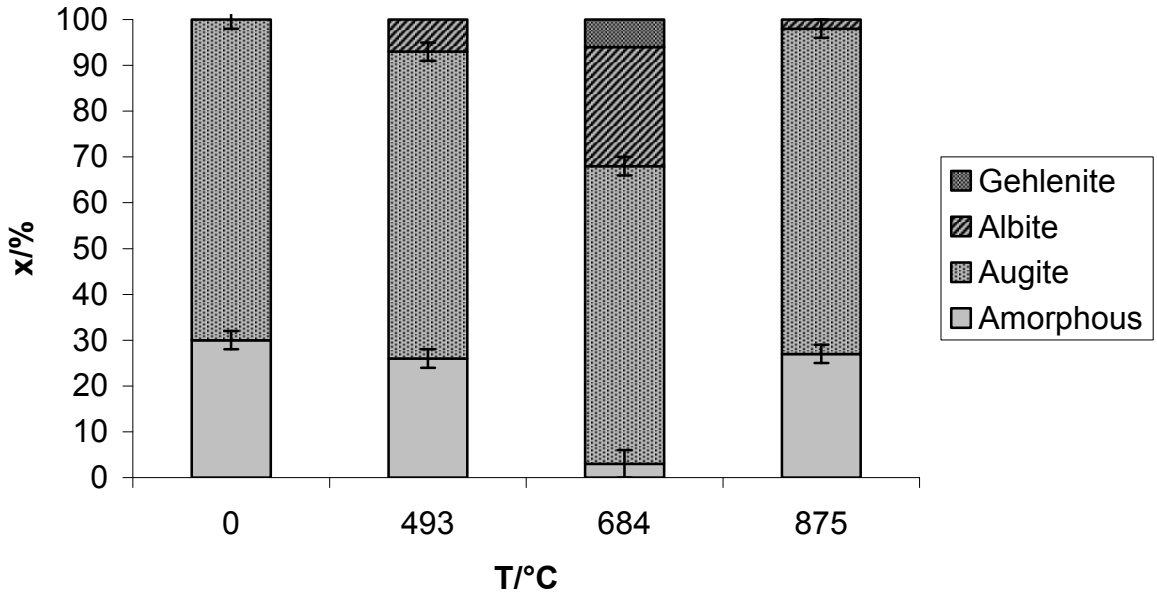

Figure 40: Phase composition x as a function of the temperature T of the pre-heat treatment for 60 min (heat treatment for 60 min at 971 °C)

Pre-heat treatments performed above and below T_g lead to similar mineralogical compositions after the second heat treatment, whereas a pre-heat treatment at T_g leads to a different composition. This effect can be explained by the idea that during a pre-heat treatment significantly above T_g the same process, bulk crystallization, occurs which happens to untreated fibres during the second heat-treatment. This might be the reason for the similarity between the behaviour of non-pre-treated and highly pre-treated stone wool. The almost complete crystallization of the fibres which had been pre-heated at T_g might be explained by the acting of the surface crystals as heterogeneous nuclei. A lack of nuclei might lead to an incomplete crystallization in the untreated and intensively treated fibres. The formation of albite and gehlenite might be explained by the chemistry of the system. After the formation of about 70 % augite ($(Ca,Na)(Mg,Fe,Al,Ti)(Si,Al)_2O_6$) the matrix is depleted in Mg and Fe and enriched in Na, Ca, Al and Si. These elements are the constituents of albite ($NaAlSi_3O_8$) and gehlenite ($Ca_2Al(Al,Si)O_7$). Hence the amorphous rest which remains after the crystallization of augite crystallizes to albite and gehlenite. Alternatively it might be possible that an exsolution takes place. During the pre-heat treatment the new-formed trivalent iron might displace the Al from the tetrahedrons. If this exchange takes place only in a part of the sample there will be regions where Fe is tetrahedral and Al octahedral coordinated and regions where

it is the other way around. The formation of a $Al^{[6]}$-rich phase during the pre-heat treatment might explain the formation of gehlenite during the heat treatment.

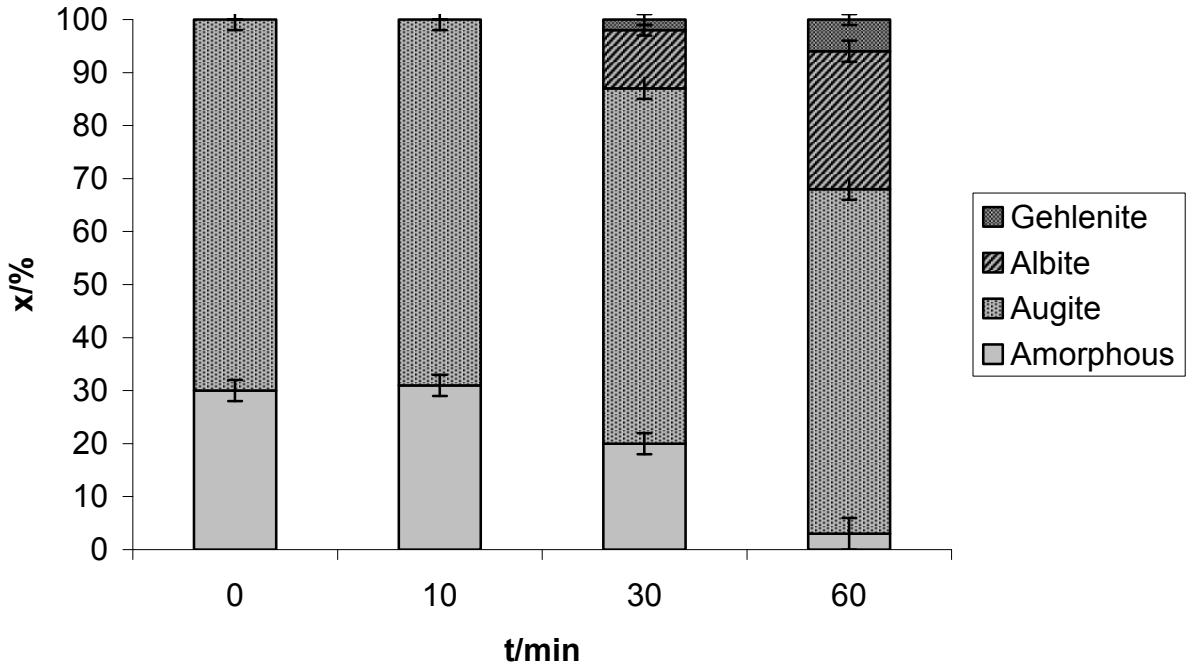

Figure 41: Phase composition x as a function of the duration t of a pre-heat treatment at 684 °C (heat treatment for 60 min at 971 °C)

Figure 41 shows that the longer the pre-heat treatment is performed at T_g, the smaller becomes the amorphous percentage after the second heat treatment. A pre-heat treatment of 10 minutes has no effect on the final mineralogical composition although it already causes the formation of some surface crystals (chapter 4.1.2). Fibres pre-heated for one hour are crystallized almost completely after the second heat treatment. This might be explained by the increasing number of surface crystals which act as nuclei and accelerate the bulk crystallization. It can be seen that 70 % of the material can crystallize without previous pre-heat treatment, e.g. they do not need heterogeneous nuclei. This might be explained by the following idea: Due to the chemical composition (Table 1) the amorphous amount will be replaced by albite (25 %) and gehlenite (5 %) when the duration of the pre-heat treatment is increased. It might be that the surface crystals provide nucleation sites for these two minerals and their lack prevents their crystallization. Another explanation is that after a long pre-heat treatment almost all the iron is tetrahedral coordinated; hence no octahedral coordinated iron is available any more for the formation of augite where iron is also octahedral coordinated.

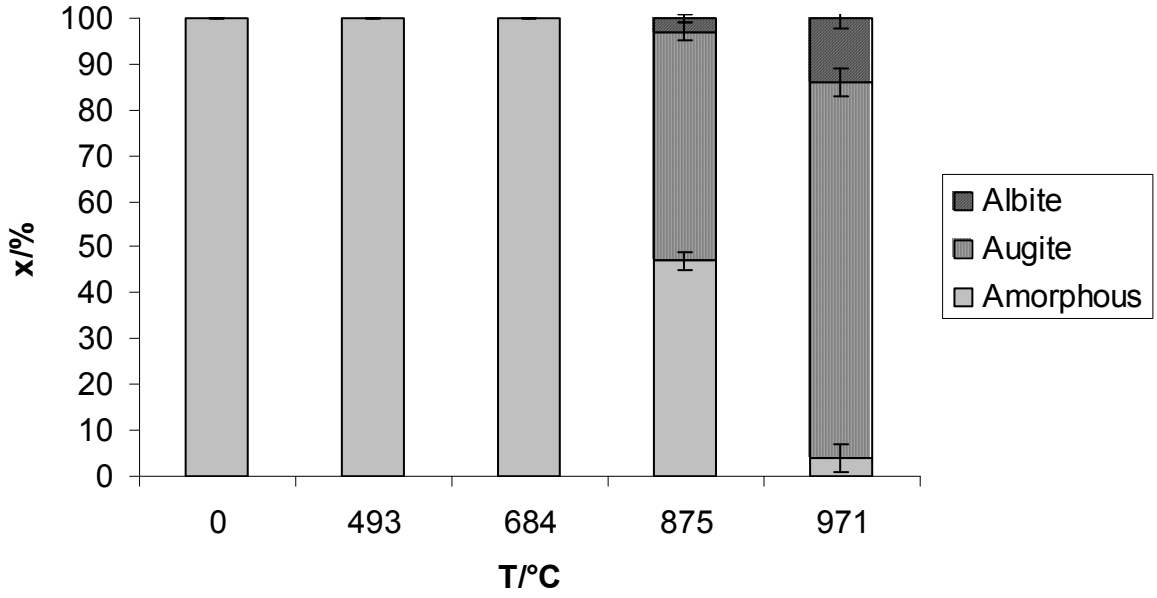

Figure 42: Phase composition x as a function of the temperature T of a one-stage heat treatment for 60 min

Figure 42 shows the development within a one-stage heat treatment which can be understood as a pre-heat treatment without further heat treatment. It can be seen that crystallization only occurs above the glass transition temperature. This can be explained because here the glass is converted into its metastable equivalent state, the undercooled melt (Heide, 2002). At 971 °C the crystallization is almost completed. The relative amount of augite is higher after a heat treatment at 875 °C than at 971 °C. Considerating that this series shows a one-stage heat treatment it might be concluded that no pre-existing nuclei are present. If this is the case the later occurrence of albite might mean that the energy which is needed to form albite nuclei is higher than that for the formation of augite nuclei. This might be associated with the more complex crystal structure of feldspars compared to pyroxenes.

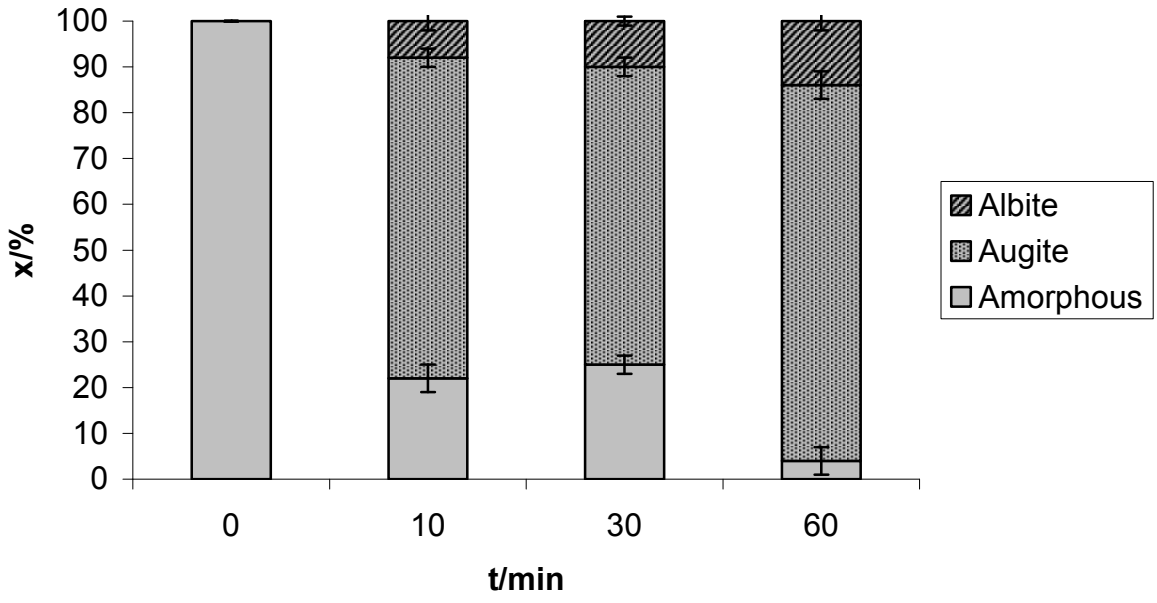

Figure 43: Phase composition x as a function of the time t of a one-stage heat treatment at 971 °C

Figure 43 shows the development of the bulk crystallization with time. The crystallization starts very rapidly. This means that both nucleation and crystallization rates are quite high at 971 °C. This seems logical because this temperature is more or less between the glass transition temperature (684 °C) and the melting temperature (1202 °C peak temperature, Moesgaard & Pedersen, 2005). Hence the temperature is high enough to enable diffusion and low enough for a strong thermodynamic driving force. This means that 971 °C are in the area in Figure 4 where both nucleation and crystal growth take place. After 10 minutes the crystallization process seems to stop. It seems probable that there is a problem with crystal growth because nuclei are already present so that nucleation cannot be the limiting factor. Crystal growth depends on diffusion; diffusion depends on the structure of the undercooled melt. This structure might change when more and more atoms are dissolved and transported to the crystals. This changed structure might consist of a residual glass network depleted in network modifiers and therefore with a higher strength and a smaller solubility. Hence the reservoir of the elements needed for crystal growth might have become smaller. After 30 minutes the crystallization rate accelerates again. According to the given explanation the availability of the atoms must increase again. Since time seems to be the dominating factor it could be imagined that a critical time must pass until the residual network is dissolved. This time might be needed to complete the breaking of a chemical bond. Since many bonds are attacked at the same time, they also break simultaneously and the atoms are released to form crystals. The observed trends are valid for both augite and albite. This supports the given

explanations because they refer only to the undercooled melt and not to a certain crystalline phase.

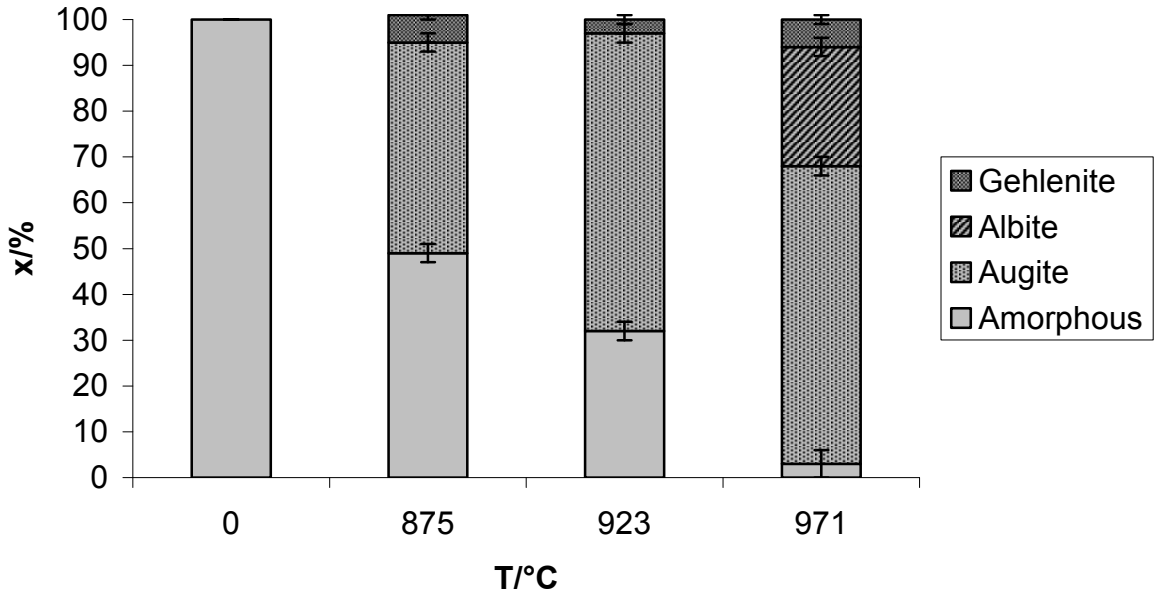

Figure 44: Phase composition x as a function of the temperature T of a heat treatment for 60 min (pre-heat treatment for 60 min at 684 °C)

Figure 44 shows the influence of the temperature of the heat treatment which is quite similar as an increase in its duration (see below), but also as an increase in the duration of the pre-heat-treatment: The amorphous percentage decreases. But here the cause is another one: Whereas the influence of the pre-heat treatment could be explained by the nucleation, here crystal growth is the decisive parameter. The crystallization rate increases with increasing temperature until a maximum which is probably at higher temperatures (Figure 4). Hence in the temperature range observed here increasing temperature decreases the amorphous amount. Albite is only present in the fibres heated up to the highest temperature (973 °C) which can be explained again by a change in the chemical composition of the matrix during the crystallization.

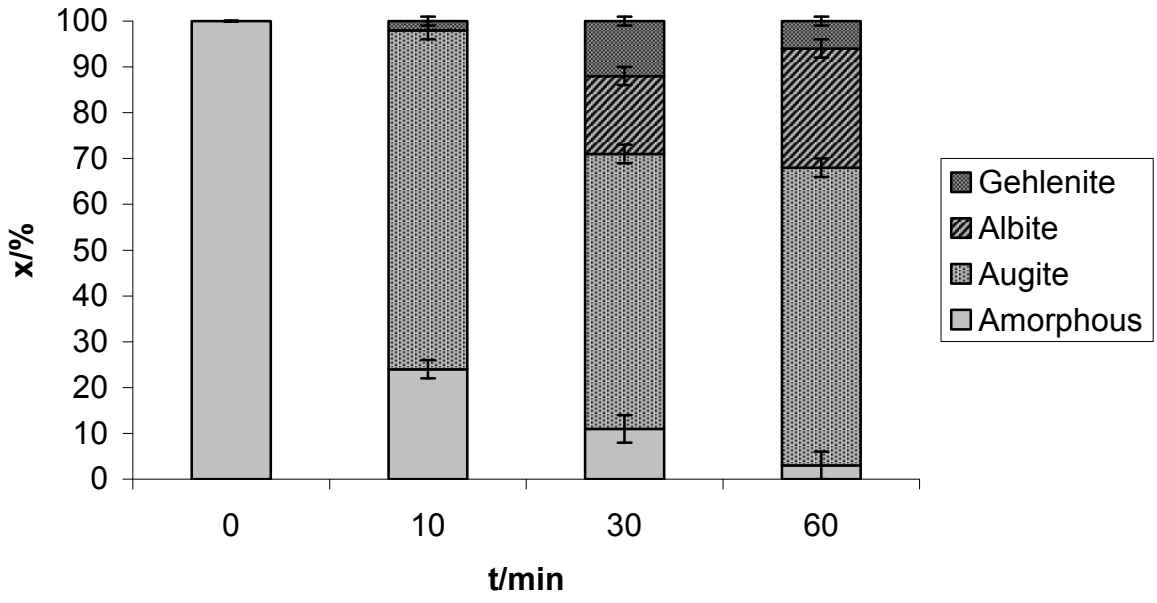

Figure 45: Phase composition x as a function of the duration t of a heat treatment at 971 °C (pre-heat treatment for 60 min at 684 °C)

An increase in the duration of the heat treatment has the same effects as an increase in its duration: The amorphous percentage decreases and the amount of albite increases. As discussed in the previous paragraph crystal growth has an influence on the amorphous amount. Whereas an increase in temperature increases the crystallization rate in this series the crystal growth proceeds by time at a constant temperature and a constant crystallization rate. But there is also one difference: The gehlenite content reaches a maximum for a medium duration whereas it is minimal for medium temperatures whereas the changes are not significant in Figure 44. It seems to dissolve partly for heat treatments of more than 30 minutes to the credit of albite. This might be interpreted in the following way: Albite incorporates Na and a smaller amount of K from the glassy matrix, Al which is also necessary for the albite crystallization lacks in the matrix. Hence it has to be dissolved from the gehlenite whose crystal structure therefore breaks down. In contrast to this in the sample 684-60-923-60 (Figure 44) the amorphous amount which contains much Al is larger; hence the gehlenite has not to be dissolved to provide the Al for the albite formation.

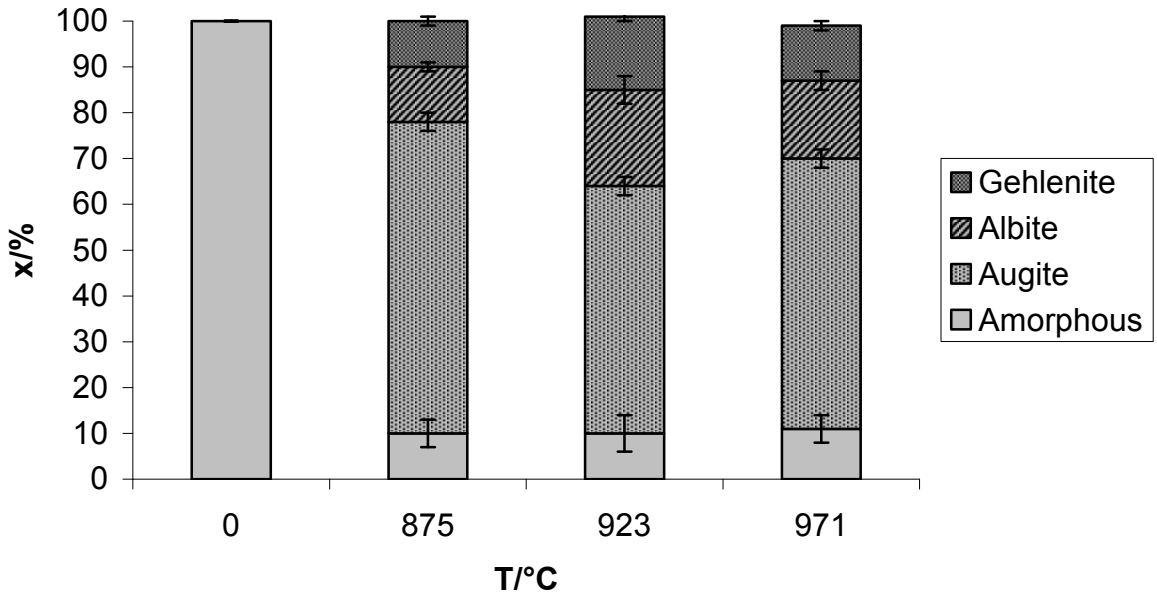

Figure 46: Phase composition x as a function of the temperature T of a heat treatment in 90 % N_2 + 10 % H_2 for 60 min (pre-heat treatment in air for 60 min at 684 °C)

Figure 46 is the first of a set of analyses made in a reducing atmosphere consisting of 90 % N_2 and 10 % H_2. The striking difference in comparison with the samples heat-treated in air is the independence of the amorphous percentage from the temperature of the heat treatment. It is interesting to remember that in contrast to this series the sample "untreated-971-60" maintains an amorphous percentage of 30 % whereas the sample "684-60-971-60" crystallizes almost completely. Since a pre-heat treatment at T_g enhances crystallization the fact that in a reducing atmosphere, however, no complete crystallization is reached in 684-60-971-60-H, might be interpreted by a smaller diffusivity of the sintered fibres which posess a denser structure. But the comparison between two samples that were heated continuously in air in the furnace normally used for the experiments in a reducing atmosphere shows that there is no difference in the amorphous amount between both atmospheres (Figure 47).

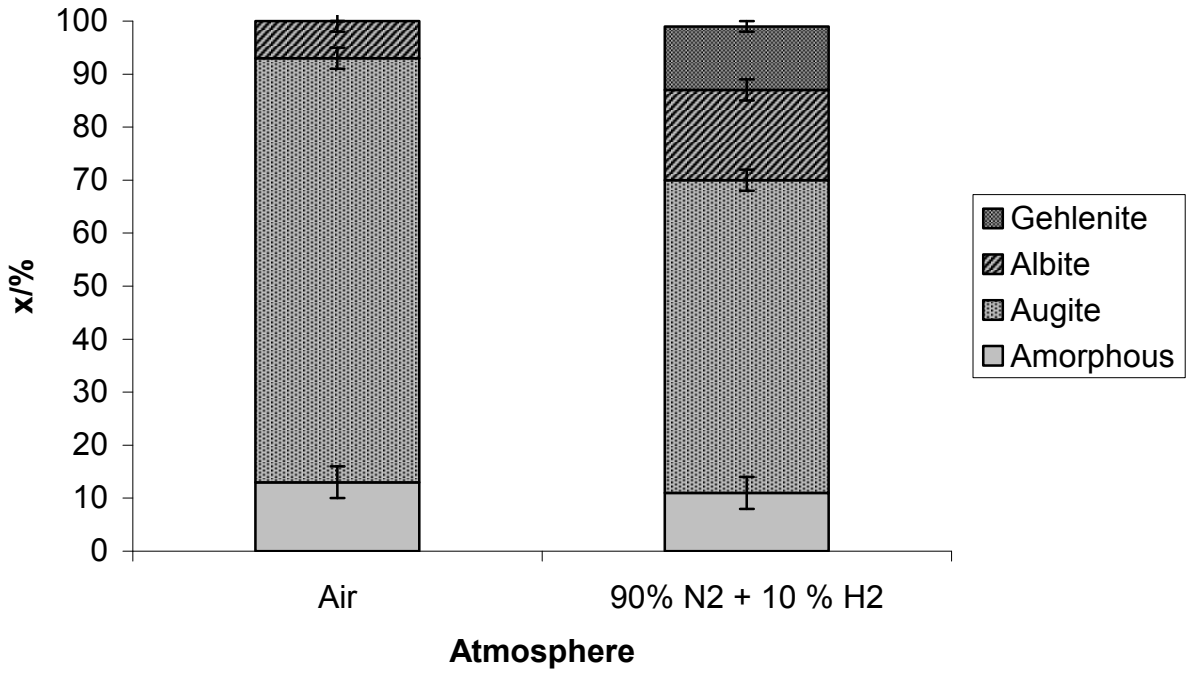

Figure 47: Phase composition x as a function of the atmosphere (pre-heat treatment in air for 60 min at 684 °C, heat treatment in the mentioned atmospheres for 60 min at 971 °C)

Since crystallization speed of undercooled melts at constant T depends on the diffusivity which depends on the structure and the temperature of the melt, the atmosphere does not seem to have any influence on these parameters. In a reducing atmosphere gehlenite and additional albite are formed to the account of augite compared with a heat treatment in air. The smaller amount of augite might be associated with a lack of trivalent iron which is needed to stabilize this mineral. Then the elements which are incorporated in the additional augite in air must be incorporated into another phase in a reducing atmosphere. Mg can be incorporated into gehlenite which forms as a new phase for this reason. Fe^{2+} can substitute for Ca in gehlenite. Ca, Al and Si can be incorporated into gehlenite and albite without any problems. From Figure 47 it can be concluded that the apparent difference between the samples 684-60-971-60 und 684-60-971-60-H concerning the degree of crystallization (3 vs. 11 %) does not result from the atmosphere but from the kind of heating. The maximum degree of crystallization is reached already below 875 °C, e.g. the crystallization temperature in a hydrogen-nitrogen-atmosphere is lower than in air (Figure 44) although augite forms in both cases. This might result from the sintering of the fibres in the reducing atmosphere. The second aspect is the change within the crystalline phases: Since the amorphous percentage remains constant, all the changes in the mineralogical composition result from different reactions between the crystalline phases at different temperatures. The problem is that data for short-time, low-

temperature heat treatments are missing. Hence the identity of the first crystals forming in a reducing atmosphere is not known. It is not clear, whether the sample heated at 971 °C had first the same composition as the sample heated at 875 °C and that this composition changed during the heat treatment. It might also be possible that the initial composition at the beginning of the crystallization is not observed in any of the samples and that from this composition all the other compositions developed. The latter possibility is more probable because the former implies that the composition of the sample heated at 875 °C remains constant after some minutes, which contradicts the results observed in Figure 48. The leads to the following theory: The trend of Figure 46 does not tell anything about an order of crystallization. What can be seen is predominantly the result of thermodynamics and only to a minor amount of kinetics. Gehlenite and albite have there stability maxima in the range of 923 °C. At lower and higher temperatures they dissolve into augite. A last interesting point is the fact that the samples rich in gehlenite shrink more than the others. But it is not clear if the gehlenite formation occurs before or after the shrinking. Hence a causal relation cannot be postulated.

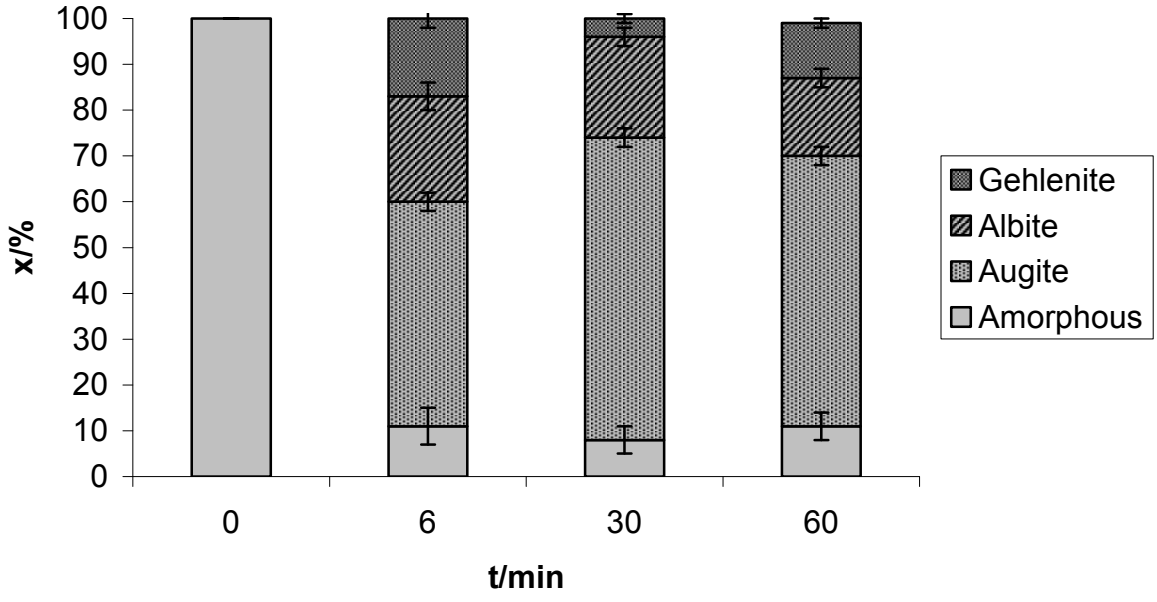

Figure 48: Phase composition x as a function of the duration t of a heat treatment at 971 °C in 10 % H_2 + 90 % N_2 (pre-heat treatment for 60 min at 684 °C)

As for a variation in temperature also for the variation in time the amorphous amount is constant at 10 %, when the heat treatment is performed in a reducing atmosphere. The constant amorphous percentage in this series means that the crystallization is a very fast process which occurs during few minutes. The remaining amorphous percentage can be

interpreted again as the result of the smaller diffusivity of the sintered fibres. Increasing duration increases the content of augite and decreases the content of albite whereas the gehlenite percentage reaches a minimum for the medium duration (30 min) at 5 %. This can be interpreted as dissolution of albite to the favour of augite, which means that the latter is the more stable phase at 971 °C. The same interpretation can be used for the initial decrease of gehlenite to the favour of augite and for the following dissolution of albite to the favour of gehlenite.

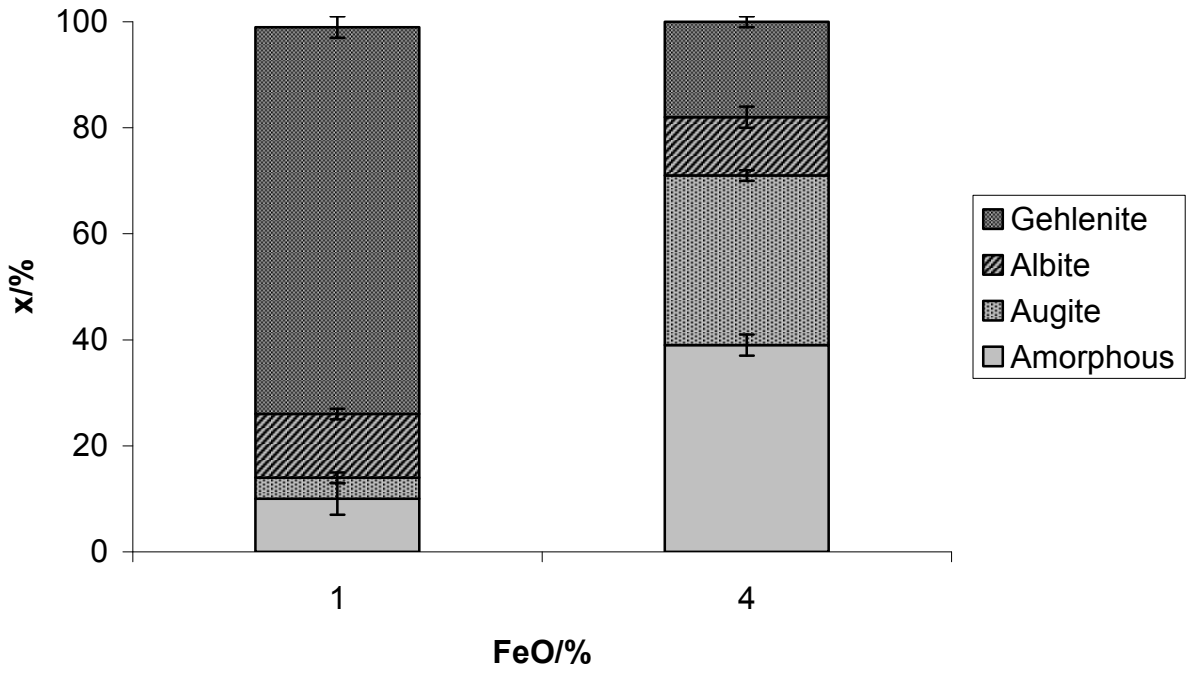

Figure 49: Phase composition x as a function of the FeO content, single heat treatment for 60 min at 884 °C

A decrease in the iron content leads to an increase in the formation of gehlenite and to a decrease in the amount of augite whereas the amorphous percentage whereas the albite content remains constant. Augite is the only present phase that contains significant amounts of iron. Therefore the augite content decreases with decreasing iron content. The Ca content of the fibres with 1 % FeO (white fibre) is higher than that of the fibres richer in iron (mixed fibre) (Table 1). This Ca can be incorporated better into gehlenite than into albite. Therefore the gehlenite content increases wheras the amount of albite remains constant. The oxidation of iron is the main reason for the surface crystallization. From the variation of the temperature of the pre-heat treatment it is known that the amorphous amount is the smallest for a pre-heat treatment at T_g (Figure 40). This was explained by the formation of the surface layer and its role as a heterogeneous nucleus. According to this theory a small iron content should lead to

less surface crystals and to a higher amorphous rest after the heat treatment. The opposite is the case. It might be an idea that the oxidation of iron which is associated with a conversion from a network modifier to a network former strengthens the glass network and thereby increases the amorphous amount. A problem in this work is that the heat treatments in air and in a reducing atmosphere were conducted in different furnaces. The most important difference was that for the heat treatment in air the samples was put into and removed from the hot furnace whereas they remained in the furnace during the heating and cooling process in the reducing atmosphere. Therefore one sample was heated in air using the hydrogen furnace and the heating technique used for the heat treatment in the reducing atmosphere to check if the heat treatments in both furnaces are comparable:

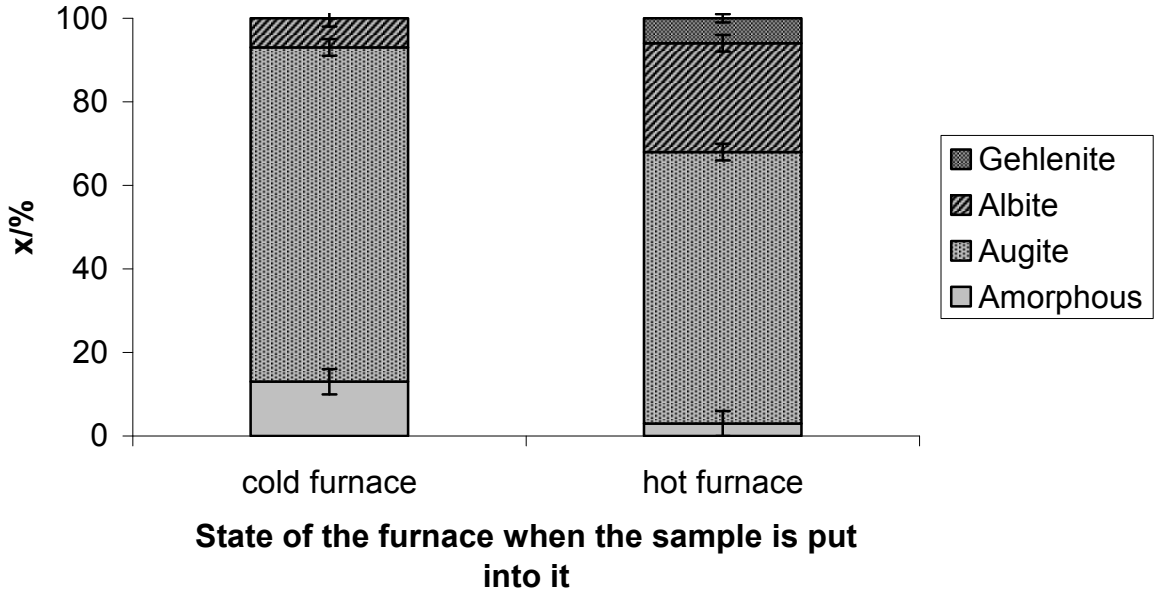

Figure 50: Phase composition x as a function of the kind of heating during the heat treatment (pre-heat treatment for 60 min at 684 °C, heat treatment for 60 min at 971 °C, in case of the cold furnace the standing time at 971 °C is meant)

If the sample is inserted into the cold furnace and is left there during the whole heating and cooling process, the mineralogical composition is different from that of a sample which is put into and removed from the hot furnace: The amorphous percentage and the augite content are higher for continuous heating whereas the concentration of albite is lower and no gehlenite forms any more. The explanation for this behaviour might be that the metastable glassy state can survive if no shocks occur. For example undercooled water remains stable in a cup as long as nobody touches it. The shake the cup suffers when it is touched makes the water freeze. In this case the shock is a thermal one and not a mechanical one. But the effect is the

same: The heating shock makes the sample crystallize. The reason for the formation of gehlenite and albite is the bulk chemistry of the sample which is out of the augite range. Two more samples were investigated by XRD: one sample which was continuously heated in air up to 1100 °C to simulate the process in the DSC, another sample was the sieve remainder from the first step of the sample preparation.

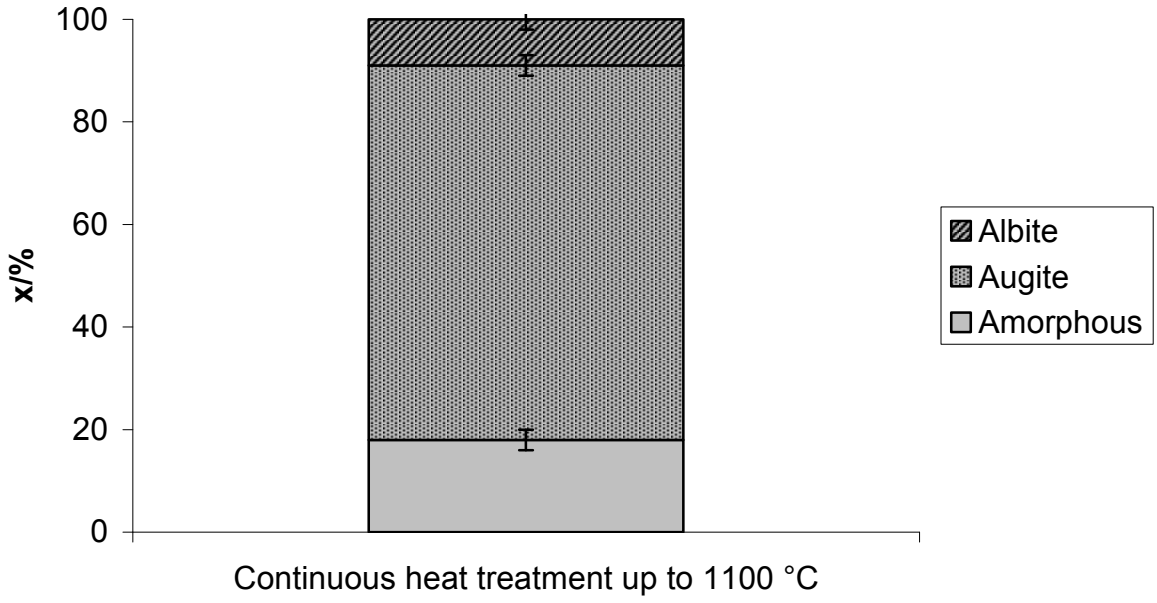

Figure 51: Phase composition x of stone wool fibres pre-heated for 60 min at 684 °C and heat-treated continuously up to 1100 °C.

The amorphous amount is much larger than for a sample which was faced to abrupt heating at 971 °C (Figure 46). This supports the thesis that without a thermal shock no complete crystallization of pre-heated stone wool fibres can be evoked. The sieve remainder was found to be completely amorphous. Since no chemical analyses of the two sieve fractions were performed it remains unclear what the difference between them is.

5 Discussion

The idea of this chapter is to evaluate critically the results and their importance for science and application by identifying and estimating error sources (chapter 5.1) and by comparing them to the literature (chapter 5.2).

5.1 Evaluation of Results

The first group of error sources is formed by the pre-heat and by the heat treatments. It has to be considered that in this thesis 4 g of material were used to obtain good quantitative XRD results. The disadvantage of such a large amount of sample is an inhomogeneous heat distribution in the sample, especially because stone wool is a thermal isolator. It seems probable that for short heat treatments the temperature gradient within the sample might be several tens of degrees. A solution might be to use µ-XRD in the future. For the pre-heat treatments and the heat treatments in air another error source is the opening of the furnace after the insertion of the samples. It was observed that the temperature decreased by about 10 °C and it needed about 3 minutes until the temperature reached the old level again. The furnace used for the heat treatments in reducing atmosphere had a by 20 °C wrong temperature calibration according to previous experiences at Aalborg University. This was tried to be corrected by just choosing a temperature 20 °C above the wished temperature. However, there seems to be a large error source. Furthermore the times given for the heat treatments in reducing atmosphere do not include the heating and cooling process. This means that the measurements in air and in a reducing atmosphere are not comparable apart from Figure 47. Hence all temperatures of thermal treatments in this series should be seen as "x ± 20 °C". The next error occurred when some mg of the fibres were used for microscopic and thermoanalytic measurements. The fault was not to homogenize the sample before to eliminate the effects of the inhomogeneous heat distribution. Hence the samples chosen for all these measurements were not representative for the whole sample. The SEM-EDX results show so large variations of the chemical composition even in untreated fibres that they would have been worthless even then, if they had been performed on fresh cross sections instead of pre-existing ones. Furthermore scans across an edge are not suitable for SEM-EDX analyses because this technique needs a flat surface. The SEM-SE pictures are not representative for the whole sample because the amount needed for the analyses (few mg) was much smaller than the amount used for the pre-heat treatment (4 g). But even in this small amount there were large differences between the fibres. Hence a statistical evaluation of about 100 pictures

per sample might be an appropriate approach. The pictures lack sharpness which might be improved by embedding all the samples and by adding copper powder to the epoxy resin to increase the electrical conductivity which should avoid charging effects. The interpretation of the SEM pictures is very speculative. Information about the chemical composition of a single white particle is needed. Using a TEM technique called electron energy loss spectroscopy (EELS) might provide this piece of information in the demanded resolution. During the thermoanalytical measurements several handling errors (switching the gas off etc.) occurred which query strongly all these results. Furthermore the use of DSC to determine the number of crystalline phases is associated with the problem that during rapid heating several crystallization peaks might interfere. This is due to the fact that at higher heating rates the first phase has just started crystallizing when the temperature is reached where the second phase crystallizes. Hence the number of crystallization peak in the DSC might not be equal to the number of crystalline phases forming. Furthermore stone wool fibres with their large heat capacity and the bad thermal contact to the crucible are examples for bad measuring conditions. Under those conditions according to Höhne et al. (1996) a temperature error up to 10 °C can occur, especially when the heating rate is high. They mention also the possibility to correct partially thermal conductivity effects by using a similar reference material. In this work the two materials (a crystalline oxide and a glassy silicate) were very different from each other; hence additional errors might occur. Against the recommendations of Höhne et al. (1996) no second zeroline was measured after each series of measurements and the calorimeter was not pre-heated above the temperature of the following measurement before. The repeatability of the measurements was not satisfying which also finds expression in the calculated enthalpies of crystallization. Hence a calculation of a relative degree of crystallization (Moesgaard & Pedersen, 2005) would be too daring. The only piece of certain information derived from DSC and TG measurements are general temperature ranges where oxidation and crystallization take place. The bad repeatability might result from unequal masses of the crucibles, differences in the lids of the crucibles and from rests of old fibres in the crucible. XRD results were presented with an error given by the Rietveld program AutoQuan which was normally about 2 % which is the best achievable value (Allmann, 2003). But it has to be considered that the Rietveld refinement refers to a texture-free sample. But it seems probable that the crystallographical orientation of crystals which form in fibres is somehow related to the orientation of the fibres. Since the diameter of the fibres (2 – 5 µm) is a bit smaller than the median particle size (4 – 6 µm) (Figure 38), they might have a preferred orientation in the sample holder. This might lead to a preferred orientation of the crystals, too.

This might lead to a larger error than the given one. This hypothesis is supported by some "wrong" intensity distributions between peaks at low and high angles. Furthermore the samples were homogenized during the preparations which increased the representativity compared to the results from all the other methods. As a conclusion it can be said that in spite of possible texture in the samples the XRD data have the highest reliability of all the data from thesis. Furthermore, in contrast to the other results, they give some really new information.

5.2 Comparison with Literature Data

The change in colour during the heat treatment might result from the diffusion of hyrdrogen into the fibres which could have led to a reduction of ions down to the native state or to the reaction with optical defects (Shelby, 2005). Since iron occurs already as Fe^{2+} in stone wool (Kirkegaard & Korsgaard, 2004) and since the concentration of Ti is very slow (Table 1) the reduction of iron to its native state might be explanation although it seems very doubtful that 5 % Fe can be incorporated in the remaining 10 % glassy matrix after the crystallization which would be necessary because no crystalline metallic phase was found (chapter 4.3.1). The oxidation temperatures found in this thesis are in the range of those observed by Kirkegaard & Korsgaard (2004). The sintered fibres that could be seen in the SEM analyses of fibres pre-heated at 1.2 T_g are in agreement of the statement of Kirkegaard & Korsgaard (2004) that sintering takes place above 1.1 T_g.

XRD analyses of stone wool fibres were already performed by Kirkegaard, L. & Korsgaard, M. (2004). They used fibres which were pre-heated for 44 hours at T_g and untreated fibres and heated them up continuously to 1100 °C in air and in argon. Afterwards they determined the crystalline phases qualitatively. They found diopside and anorthite in the un-pre-heated fibres after a heat treatment in argon and only diopside in the three other samples. Augite (calculated formula $Ca_{0.69}Fe^{2+}_{0.21}Fe^{3+}_{0.11}Mg_{0.91}Al_{0.08}[Al_{0.19}Si_{1.81}O_6]$) is only a solid solution of diopside ($CaMgSi_2O_6$), hedenbergite ($CaFeSi_2O_6$), clinoenstatite ($Mg_2Si_2O_6$) and clinoferrosilite ($Fe_2Si_2O_6$), hence the crystallographic identification is similar. But the formula chosen in this thesis was calculated from the chemical composition and seems more probable than a pure diopside. This was also supported by the peak positions. Estrup et al. (2006) found also augite in a bulk glass with Rockwool composition. In contrast to this anorthite would reflect the chemical composition better than albite, but the peak position was less suitable. For this reason it might be good to talk about plagioclases instead of talking about the end members

albite and anorthite. In this thesis no heat treatments in argon were performed; hence no data can be compared. A comparison between the data from the fibres heat treated in air, it shows that additional albite and sometimes gehlenite were found here. The differences between this work and that of Kirkegaard & Korsgaard (2004) is that in the former case the heat treatment was discontinuously and in the latter continuously. However, also in this thesis the sample 684-60-1100-cont was heated continuously, but the time of the pre-heat treatment was with one hour much shorter than the 44 hours. Hence it can not be said if the presence of albite only occurs under the conditions chosen in this thesis or if it could not be identified in the other work. Burkhard (2000) also found pyroxenes in plagioclases in heat-treated natural basaltic glass with a similar composition like Rockwool® HT fibres. She also observed similar crystallization temperatures. In contrast to Augustesen (2005) who found nepheline ($(Na,K)[AlSiO_4]$), periclase (MgO) and cristobalite (SiO_2) in HT fibres after a heat treatment at 1000 °C these phases could not be identified in this thesis. Moesgaard & Pedersen (2005) found that after a pre-heat treatment for two hours at 860 °C and a continuous heat treatment up to 1000 °C the amorphous amount according to XRD analyses is 22 %. In this thesis the sample 875-60-971-60 has an amorphous percentage of 27 ± 2 % which is in the same range. Moesgaard & Pedersen (2005) identified only one crystallization peak in the DSC between 910 °C and 930 °C depending on the duration of the heat treatment, which was performed at 860 °C. This agrees with the findings of this work. Pakosch (2006) studied the influence of the temperature and observed that an oxidation for more than two hours at 691 °C led to the development of a crystallization peak at 830 °C in the DSC diagram. This is in the same range as the onset temperatures found in this work. In contrast to Pakosch (2006) it could not be found in this thesis that increasing the temperature of the pre-heat treatment up to 836 °C increased the crystallization temperature up to 941 °C and led to sharper and higher crystallization peaks in the DSC diagram. It could also not be confirmed that the crystallization temperature decreases by 50 °C continuously when the duration of the pre-heat treatment increases from 5 minutes to 4 hours at 691 °C (Pakosch, 2006). Furthermore the second crystallization peak for pre-heat treatments up to 30 minutes between 780 °C and 800 °C (Pakosch, 2006) could not be found in this thesis. A second crystallization peak at 827 °C after a pre-heat treatment of 5 minutes at 739 °C might correspond to the small side peak found in this thesis at 880 °C. Furthermore it could not be confirmed clearly that the crystallization temperature is lower in argon than in air. In contrast to this there is an agreement that no shoulder peaks occur in argon. However, the general temperature range where the crystallization takes place is in agreement with Pakosch (2006), but also with

Andersen et al. (2006). Finally the results of the identification of the crystalline phases shall be compared with a phase diagram (Figure 52):

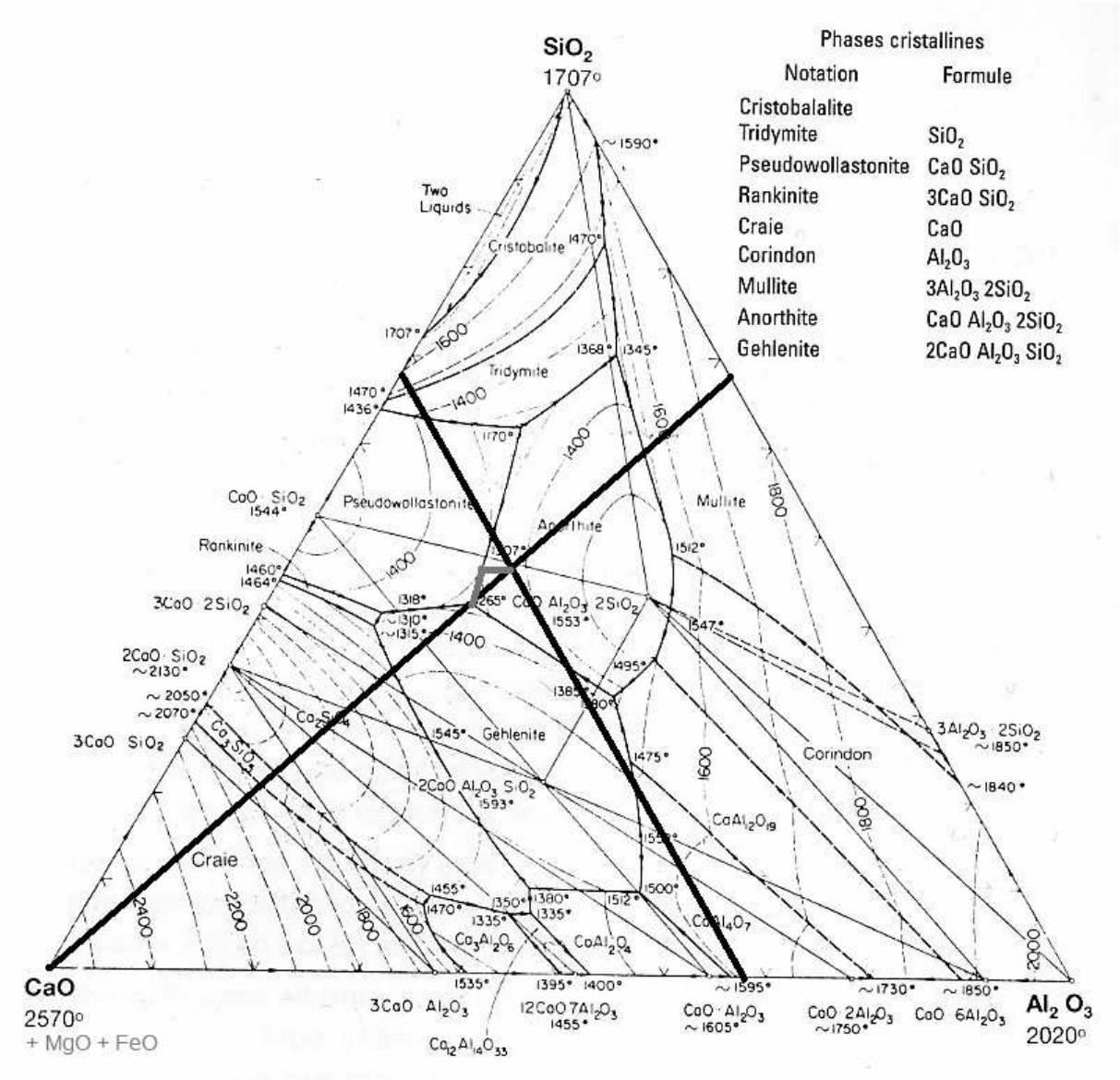

Figure 52: Phase diagram CaO-Al2O3-SiO2 with the chemical composition of stone wool fibres where CaO, MgO and FeO are concluded to CaO (modified after Osborn & Muan, 1960)

It can be seen that the approximation of the real chemical composition by a three-components phase diagram can give some explanation for the mineralogical assemblage. Considering all divalent ions as Ca the chemical composition of HT Rockwool® fibres can be inserted into this phase diagram which can explain the order in which the different phases crystallize from a melt. In this thesis the crystallization occurs far below the melting point, hence the order can not be used, but the composition which should be anorthite + pseudowollastonite + gehlenite according to the phase diagram. The presence of Na and K explains why anorthite is replaced

by albite, the presence of Mg and Fe causes the formation of augite instead of pseudowollastonite ($Ca_2Si_2O_6$).

5.3 Relation between the Crystalline Phases and the High-Temperature Stability

Finally the relation between the crystalline phases and the shape stability at high temperatures shall be discussed. Both a pre-heat treatment and a reducing atmosphere decrease the amount of augite. But the former increases the high-temperature stability whereas the latter decreases it. Hence the augite content is independent from the high-temperature stability. On the one hand both a reducing atmosphere and a decreasing amount of FeO increase the gehlenite content and decrease the shape stability. On the other hand a pre-heat treatment increases both the gehlenite content and the high-temperature stability. Hence the gehlenite content is independent from the high-temperature behaviour. Both a pre-heat treatment and a reducing atmosphere increase the albite content, but the former increases the high-temperature stability whereas the latter decreases it. Hence also the albite content is independent from the shape stability. This means that the whole phase composition is independent from the high-temperature stability.

6 Conclusion

In this thesis the crystallization behaviour of stone wool fibres was investigated using a two-step heat treatment. The consequences of its first step which was conducted around T_g are an oxidation of iron between 500 and 700 °C and the formation of surface crystalls. The effect of its second step which was performed above T_g was the bulk crystallization of the fibres. The mineralogical assemblage which forms is augite ± albite ± gehlenite. The latter two form especially for higher temperatures of the heat treatment, lower iron contents and longer durations of both the pre-heat and the heat treatment. If the second heat treatment is conducted in a reducing atmosphere or in argon they sinter and become black. This can be prevented partially in argon, but not in a reducing atmosphere by a pre-heat treatment. However, the sintering has no effect on the amorphous amount which is independent from the redox conditions, but decreases with increasing duration of both the pre-heat and the heat treatment and with increasing temperature of the heat treatment. The former effect is based on nucleation, the latter two on crystal growth. A pre-heat treatment above or below T_g increases

the amorphous amount because less surface crystals form before the bulk crystallization and can act as nuclei afterwards.

7 Further Experiments

This thesis provides basic knowledge about the crystalline phases which form in thermally treated stone wool. In the future additional work can be done to close the gaps which remain after this study. The pre-heat treatment should be performed in the future with a "denser" experimental design, e.g. with more different durations and temperatures. It should also focus on the ranges that have turned out to be most interesting by this thesis:

Table 16: Proposal for further pre-heat treatments

	0.9 T_g = 588 °C	0.95 Tg = 636 °C	1.0 T_g = 684 °C	1.05 T_g = 732 °C	1.1 T_g = 780 °C
15 min					
30 min					
45 min					

To improve the comparability of DSC and XRD results μXRD should be applied which allows smaller amounts of samples. Hence the second heat treatment could be replaced by a DSC measurement and the sample could be used afterwards for μXRD. This would add the quantitative information to the qualitative one which was won by Kirkegaard & Korsgaard (2004). Then these results could be compared with those from this thesis concerning the influence of the sample amount during the heat treatments and of the difference between continuous heating during a DSC and the abrupt heating in the furnace on the phase composition. The DSC measurement could be performed up to different temperatures (1.1 Tg = 780 °C, 1.15 Tg = 828 °C, 1.2 Tg = 875 °C, 1.25 Tg = 923 °C, 1.3 Tg = 971 °C) which should be held for different times (0 min, 5 min, 10 min 15 min, 20 min). The TEM measurements in Risø might provide some more information about the chemical composition of the surface crystals when a TEM-EDX or the electron energy loss spectroscopy (EELS) is applied.

8 Acknowledgement

There are several people who supported this work and who shall be mentioned therefore here: First of all Yuanzheng Yue (Aalborg University) and Gerhard Heide (TU Bergakademie Freiberg) who supervised this project. Furthermore I would like to thank Dorthe Lybye (Rockwool International A/S) for the general scientific support, Reinhard Kleeberg and Gerhild Landers (TU Bergakademie Freiberg) for the help with the XRD measurements and Xiaoxu Huang and Gitte Christiansen (Risø National Laboratory) for the TEM measurements which shall still be performed.

References

Allmann, R. (2003): Röntgenpulverdiffraktometrie: rechnergestützte Auswertung, Phasenanalyse und Strukturbestimmung. 2. Auflage. Berlin u.a. Springer-Verlag. ISBN 3-540-43967-6.

Augustesen, M. (2005): High-temperature properties of mineral wool. Master thesis. Aalborg University.

Andersen, R.; Bobach, C.; Mogensen, M.; Rosendahl, M. (2004): Betydningen af MgO-nanokrystallag for krystallisering og dermed varmebestandighed af HT-Rockwoolfibre. Project Paper. Aalborg University.

Askeland, D. (1996): The Science and Engeneering of Materials. Third Editon. Chapman & Hall. Oxford. ISBN 978-0748740833.

Becker, W.; Kleinsmith, L.; Hardin, J. (2003): Guide to Microscopy. Benjamin Cummings. San Francisco. ISBN 0-8053-4869-7.

Burkhard, D. (2001): Crystallization and Oxidation of Kilauea Basalt Glass: Processes during Reheating Experiments. In: Journal of Petrology. Vol. 42. No. 3, pp. 507 – 527.

Deutsches Insitut für Normung e.V. (2001): DIN 1259: Glas. Teil 1: Begriffe für Glasarten und Glastypen. Berlin.

Estrup, M.; Jensen, M.; Kristjansson, M.; Smedskjær, M. M.; Stougaard, A. (2006): Effect of High Temperature Treatment of a Basaltic Bulk Glass on Hardness and Crystallization Degree. Project Paper. Aalborg Universitet.

Götze, J. (2006): Technische Mineralogie II – Massenprodukte. Skript zur Vorlesung. TU Bergakademie Freiberg.

Goldstein, J. et al. (1981): Scanning electron microscopy and X-ray microanalysis. Plenum Press. New York and London.

Heide, G. (2002): Zur Systematik nichtkristalliner Materialien. Habilitationsschrift. TU Clausthal. Accesible as pdf file in the internet: http://deposit.d-nb.de/cgi-bin/dokserv?idn=973329203

Höhne, G. Hemminger, W. & Flammersheim, H.-J. (1996): Differential Scanning Calorimetry – An introduction for Practioners. Springer-Verlag. Berlin. ISBN 978-3540590125.

Kelting, R. & Traut, S. (2004): Einführung in die Thermogravimetrische Analyse. Praktikumsarbeit. Universität Karlsruhe. Used as internet source under www.stud.uni-karlsruhe.de/~urv5/Thermogravimetrie.doc on 2008-03-30.

Kirk, C. (in preparation): Development of inorganic binder for stone wool fibres. Masters Thesis. Aalborg University.

Kirkegaard, L. & Korsgaard, M. (2004): Impact of redox state and pre-oxidation on diffusion, crystallisation, and high temperature behaviour of iron containing alumino-silicate glass fibres. Master Thesis. Aalborg University.

Kirkegaard, L.; Korsgaard, M.; Yue, Y.; Mørup, S. (2005): Redox behaviour of iron bearing glass fibres during heat treatment under atmospheric conditions. In: Glass Science and Technology. Vol. 78. No. 1. pp. 1-6.

Korsgaard, M. et al. (2001, unpubl.): Oxidation, diffusion and recrystallization in ferrous iron rich glass fibres.

Mackenzie, R. C. (1979): Nomenclature in Thermal Analysis, Part IV. In: Thermochimica Acta. Vol. 28. pp. 1 - 6.

Moesgaard, M. & Pedersen, H. (2005): Investigation of the Crystallization Process occuring in Stone Wool Fibres during High Temperature treatments. Project Paper. Aalborg University.

Moesgaard, M.; Pedersen, H.; Yue, Y.; Nielsen, E. (2007): Crystallization in stone wool fibres. In: Journal of Non-Crystalline Solids. Vol. 353. pp. 1101–1108

Navrotsky, A. (1995): Thermodynamic Properties of Minerals. In: Mineral Physics and Crystallography. A Handbook of Physical Constants. American Geophysical Union. http://www.agu.org/reference/minphys/5_navrotsky.pdf

Osborn, E.F. & Muan, A. (1960): Phase Equilibrium Diagrams of Oxide Systems. Plate 1, published by the American Ceramic Society and the Edwart Orton jr. Ceramic Foundation. Diagram found in: Shieldalloy Metallurgical Cooperation (1995): Synthetic Slags for Steelmaking http://www.metallurgvanadium.com/downloads/synthetic_slags.pdf

Pakosch, D. (2006): Impact of the pre-heat treatment on the crystallisation behaviour of iron containing alumino-silicate glass fibres. Student Research Report. Aalborg University.

Rietveld, H. M. (1969): A profile refinement method for nuclear and magnetic structures. in: Journal of Applied Crystallography. Vol. 2. pp. 65-71.

Rueda, D. R., Gutiérrez, M. C. García, Calleja, F. J. Baltá and Piccarolo, S. (2002): Order in the amorphous state of poly(ethylene terephthalate) as revealed by microhardness: Creep behaviour and physical aging. In: International Journal of Polymeric Materials. Vol. 51. Issue 10. pp. 897 – 908.

Shelby, J. E. (2005): Introduction to Glass Science and Technology. 2nd Edition. The Royal Society of Chemistry. Cambridge. ISBN 978-0854046393.

Sørensen, P. et al. (2005): Effect of the redox state and concentration of iron on the crystallization behaviour of iron rich aluminosilicate glasses. In: Journal of Non-Crystalline Solids, Vol. 351, pp. 1246 – 1253.

Vogel, W. (1992): Glaschemie. 3. Auflage. Springer-Verlag. Berlin, Heidelberg. ISBN 978-3540551713.

Wenk, H.-R.: (1976): Electron Microscopy in Mineralogy. Springer-Verlag. Berlin, Heidelberg, New York.

Yue, Y. Z.; von der Ohe, R.; Jensen, S. L. (2004): Fictive temperature, cooling rate and viscosity of glasses. In: J. Chem. Phys., Vol. 120, No. 17, pp. 8053 – 8059.

Young, R. A. (editor) (1995): The Rietveld Method. Oxford University Press. Oxford. ISBN 0198559127

Zachariasen, W. (1932): The Atomic Arrangement in Glass. In: J. Am. Ceram. Soc., Vol. 54, pp. 3841 – 3851.

http://www.mineralienatlas.de/lexikon/index.php/Melilith, used 2008-03-30.

Affidavit

Hereby I confirm that I produced this thesis without illegal help of others and without other sources than the mentioned ones; minds adopted from other sources directly or indirectly are marked as those.

Daniel Höllen

Eidesstattliche Erklärung

Hiermit versichere ich, dass ich die vorliegende Arbeit ohne unzulässige Hilfe Dritter und ohne Benutzung anderer als der angegebenen Hilfsmittel angefertigt habe; die aus fremden Quellen direkt oder indirekt übernommenen Gedanken sind als solche kenntlich gemacht.

Daniel Höllen

Edsvoren erklæring

Hermed forsikrer jeg, at jeg har udfærdiget dette speciale uden ulovlig hjælp fra andre mennesker og uden at benytte andre kilder undtagen de nævnte. Hvor direkte og indirekte ideer fra fremmede kilder er anvendt er dette markeret.

Daniel Höllen

Appendix

A Theoretical background of analytical techniques

A1 Scanning electron Microscopy (SEM)

The interaction of an electron beam with a piece of matter creates secondary electrons (SE), backscattered electrons (BSE), Auger electrons, characteristic and continuum x-rays, photons (including cathodoluminescence), electron-hole-pairs, lattice vibrations and electrons oscillations. Secondary electrons are loosely bound electrons from the outer shells which are released when inelastic scattering of the electron beam takes place (Goldstein et al., 1981). Inelastic means that the electrons loose a part of their energy in the sample (Wenk, 1976). The spatial resolution of a SEM-SE picture accounts for 5 nm, the penetration depth is 10 nm. The release of an electron from the inner shells leads to an excited state of the atom and to a subsequent emission of characteristic x-rays and Auger electrons. The characteristic x-rays can be determined both by energy-dispersive and wavelength-dispersive spectrometers (EDX and WDX). The energy and the wavelength of the x-rays are characteristic for a certain element and allow therefore a chemical analysis. The information volume of characteristic x-rays reaches up to a depth of some tens of µm. The deceleration of the electrons in the electric field of the atom creates the so-called Bremsstrahlung ("braking radiation"). In contrast to all these types where energy is transferred from the impacting electrons, 30 % of all electrons are scattered out as backscattered electrons from a 450 nm thick surface layer (Goldstein et al., 1981).

A2 Transmission electron microscopy (TEM)

The sample preparation of silicates for TEM measurements can be done by replicas, powder fragments and ion thinning devices. TEM measurements provide information about the crystal structure, twins, dislocations, precipitations and exsolution lamellae. The crystal structure can be seen due to the elastic scattering of the electrons on the atoms. Elastic means that the electrons do not loose any energy in the sample. Selected area electron diffraction (SAED) allows phase identification. Electron dark field and lattice-fringe microscopy are TEM techniques to investigate the structure of non-crystalline solids (Wenk, 1976).

A3 Thermogravimetry (TG) and differential scanning calorimetry (DSC)

Thermoanalytical methods are defined as “a group of techniques in which a physical property of a substance is measured as a function of temperature whilst the substance is subjected to a controlled temperature programme” (Mackenzie, 1979). In this thesis thermogravimetry (T_g) is used to investigate the oxidation and differential scanning calorimetry (DSC) to observe the crystallization of stone wool during a thermal treatment. In this chapter the fundamentals of both methods are explained.

During **Thermogravimetry (TG)** a sample is heated with a constant rate and the change in mass resulting from the release of gases is determined (Pakosch, 2006). Besides the vaporization also the oxidation, absorption, desorption, decomposition, sublimation and reduction of a sample can be measured. For TG analyses it is necessary that no phase transitions occur during the measurement. Applications of TG analyses are the investigation of the setting of cement where water reacts with the clinker phases, the determination of the ash content of coal and the determination of the Curie temperature (Kelting & Traut, 2004). In this work a so-called Simultaneous Thermal Analyses (STA) is used which is a combination of Thermogravimetry (TG) and Differential Scanning Calorimetry (DSC).

Parallely to the heat treatment in the two types of furnaces mentioned above the pre-heated fibres were also subjected to a thermoanalytical method called **differential scanning calorimetry (DSC)**. According to the International Confederation for Thermal Analysis and Calorimetry (ICTAC) this is “a technique in which the heat flow (power) to the sample is monitored against time or temperature, while the temperature of the sample, in a specific atmosphere, is programmed” (Höhne et al., 1996). In this work this method was chosen for the following reasons: For a deeper understanding of the crystallization process and the crystallization products in thermally treated stone wool both the crystallization temperature and the crystallization enthalpy are important. DSC analyses can provide both parameters without complicated sample preparation. By measuring a series of differently pre-heated samples the influence of both parameters on the crystallization temperature and the crystallization enthalpy could be investigated. The main idea is that changes which have already occured during the pre-heat treatment do not happen any more during a subsequent thermoanalytical measurement. Hence the progress of a pre-heat treatment in time and temperature should be reflected in a trend in the DSC signal.

There are two types of DSC machines, the heat flux DSC and the power compensation DSC (Höhne et al., 1996) among which in this work the former is used (Fig. 53):

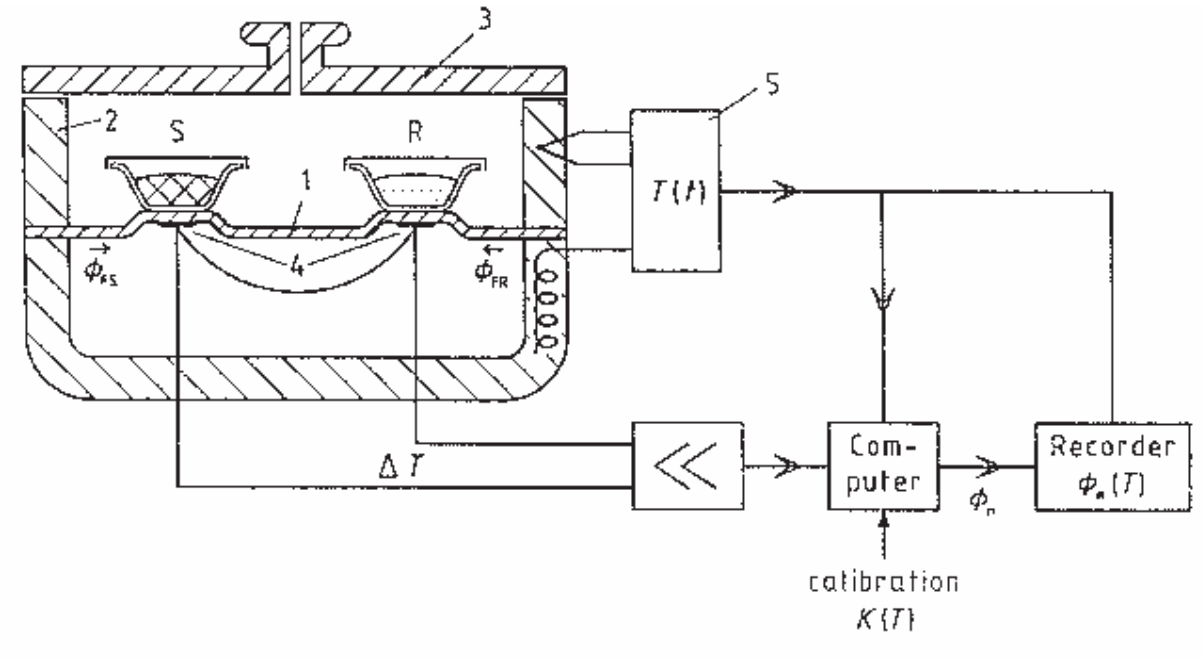

Figure 53: Scheme of a heat flow DSC. S: sample, R: reference, 1) disc where the heat flows from the furnace to the crucibles, 2) furnace, 3) lid, 4) temperature sensors, 5) controller system (Höhne et al., 1996)

A DSC works in the following way: During the measuring heat is transferred to both a sample and to the reference chamber. The two samples are arranged symmetrically to the disk which is used as transport medium for the heat. Therefore in the case of two identical samples the heat flow rates towards them should be identical. Practically the arrangement is not completely symmetrical, hence a zeroline is measured and subtracted from the measured data to correct this effect. If the samples are different, the heat flows to the sample, Φ_{FS}, and to the reference chamber, Φ_{FR}, are different. The difference of the heat flows, the heat flow rate Φ_m, is proportional to the temperature difference ΔT between the reference material (T_S) and the standard T_R) which can be measured as electrical voltage:

$$\Delta T = T_S - T_R$$

$$\Phi_m = \Phi_{FR} - \Phi_{FS} = -k' \bullet \Delta T$$

This calculation is done automatically by the computer. Hence the measurement signal output by the DSC is the heat flow rate Φ_m. This heat flow rate should be proportional to the reaction heat flow rate Φ_r which is needed to make a point about the energy consumed or released by the sample:

$$\Phi_r = -K \bullet \Delta T$$

K is a proportional constant which is given by the heat conduction path between the furnace and the samples. This relation is only valid for a constant heat flow rate (steady state). Furthermore there must not be any interaction between sample and reference sample, the devices of the instrument must neither consume nor release heat and no heat may leave the apparatus. A DSC measurement consists of preliminary and main measurements. First a baseline zero line has to be measured with an empty crucible. Then a reference material is measured and finally the sample. Figure 54 shows an endothermic peak with its characteristic parameters:

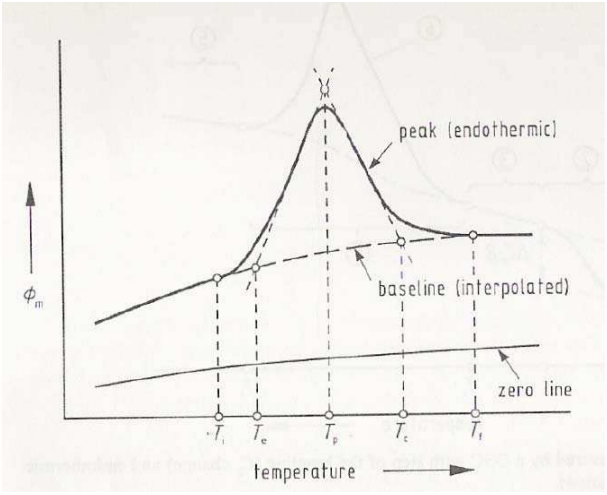

Figure 54: Characteristic features of a DSC diagram (Höhne et al., 1996)

Endothermic reactions like melting are characterized by positive DSC peaks whereas exothermic reactions like crystallization have negative peaks. A glass transition does not occur as a peak but only in a change of the shape of the curve. The term baseline means in Figure 54 the connection between the two basis points of a peak. The subtraction of this baseline removes the influence of the crucible and the apparatus from the signal. The peak contains five characteristic points. The initial peak temperature T_i marks the beginning of the peak, the extrapolated peak onset temperature T_e is the cross section of a straight line approximating the slope of the peak and the baseline. The peak maximum temperature T_p is defined as the point where the slope of the curve equals zero. The extrapolated peak completion temperature T_c and the final peak temperature T_f correspond to the analogous onset temperatures. DSC can be used in this work to determine the crystallization temperature and enthalpy. The area of a peak is the enthalpy of the associated chemical reaction. To calculate this area the baseline of the peak has to be determined. In this work a very simple

approach is used: The two maxima beneath the negative crystallization peak are connected with a straight line. However, there are more sophisticated methods: For irreversible transformations the measurements can be repeated with the used sample. In this case the difference area is the crystallization enthalpy. If the degree of reaction is known, mathematical solutions can be applied. From the crystallization enthalpy the degree of crystallization can be calculated. Other attempts base on an integration of the C_p curve (Höhne et al., 1996). The crystallization enthalpy which is released during a DSC measurement is always only a part of the theoretical crystallization enthalpy of the forming phase. This means that only a part of the whole sample crystallizes. Hence the percentage of the observed enthalpy on the theoretical enthalpy is the degree of crystallization. This method was compared with XRD and both methods were found to give similar results (Moesgaard & Pedersen, 2005).

A4 X-ray diffraction (XRD)

X-ray diffraction (XRD) is a method to identify a material by means of the parameters of its crystal lattice. Additionally XRD analyses were also performed for the samples after the pre-heat treatment to find out if there is a measurable amount of crystalline phases. XRD on the crystal lattice was discovered in 1912 by Friedrich, Knipping and von Laue and is used nowadays as a gentle phase identification method where the changes the sample undergoes remain smaller than in other methods like DSC. X-rays which are diffracted on different atomic planes of the crystal lattice can interfere if their phase difference equals a multiple of their wave length. The phase difference depends on the spacing d and the diffraction angle Φ between the incident ray and the scattering lattice planes. Hence a relation between the spacing d and the diffraction angle θ of the interference peak, Bragg´s law, can be deviated:

$$n \cdot \lambda = 2 \cdot d \cdot \sin\Theta$$

In x-ray powder diffraction analyses the diffraction angle is the measured parameter, the wave length of the X-rays is known (CoKα = 1.78901 Å). Hence all the d-values and therefore also the crystal structure can be calculated (Allmann, 2003).

In this work the quantification of the phases is done with the Rietveld program autoquan. The principle of this method is to describe all measured points of an X-ray powder diffraction pattern by analytical functions. The parameters of these functions are refined simultaneously by the root least squares method in order to fit the calculated pattern to the observed one. The

structural parameters are optimized simultaneously with the intensity distribution to the different overlapping peaks. By this method thousands the number of points is increased by the factor ten compared with an approach which only considers a single point per peak. The Rietveld method needs a starting model for the crystal structure. Starting from this model the parameters of the numerical peak profile functions (peak position, integral peak intensity, peak width at half height, peak flank shape and asymmetry) are fitted to the measured diffraction pattern (Allmann, 2003). Hence the method can also be called whole powder pattern fitting structure refinement (WPPSR) (Allmann, 2003; Young, 1995). For the fitting of the peak profile functions the parameters for the crystal structure (atom positions, overall temperature factor, anisotropic thermal factors, site-occupancy factors), but also those for the diffraction optics effects, instrumental factors and other specimen characteristics (transparency, amorphous amount, crystallite size, microstrain, preferred orientation) are refined. For phase quantification the simultaneous comparative refinement of the overall scale factors of the different phases is the most important step (Young, 1995). The starting model consists of a structural model and models for the refinement of the properties of the sample and the apparatus. After the selection of a starting model and the start parameters the order in which the parameters are decontrolled has to be determined. The first factor which should be refined is the scale factor mentioned above. A problem is that some parameters depend on each other. This mutual dependence is shown in a correlation matrix. If the correlation accounts for more than 97 % only one of the two parameters should be refined. Another problem is that the refinement might lead to local instead of to the global minimum of a certain parameter. Therefore the starting model must be sufficient good which can be tested by the choice and comparison of several different starting models. The fitting starts from the observation that every intensity at a certain diffraction angle is composed of a structural and a background component. Furthermore it can be said that the intensity distribution around a certain peak depends on three fundamental parameters: the intensity distribution of the incident X-rays, the apparatus-dependent factors like aperture openings and the size of the sample holder and sample-dependent factors like the absorption, the crystallite size and the lattice strain. Then the weighted sum of the squares of the deviations of the observed from the calculated intensity is minimized. The weighting factor is the reciprocal variance of the observed intensity under the assumption of a Gaussian distribution of the statistical intensity fault. The success of a Rietveld refinement can be evaluated by the residuals and by the difference plots (Allmann, 2003). Rietveld analysis was not invented for quantification of crystalline phases but in order to refine their nuclear and magnetic structure (Rietveld, 1969).

The precision of quantitative XRD measurements is maximal 2 %. The grain size of the samples should lie between 1 and 10 µm (Allmann, 2003).

B XRD Diagrams

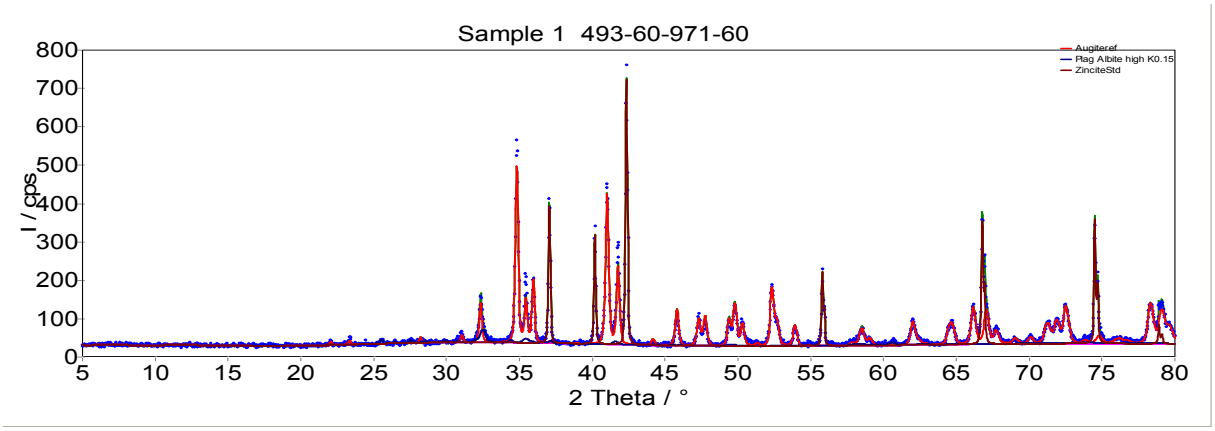

Figure A 1: XRD pattern of the sample 493-60-971-60

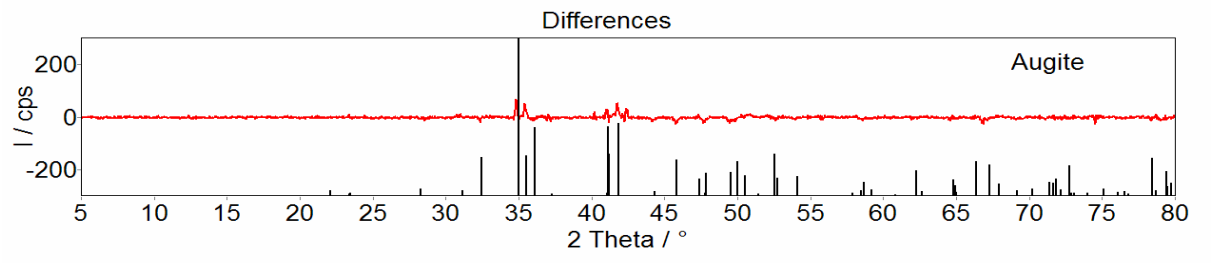

Figure A 2: Difference plot of the sample 493-60-971-60

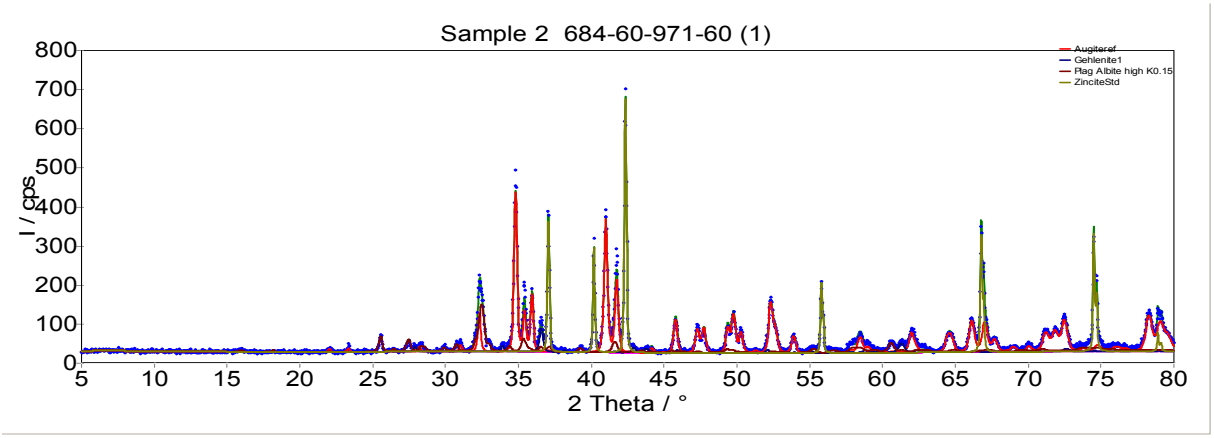

Figure A 3: XRD pattern of the sample 684-60-971-60 (1)

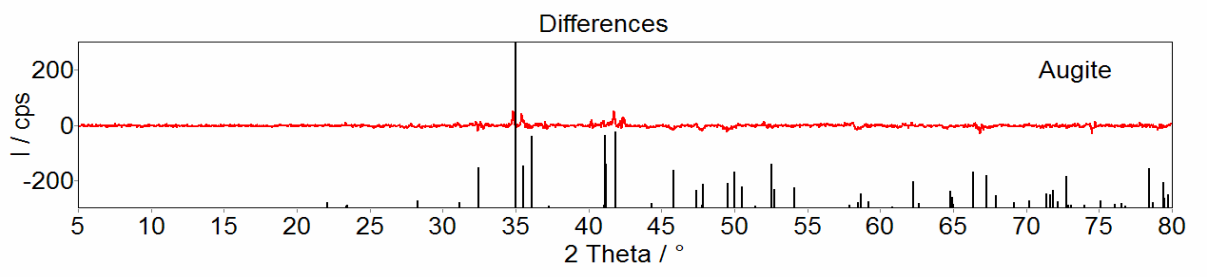

Figure A 4: Difference plot of the sample 684-60-971-60 (1)

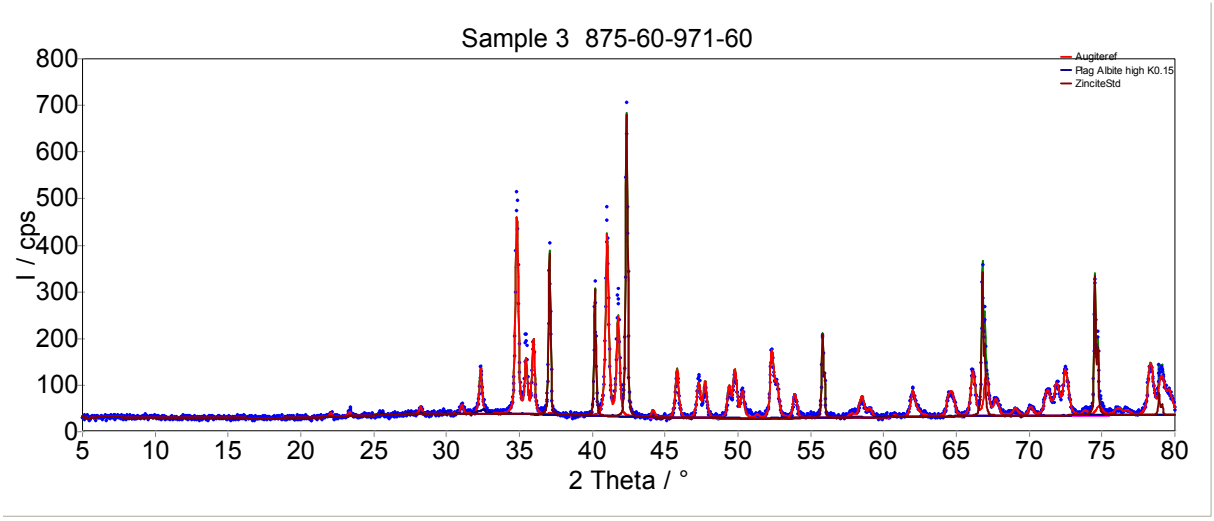

Figure A 5: XRD pattern of the sample 875-60-971-60

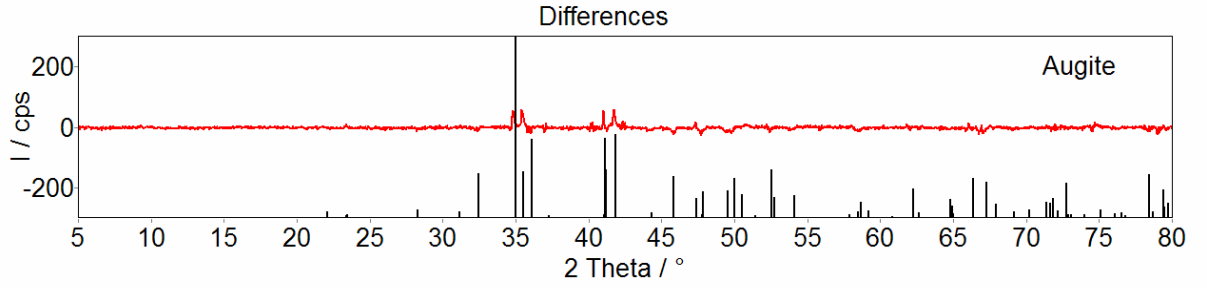

Figure A 6: Difference plot of the sample 875-60-971-60

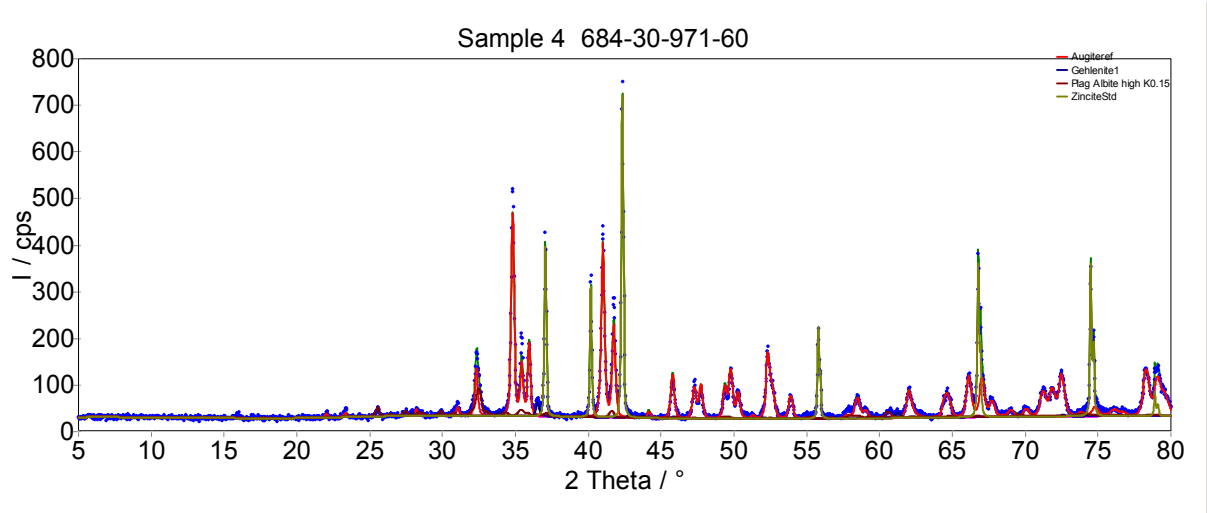

Figure A 7: XRD pattern of the sample 684-30-971-60

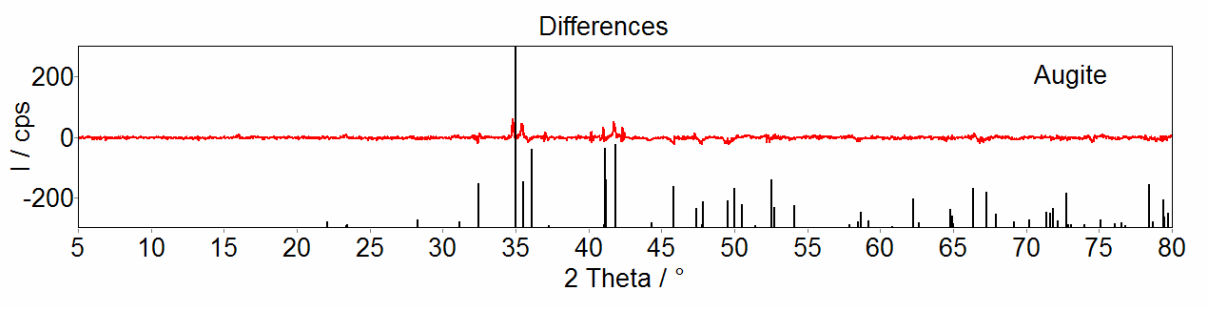

Figure A 8: Difference plot of the sample 684-30-971-60

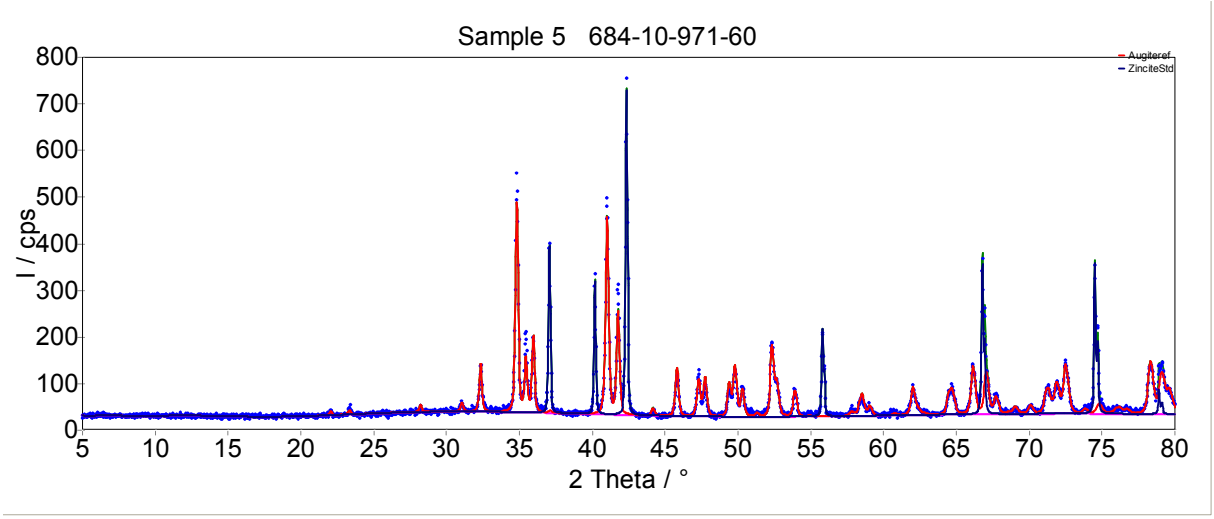

Figure A 9: XRD pattern of the sample 684-10-971-60

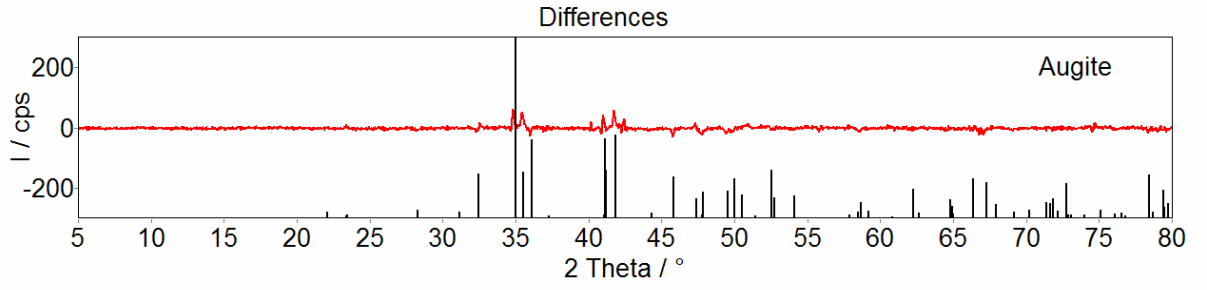

Figure A 10: Difference plot of the sample 684-10-971-60

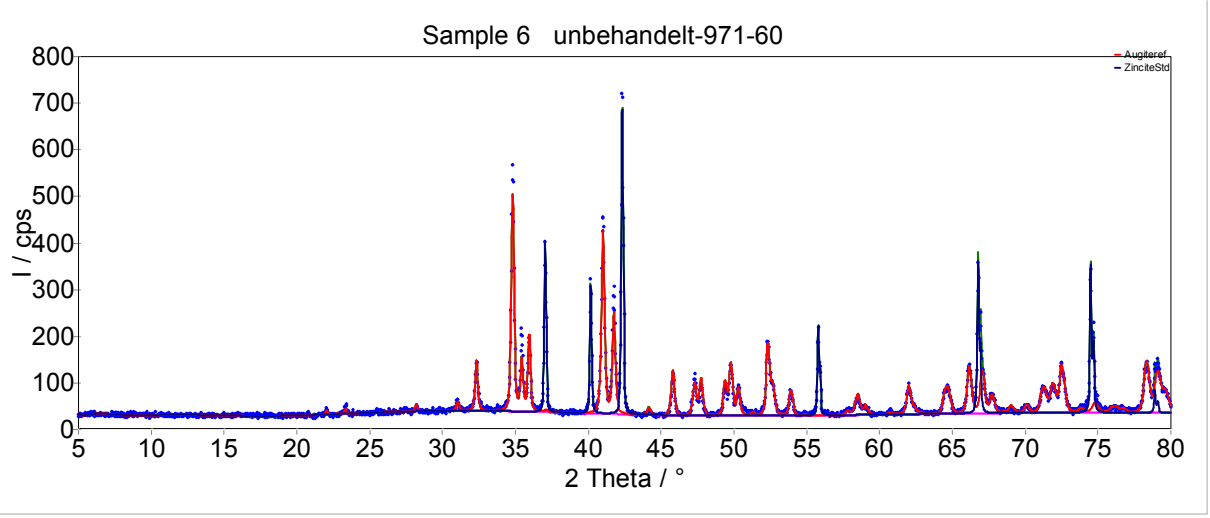

Figure A 11: XRD pattern of the sample untreated-971-60

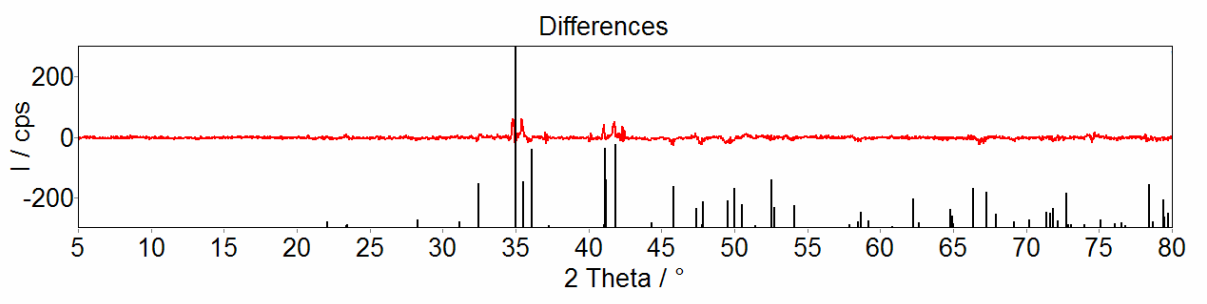

Figure A 12: Difference plot of the sample untreated-971-60

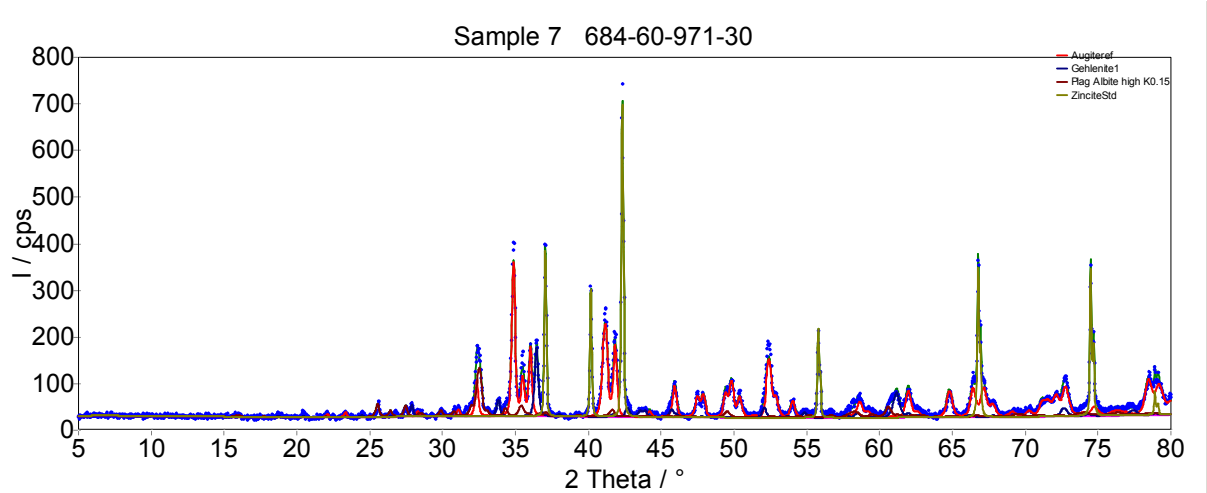

Figure A 13: XRD pattern of the sample 684-60-971-30

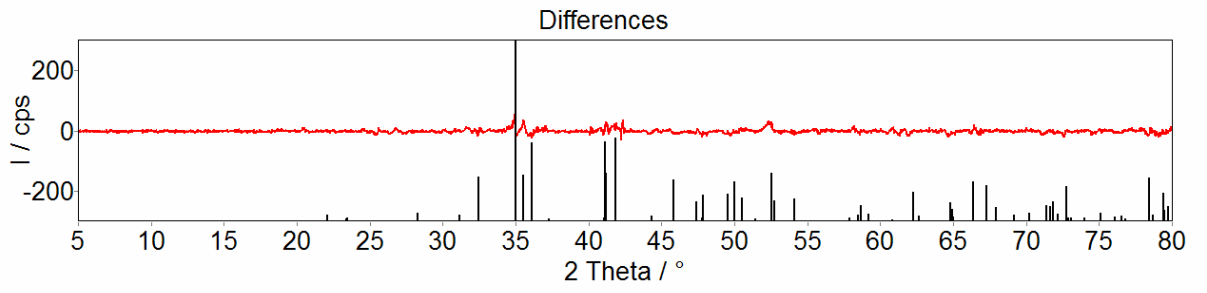

Figure A 14: Difference plot of the sample 684-60-971-30

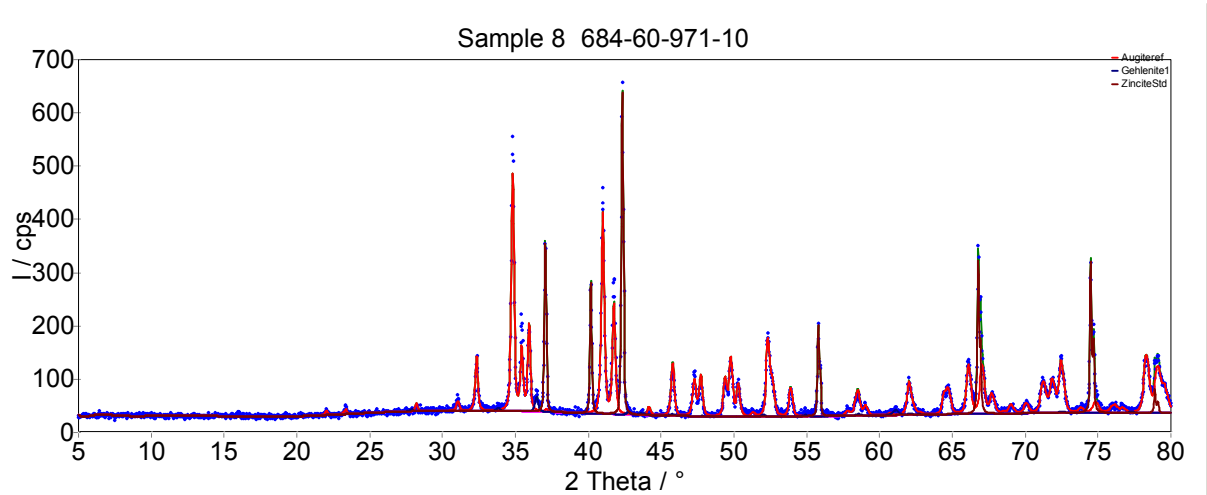

Figure A 15: XRD pattern of the sample 684-60-971-10

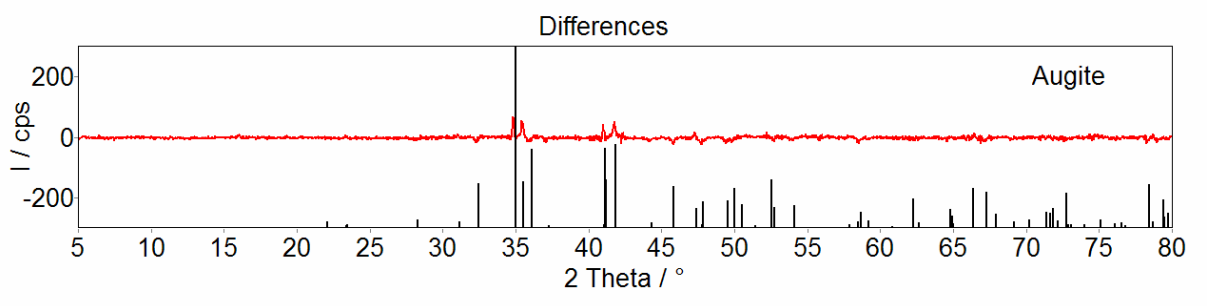

Figure A 16: Difference plot of the sample 684-60-971-10

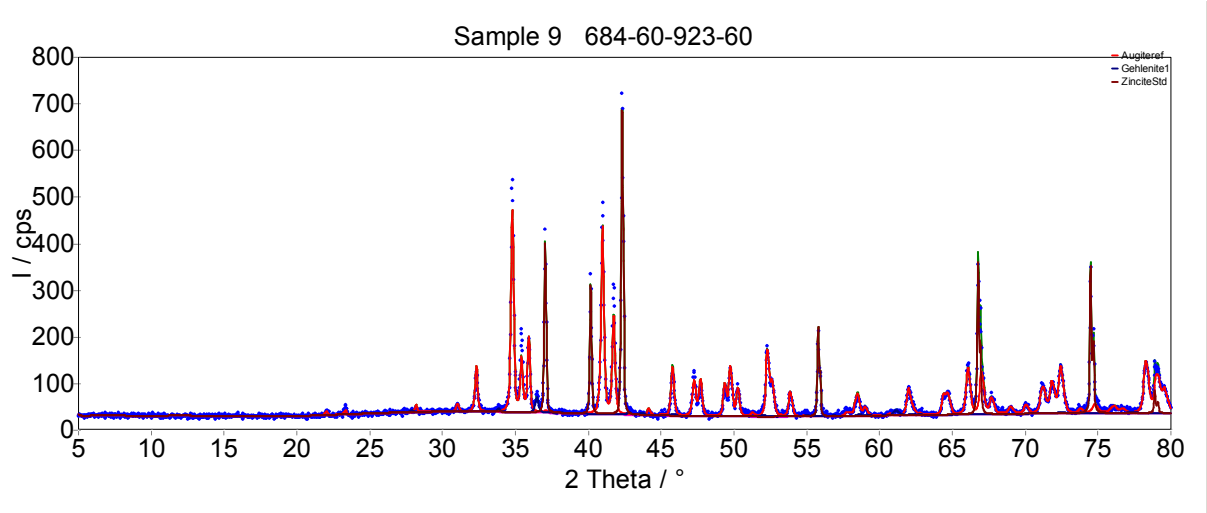

Figure A 17: XRD pattern of the sample 684-60-923-60

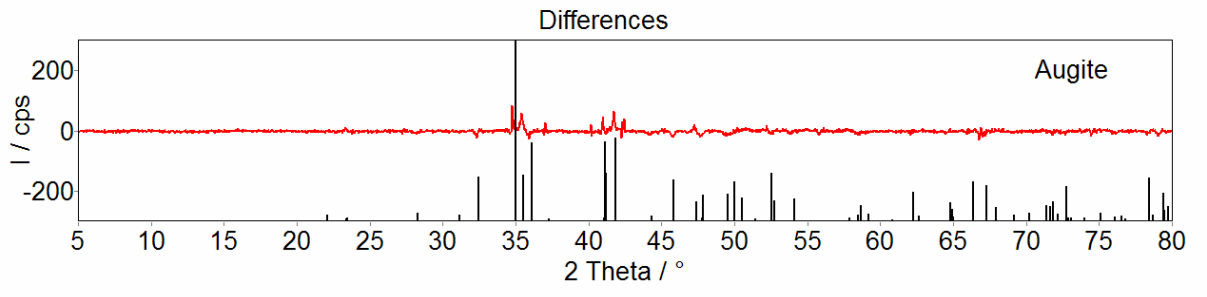

Figure A 18: Difference plot of the sample 684-60-923-60

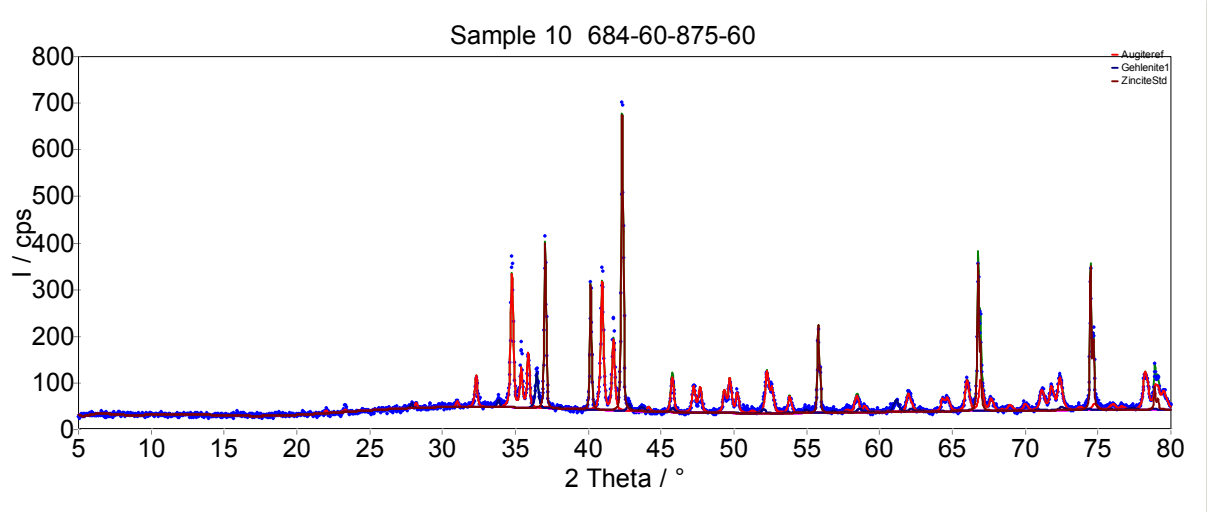

Figure A 19: XRD pattern of the sample 684-60-923-60

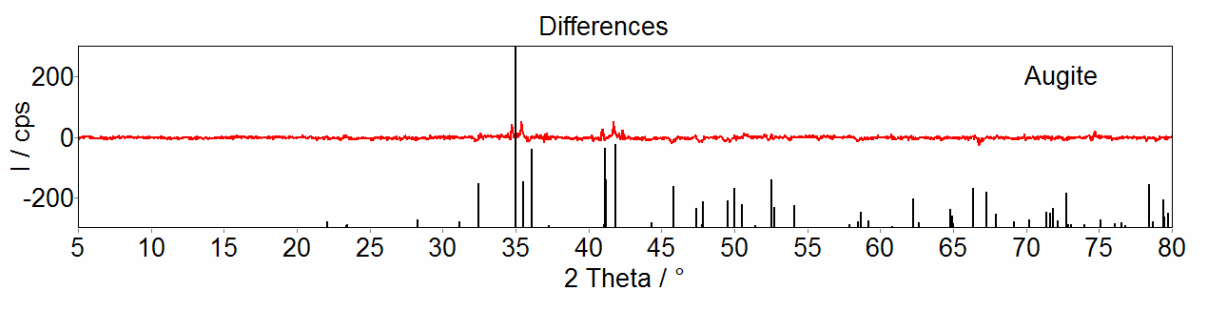

Figure A 20: Difference plot of the sample 684-60-923-60

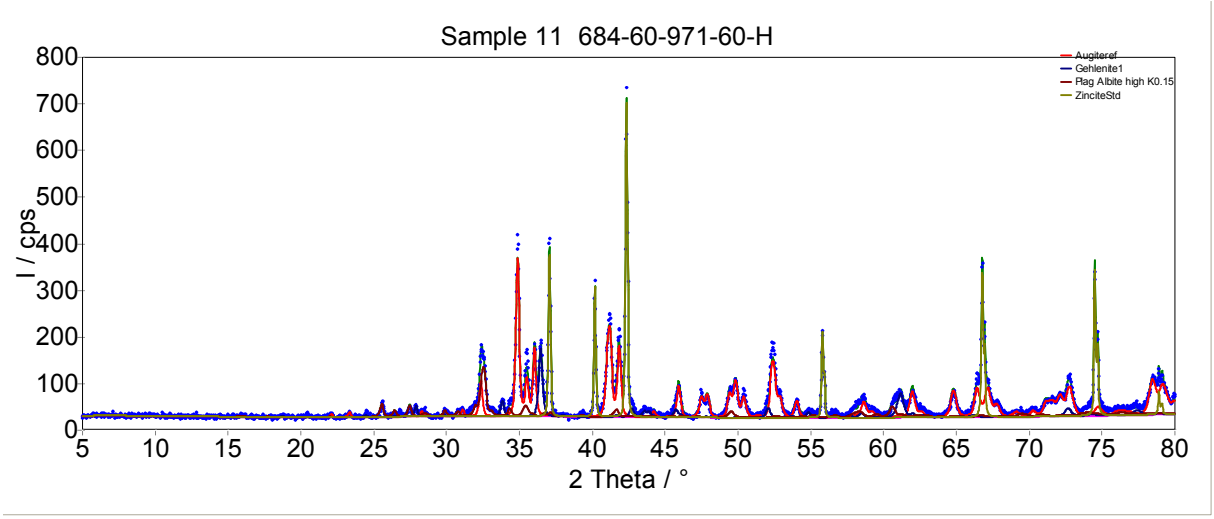

Figure A 21: XRD pattern of the sample 684-60-971-60-H

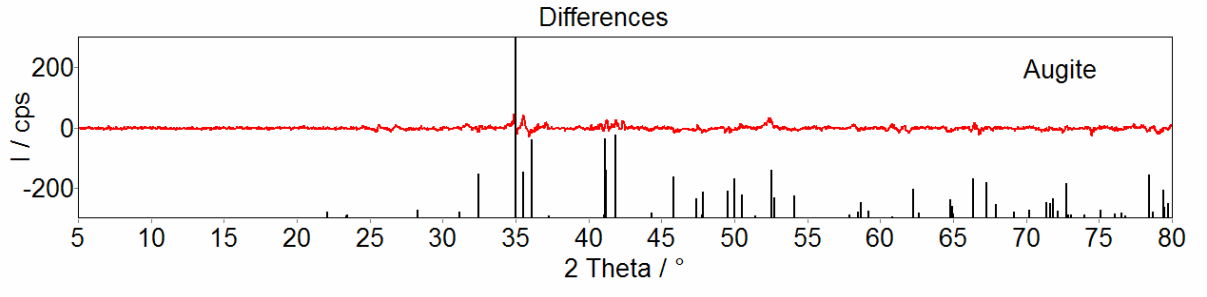

Figure A 22: Difference plot of the sample 684-60-971-60-H

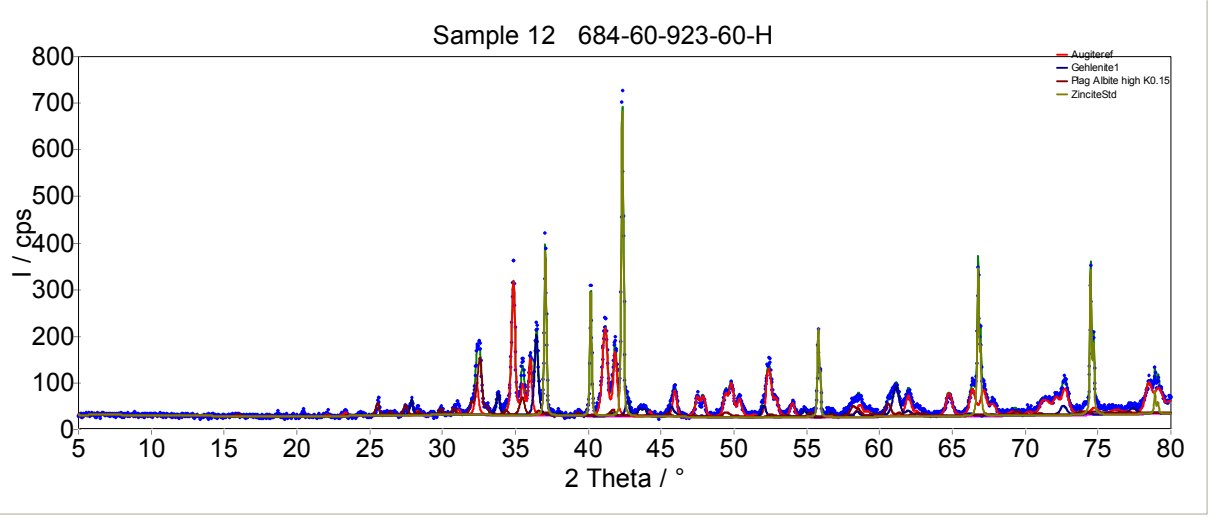

Figure A 23: XRD pattern of the sample 684-60-923-60-H

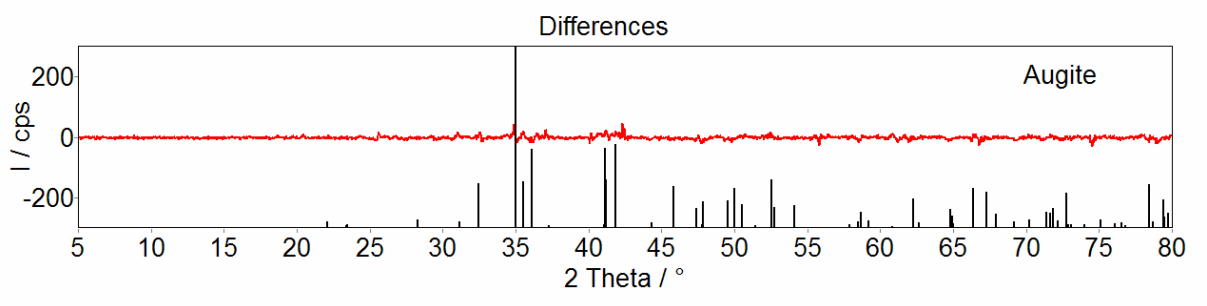

Figure A 24: Difference plot of the sample 684-60-923-60-H

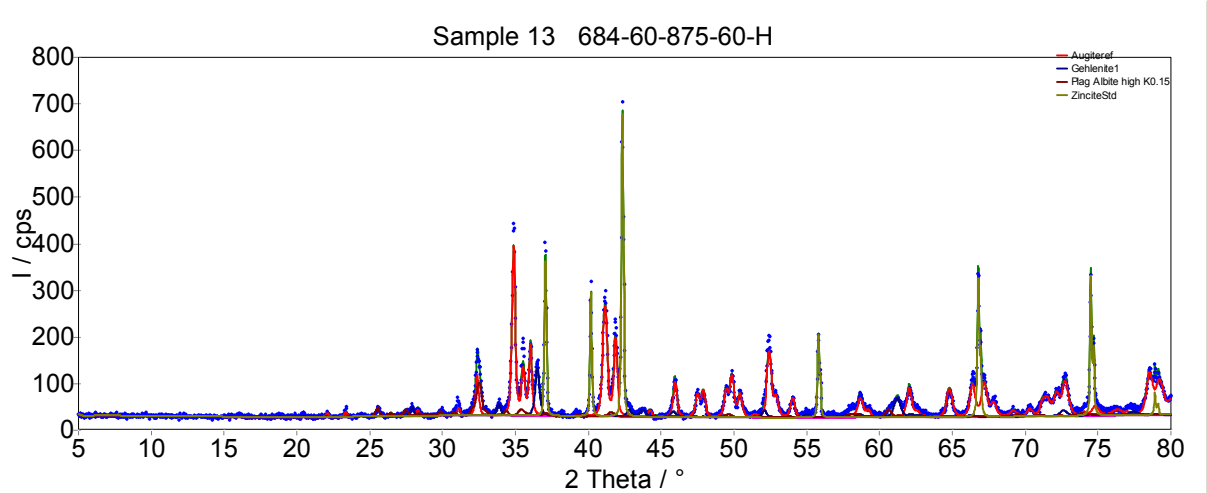

Figure A 25: XRD pattern of the sample 684-60-875-60-H

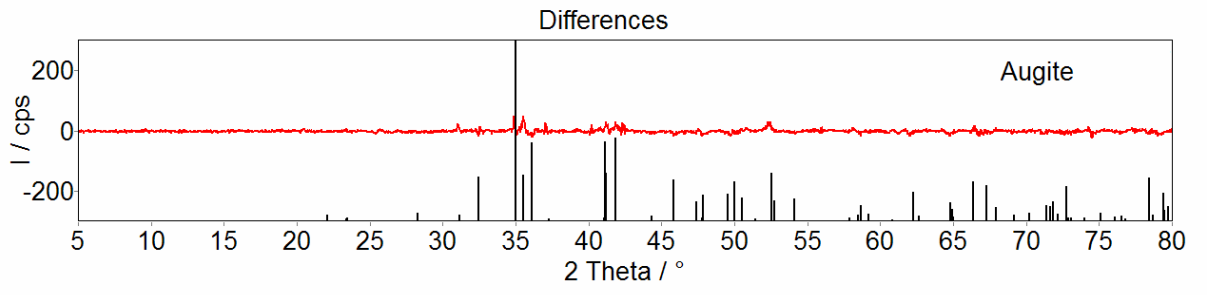

Figure A 26: Difference plot of the sample 684-60-875-60-H

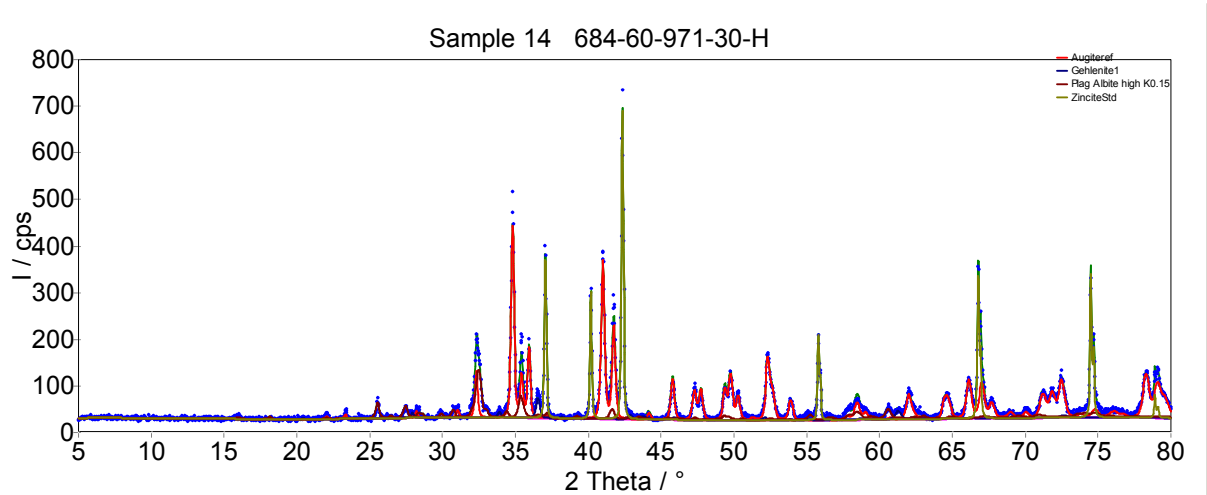

Figure A 27: XRD pattern of the sample 684-60-971-30-H

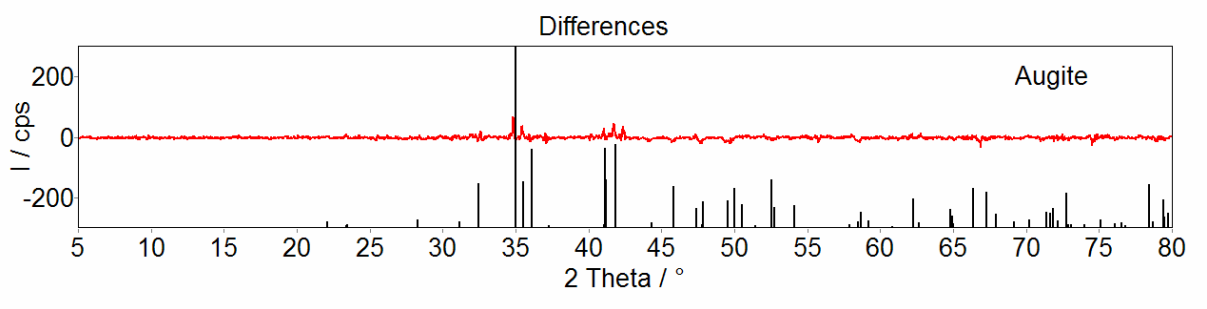

Figure A 28: Difference plot of the sample 684-60-971-30-H

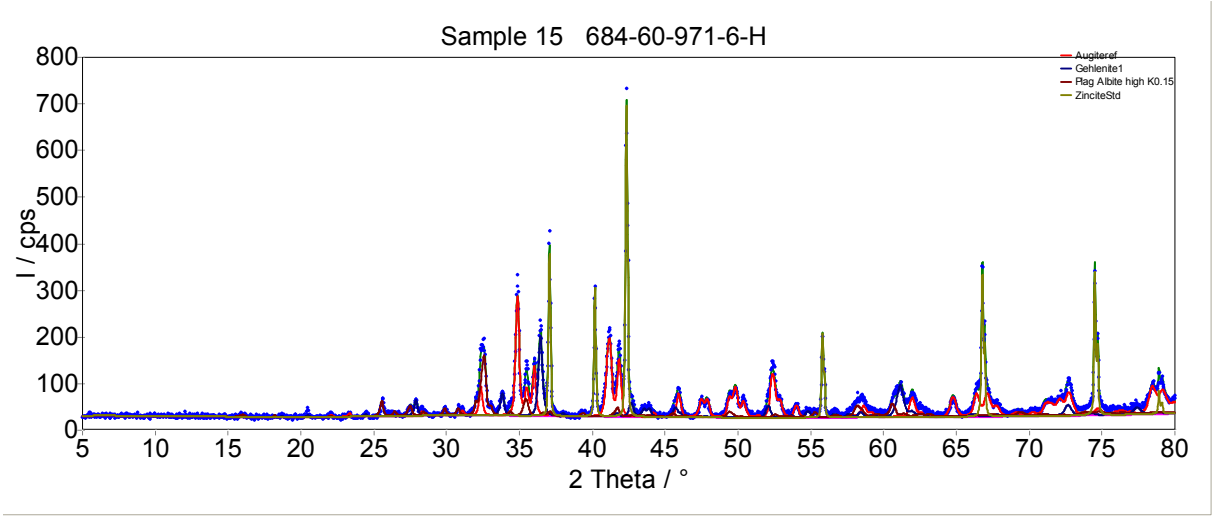

Figure A 29: XRD pattern of the sample 684-60-971-6-H

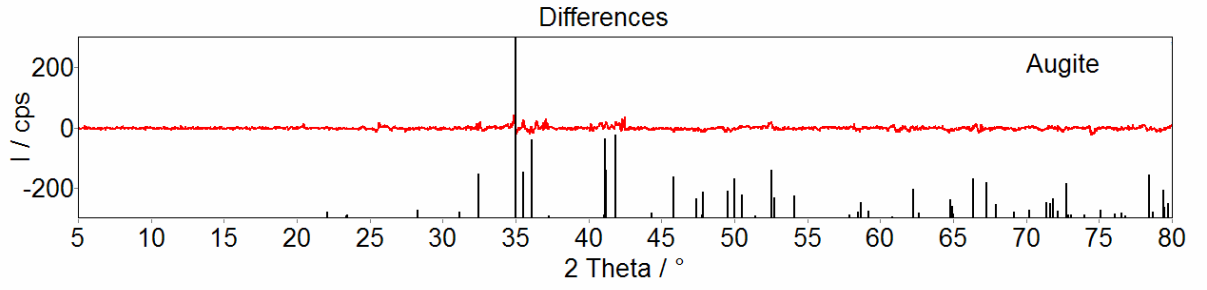

Figure A 30: Difference plot of the sample 684-60-971-6-H

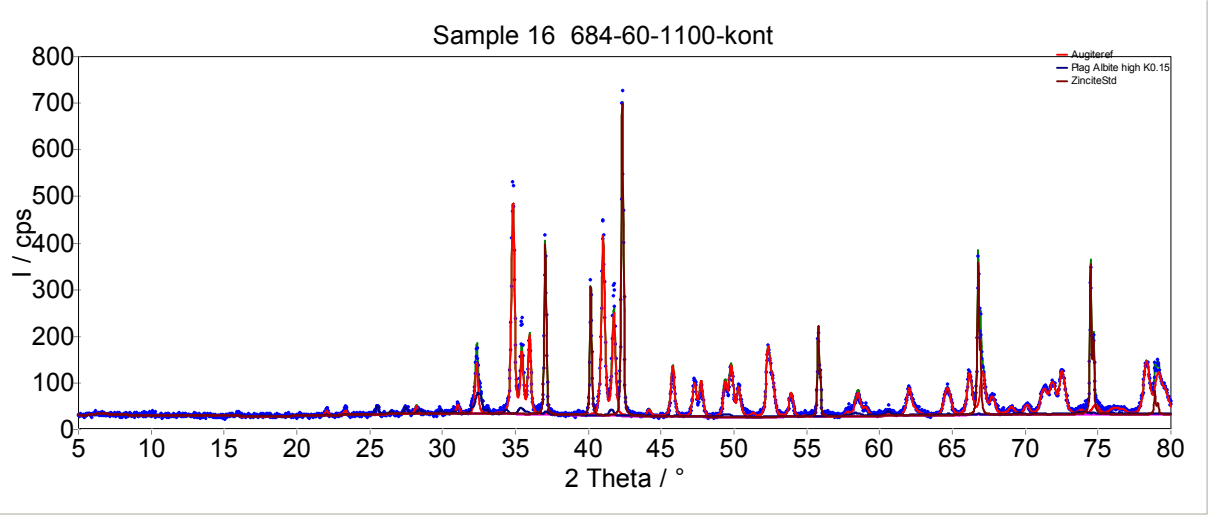

Figure A 31: XRD plot of the sample 684-60-1100-kont

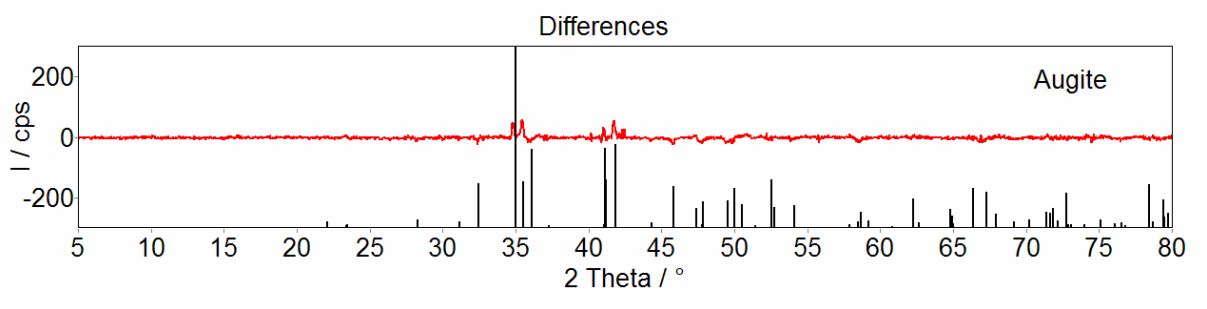

Figure A 32: Difference plot of the sample 684-60-1100-kont

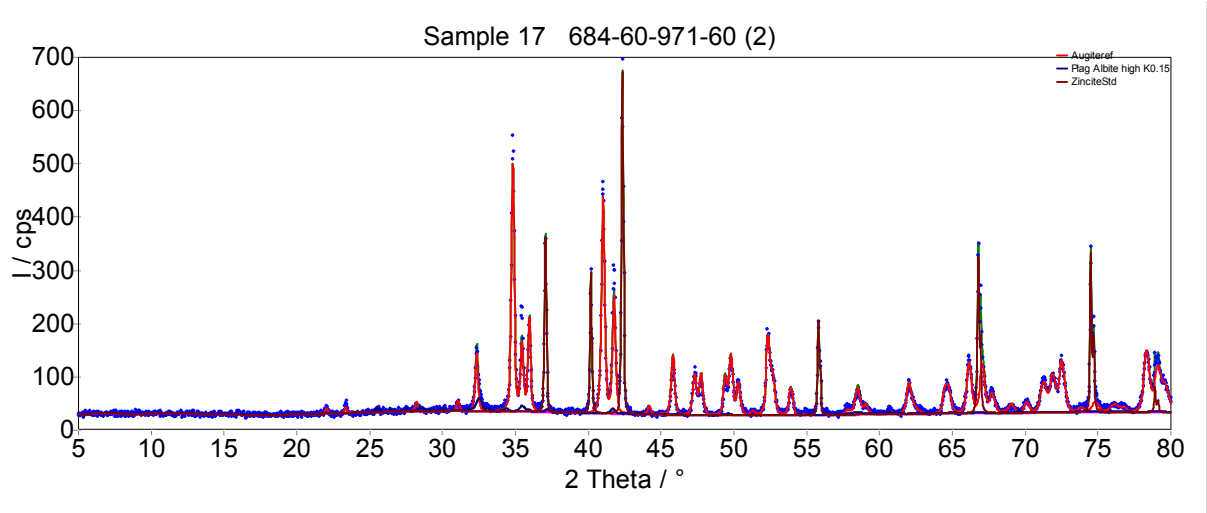

Figure A 33: XRD pattern of the sample 684-60-971-60 (2)

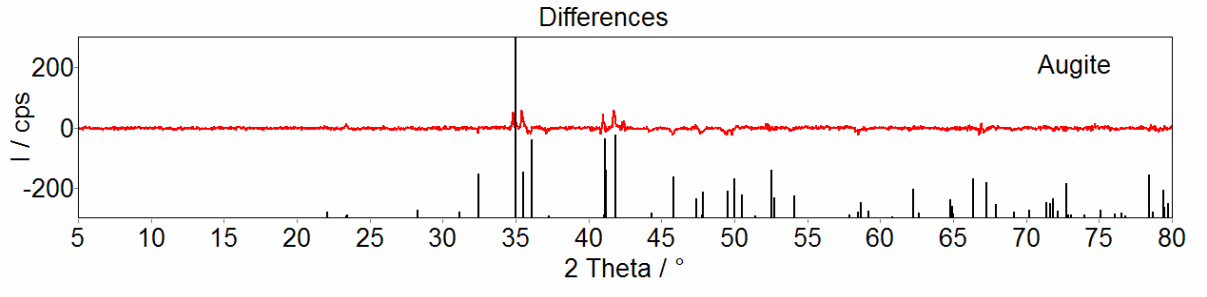

Figure A 34: Difference plot of the sample 684-60-971-60 (2)

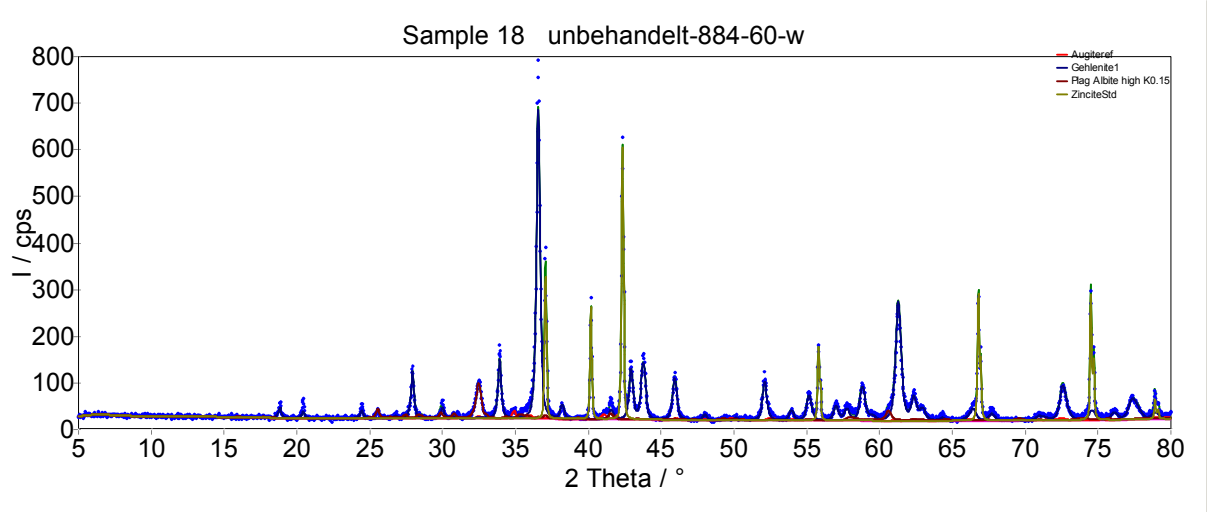

Figure A 35: XRD pattern of the sample untreated-884-60-w

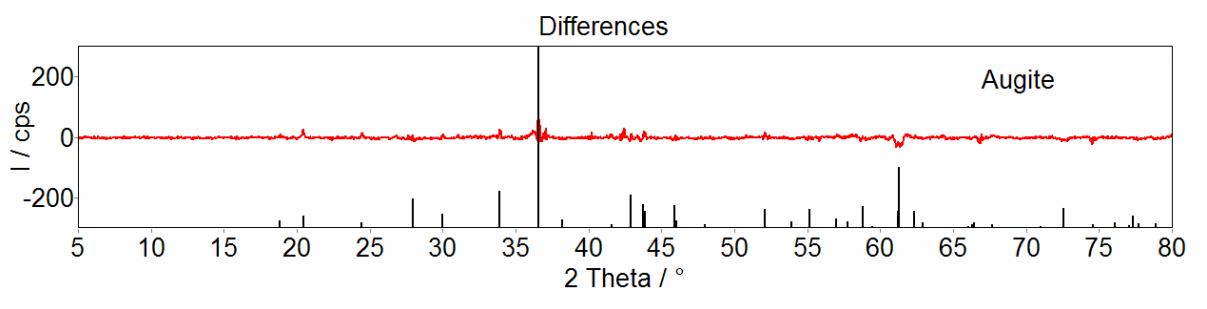

Figure A 36: Difference plot of the sample untreated-884-60-w

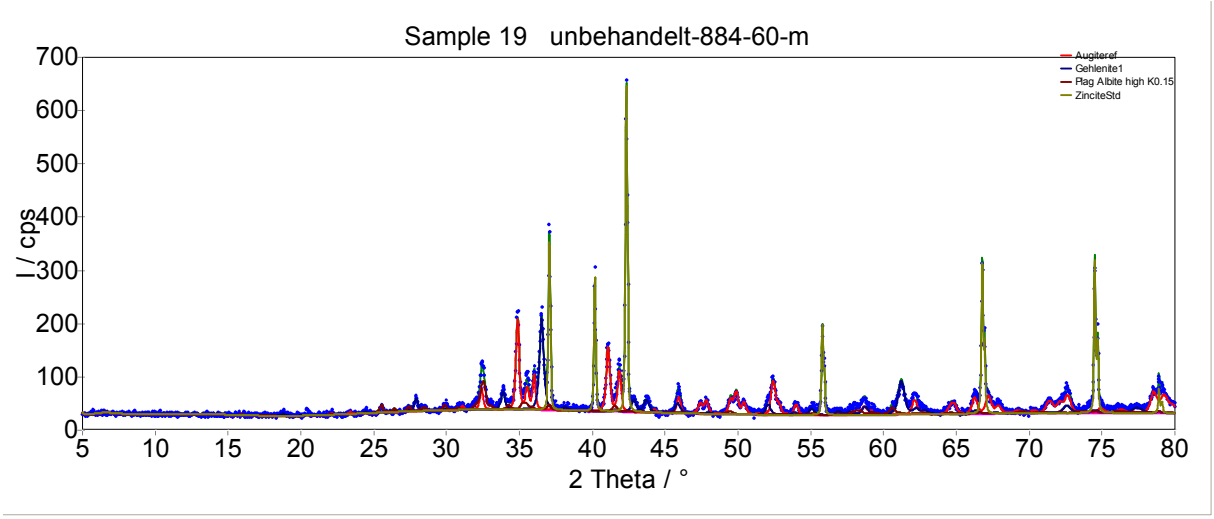

Figure A 37: XRD pattern of the sample untreated-884-60-m

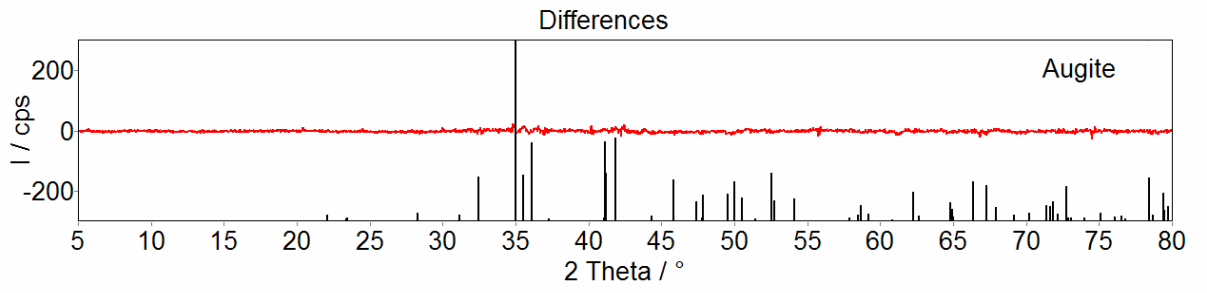

Figure A 38: Difference plot of the sample untreated 884-60-m

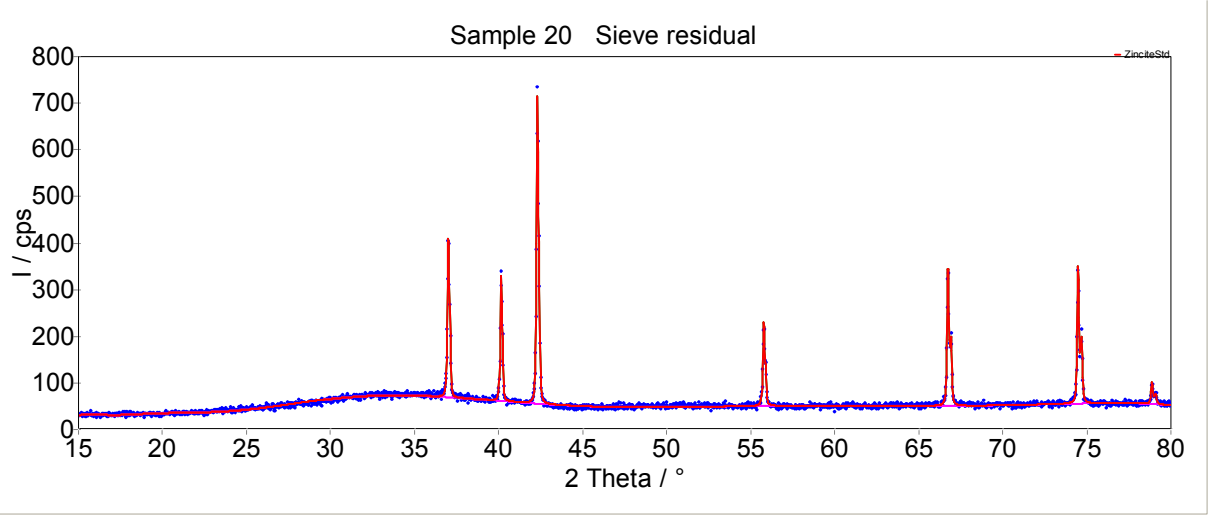

Figure A 39: XRD pattern of the sieve residual

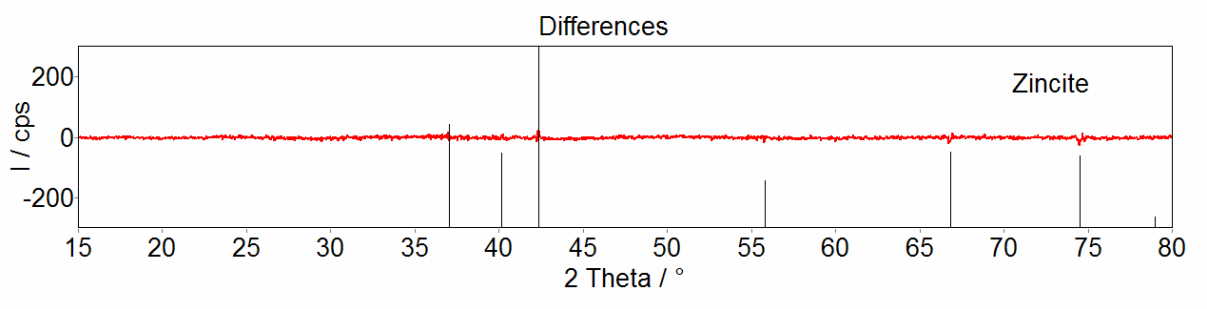

Figure A 40: Difference plot of the sieve residual